2011

AN INVESTIGATION OF THE REYNOLDS NUMBER DEPENDENCE OF THE NEAR-WALL PEAK IN CANONICAL WALL BOUNDED TURBULENT CHANNEL FLOW

Bahareh Estejab
University of Kentucky, bahareh.estejab@uky.edu

ABSTRACT OF THESIS

AN INVESTIGATION OF THE REYNOLDS NUMBER DEPENDENCE OF THE NEAR-WALL PEAK IN CANONICAL WALL BOUNDED TURBULENT CHANNEL FLOW

An experimental investigation into fully developed high aspect ratio channels was undertaken. A review of the literature reveals that there is a need for accurate measurement of the inner peak value of streamwise turbulence intensity despite the large number of studies already completed. The scattered data on this subject could be attributed either to insufficient channel size (aspect ratio or length) or to hot-wire spatial filtering.

A new, high quality, channel flow facility was designed and constructed, considering the most recent geometric limitation provided in the literature. To obtain accurate results, data were acquired using hot-wire probes with constant viscous-scale sensing length and were corrected using the most recent correction formula proposed by Smits *et al.* (2011). The results show dependence of inner peak value on Reynolds number in channels flow - its magnitude increasing with increasing Reynolds number.

KEYWORDS: channel flow, inner-peak value, streamwise turbulence intensity, hot-wire anemometry, turbulent flow

Bahereh Estejab

07/26/2011

AN INVESTIGATION OF THE REYNOLDS NUMBER DEPENDENCE OF THE NEAR-WALL PEAK IN CANONICAL WALL BOUNDED TURBULENT CHANNEL FLOW

by

Bahareh Estejab

Dr. Sean C. Bailey

Director of Thesis

Dr. James M. McDonough

Director of Graduate Studies

26/07/2011

RULES FOR THE USE OF THESES

Unpublished theses submitted for the Master's degree and deposited in the University of Kentucky Library are as a rule open for inspection, but are to be used only with due regard to the rights of the authors. Bibliographical references may be noted, but quotations or summaries of parts may be published only with the permission of the author, and with the usual scholarly acknowledgments.

Extensive copying or publication of the thesis in whole or in part also requires the consent of the Dean of the Graduate School of the University of Kentucky.

A library that borrows this thesis for use by its patrons is expected to secure the signature of each user.

Name	Date

THESIS

Bahareh Estejab

The Graduate School

University of Kentucky

2011

AN INVESTIGATION OF THE REYNOLDS NUMBER DEPENDENCE OF THE NEAR-WALL PEAK IN CANONICAL WALL BOUNDED TURBULENT CHANNEL FLOW

THESIS

A thesis submitted in partial fulfillment of the
requirements for the degree of Master of Science in the
College of Engineering
at the University of Kentucky

By

Bahareh Estejab

Lexington, Kentucky

Director: Dr. Sean Bailey, Assistant Professor of Mechanical Engineering

Lexington, Kentucky

2011

Dedicated to the memory of my mother and also to my husband and my family

TABLE OF CONTENTS

NOMENCLATURE

A	Universal constant in the logarithmic law of the wall
A_2	Constant in Chin *et.al.* (2010) correction formula
B_1	Constant in Hutchins *et.al.* (2009) correction formula
B	Large scale characteristic constant in the velocity defect log law
B_2	Constant in Chin *et.al.* (2010) correction formula
C_1	Constant in Hutchins *et.al.* (2009) correction formula
C_2	Constant in Chin *et.al.* (2010) correction formula
C_f	Local skin friction coefficient
D_2	Constant in Chin *et.al.* (2010) correction formula
d	Diameter of Hot-wire filament
E	Constant in Smits *et.al.* (2011) correction formula
H	Channel height
h	Channel half height
K_f	Thermal conductivity of the fluid
Kw	Thermal conductivity of the wire material
k	Wavenumber
k_x	Streamwise wavenumber
$k_x\emptyset_{uu}$	Pre-multiplied velocity spectra
L	Length scale
l	length of hot wire filament
l^+	Hot wire Viscous-scale wire length
Nu	Nusselt number

P	Pressure
R	pipe radius
Re_D	Reynolds number based on bulk mean velocity and pipe diameter
Re_h	Reynolds number based on mean centerline velocity and channel half height
Re_m	Reynolds number based on bulk mean velocity and channel height
Re_θ	Reynolds number based on momentum thickness Reynolds number
Re_τ	Friction Reynolds number
U	Mean velocity
$U(t)$	Streamwise component of the time-varying velocity
U_b	Bulk (area averaged) velocity
U_{CL}	Centerline velocity
U_e	Free-stream velocity
U^+	Mean velocity scaled with friction velocity
u_{rms}	Root-mean-square of the streamwise velocity fluctuations
u_τ	Friction velocity
$u'(t)$	Streamwise velocity fluctuation
$\overline{u^2}$	Streamwise component of the Reynolds stresses
$\overline{u'(t)}$	Time averaged streamwise velocity fluctuation
$\overline{u^2}^{1/2}$	Root-mean-square of the streamwise velocity fluctuations

$\overline{u^2}_m^+$	Measured streamwise turbulent intensity
$\overline{u^2}_T^+$	True streamwise turbulent intensity
$\Delta\overline{u^2}^+$	Value of difference between true streamwise turbulent intensity, $\overline{u^2}_T^+$, and the measured value, $\overline{u^2}_m^+$
V	velocity scale
x	Streamwise distance along the channel
y	Spanwise location across the channel
z	Distance from the wall in the wall-normal direction
z_0	The distance of the sensor from the wall
z^+	Distance from the wall in the wall-normal direction scaled with viscous length
α	Constant in Smits *et.al.* (2011) correction formula
β	Constant in Smits *et.al.* (2011) correction formula
γ	Resistance ratio
δ	Boundary layer thickness
δ_v	Viscous length
ε_T	three-dimensionality factor
θ	Momentum thickness
κ	Universal constant in the logarithmic law of the wall
μ	Fluid dynamic viscosity
ν	Fluid kinematic viscosity
ρ	Fluid density

τ_w	Wall shear stress
$\emptyset_{uu}$	Spectral density of streamwise velocity fluctuations

LIST OF TABLES

LIST OF FIGURES

Chapter 1

INTRODUCTION

Most flow occurring in nature is turbulent. The atmospheric boundary layer over the earth, the photosphere of sun, flow of water in rivers, majority of oceanic currents and strong winds are just a few examples of turbulent flow. It has even recently been proposed that current form of universe was affected by turbulent flow following the Big Bang theory.

Most flow encountered in engineering is also turbulent. Air flow around airplanes, water flow around ships, flow of oil or natural gas in pipelines, water flow in channels, as well as pump and turbine flows are just some important examples.

Prevalence of turbulence in the everyday life of human beings goes even back to first peoples' life without it being recognized: they hunted using hunting spears, which produce turbulent flow, they communicated with other tribes using smoke signals, and they blew on the fire to propagate the flame. The presence of turbulence is more obvious in our lives today. A quick look around reveals the turbulent smoke emerging from smoke stacks, the fast flow of water towards the drain and flow around golf balls are just a few examples. The ubiquity of turbulence in our surroundings and everyday life has made it an active research topic for years with the very first formal recognition of turbulence as a physical phenomenon attributed to Leonardo da Vinci. He explained turbulence in his sketch book as "... the smallest eddies are almost numberless, and large things are rotated only by large eddies and not by small ones, and small things are turned by small eddies and large."

From da Vinci until the present, countless researchers have devoted part or even their entire scientific career towards understanding turbulence.

Despite long years of study and despite the importance of turbulence, much remains unknown and much remains to be discovered. In fact, turbulent flow is the only problem from classical physics that is still considered 'unsolved'.

An exact description of the nature of turbulence is nonexistent, even today. Therefore, it is often described by its characteristics. Turbulence exhibits a disorganized, chaotic, and seemingly random behavior, which is three-dimensional, time dependent and rotational. It is sensitive to initial but boundary conditions and can contain a large range of length and time scales. Turbulence enhances diffusion and dissipation rates and has intermittency in both space and time.

Here, we review a few of the experimental works that have enhanced our current understanding of turbulence.

Osborne Reynolds' glass pipe experiment (Reynolds, 1883) is among the most important works on the subject of turbulence. His experiment consisting of a simple glass pipe with dye injected into flow of different velocity, led to proposing the important and well-known non-dimensional Reynolds number, formed from a length scale L, a velocity scale V, and the kinematic viscosity of the fluid, ν, as $Re = LV/\nu$. This parameter can be used as a yardstick to determine laminar to turbulent flow transition. For Reynolds' pipe experiment, he proposed $Re = 517$ as the transition Reynolds number, which is not far from the number cited in modern textbooks, $Re = 1{,}750$. (McDonough, 2011)

Interestingly, Reynolds was not the first scientist who observed the transition to turbulence. Hagen in 1839 observed that the parallel moving lines of saw-dust particles in a low temperature pipe began to move around randomly by increasing the temperature. Although he attributed the results to temperature changes and did not get any credit for his observations of turbulence, his name along with that of Poiseulle, who conducted the similar experiment at the same time, is commonly connected to the parabolic velocity profile of laminar flow, referred to as Hagen-Poiseuille flow.

Following Reynolds pioneering work, Ludwig Prandtl in 1904 (Prandtl, 1904) proposed his boundary layer theory. He divided a flow over a solid boundary into two regions: first, a region very close to the wall where viscosity is important and called it boundary layer, and second, the rest of flow where viscosity has no role. Without exaggeration, his work can be described as the foundation of all subsequent work in wall-bounded flows.

Although there are some well-known experiments conducted in pipes even before Prandtl formed his boundary layer theory, e.g., Du Buat in 1779, Henry Darcy between 1850 and 1858 years, experiments performed in turbulent channel flows, where the flow is bounded by two parallel plates, received much less attention until relatively very recently. Two reasons may be considered for this lack of detailed studies: first, the ambiguity of the proper channel aspect ratio to best mimic two dimensional flow by eliminating sidewall effects, and second, the upsurge in direct numerical simulations (DNS) of channel flows, for which the geometric effects provide numerical simplifications for gridding and application of periodic boundary conditions. The reason of this lack before Prandtl's time might be explained by the intended application of the

research, typically either for military or civil uses, which resulted in researchers focusing on turbulent boundary layers and pipe flows.

Among the few channel experiments, some have influenced our modern understanding of turbulent flows. Herman Schlichting conducted a series of smooth- and rough-wall rectangular duct studies and the results were published in 1936 (Schlichting, 1936), becoming the first channel flow experiment performed after Prandtl had proposed his theory. Laufer's channel experiment in mid 20^{th} century (Laufer, 1950) can be considered as the benchmark of smooth wall channel studies. He was also the first person used hot-wire anemometry for turbulence measurements in a channel. Dean's experiments (Dean, 1978) are one of the most cited studies, which solved the sidewall effects issue by determining the required channel aspect ratio. More recently, Zanoun (2002, 2003, 2009) and Monty (2005) conducted channel experiments at moderate Reynolds numbers.

The objectives of the present study are threefold:

1. Due to a lack of channel experiments at high Reynolds number, one objective was to build a channel facility to increase the range of Reynolds numbers currently achievable in facilities employing the current body of knowledge about the geometry necessary to diminish the sidewall effects on the flow and ensure full development in the streamwise direction.

2. Discrepancies between canonical wall-bounded flows in the inner region have been recently observed, where previously the flow was thought to depend only on wall friction and therefore were expected to be independent of large-scale flow geometry. A second objective was to further investigate these differences using accurate measurements,

particularly with regards to the magnitude of inner peak of streamwise velocity fluctuations.

3. New corrections have been recently proposed to address the limited spatial resolution issue of hot-wire probes. A third objective was to investigate their applicability to turbulent channel flow.

Chapter 2

LITERATURE REVIEW

The importance of turbulent wall-bounded flows in engineering and nature is reflected in the numerous studies in broad areas of this subject. Among them, there are certain subjects, which are applicable to the current research, including:

(1) Spatial filtering of hot-wire probes and its effects on inner peak magnitude of streamwise turbulence velocity fluctuations.
(2) Inner peak position and magnitude in boundary layers, pipe and channel flows.
(3) Effects of outer region on the inner region.
(4) Differences between canonical wall-bounded flows.

Before addressing these topics, it will be useful to review of some of the broad concepts in turbulent wall-bounded flow.

Wall bounded flows can be divided into two categories: internal flows and external flows. Flow through pipes and channels are examples of internal flows and flow around airplanes or ships and flow of rivers are examples of external flows. Due to their simplicity, the turbulent flows that are most commonly studied are the so-called canonical flows: fully developed channel flow, fully developed pipe flow, and the zero-pressure-gradient turbulent boundary layer.

These wall-bounded flows can be divided into two main regions, an "inner layer" and an "outer layer".

Prandtl (1925) was the first person who defined the "inner layer" concept, the region close to the wall in which, at sufficiently high Reynolds number, the mean velocity profile depends only on kinematic viscosity, ν, and wall shear stress, τ_w. Appropriate velocity and length scales for the flow can then be defined on the basis of these two parameters. The velocity scale, referred to as "friction velocity" is found from

$$u_\tau = \sqrt{\frac{\tau_w}{\rho}}, \tag{2.1}$$

where ρ is fluid density and the length scale, referred to as the "viscous length" is found from

$$\delta_\nu = \frac{\nu}{u_\tau}. \tag{2.2}$$

The Reynolds number based on just the viscous parameters is therefore equal to unity.

Further away from the wall, in the "outer layer", viscous force is not important and is replaced by inertial effects. The velocity scale in this region is still friction velocity, u_τ, but the length scale becomes the thickness of shear layer, such as boundary layer thickness, δ, pipe radius, R, or channel half height, h.

In wall bounded flow studies, the friction Reynolds number, which is also known as Karman number, is often used as a common Reynolds number to compare Reynolds number effects among different types of flows. It is defined as the ratio of inner and outer length scales, $Re_\tau = \frac{\delta u_\tau}{\nu}$, where here δ represents the outer layer length scale for the flow under consideration.

In many references, such as Pope (2000), the inner and outer regions are commonly defined on the basis of Re_τ as, the inner region in the range of $0 < z^+ < 0.15Re_\tau$, and the outer region in the range of $\frac{30}{Re_\tau} < \frac{z}{\delta} < 1$, where z is the distance from the wall in the wall-normal direction and z^+ is this distance scaled with viscous length, $z^+ = \frac{z\,u_\tau}{\nu}$. Note that, in general, within this document, a superscripted + will be used to indicate quantities normalized using the inner length and velocity scales.

It is also common practice to further divide wall-layers into subregions as follows:

1. Viscous wall region at $z^+ < 50$, where molecular viscosity affects directly on shear stress.
2. Viscous sublayer at $z^+ < 5$, where viscous stress is the only important parameter.
3. Logarithmic, or overlap region, at $30 < z^+ < 0.1Re_\tau$, where characteristics of both the inner region and outer region exists. Here, the mean velocity follows the so-called "log-law", meaning that the relationship between mean velocity and z^+ follows

$$U^+ = \frac{1}{\kappa} \ln z^+ + A \tag{2.3}$$

   where κ and A are constant

4. Buffer layer at $5 < z^+ < 30$, which is the median layer between viscous sublayer and the logarithmic layer.
5. Outer layer at $z^+ > 50$, where effects of viscosity on mean velocity is negligible.

Although the abovementioned divisions were accepted for years, it is now known that they are not exact. For example, Zagarola & Smits (1998) observed that in pipe flows, the logarithmic region begins at $z^+ \geq 600$. Nagib *et al.* (2007) and Sreenivasan and Sahay (1997) found that in turbulent boundary layers $z^+ = 200$ is approximately the beginning point for log law region.

Regardless of classical or modern definition of these divisions, the mean velocity profile, when appropriately scaled using inner or outer length and velocity scales, is independent of Reynolds number.

Wall-normal profiles of the Reynolds stresses, in particular its streamwise component

$$\overline{u^2} = \overline{u'(t)u'(t)} \tag{2.4}$$

have not been found to follow the same scaling behavior. Here

$$u'(t) = U(t) - \overline{U}, \tag{2.5}$$

and $U(t)$ is the streamwise component of the time-varying velocity, $\overline{U}$ is the mean velocity and the overbar indicates a time average. Wall-normal profiles of the streamwise Reynolds stress, also often referred to as the turbulence intensity profiles, are therefore dependent on Reynolds number when normalized using the traditional inner length and velocity scales. Most notably, there is an "inner peak" in the profiles, occurring at $z^+ \approx 15$ corresponding to the location of maximum turbulence production. The magnitude of the inner peak has been found to be Reynolds number dependent (see Section 2.2).

As a result, predicting the turbulence intensity at high Reynolds number (beyond those achievable in most laboratories) is not yet possible. Therefore, determining appropriate scaling parameters for the Reynolds stress has become an important subject of interest in the study of turbulent wall-bounded flows and is the focus of many studies, e.g., George and Castillo (1997), DeGraaff and Eaton (2000), Wie *et al.* (2005), Monkewitz *et al.* (2007), and Panton (2007). In spite of these efforts, the influence of Reynolds number on turbulent statistics is still unknown.

2.1. Spatial filtering of hot-wire probes

One factor contributing to the confusion regarding the Reynolds number scaling of turbulence quantities is the temporal and spatial filtering of hot-wire probes. Hot-wire probes are employed for turbulent studies due to their high frequency response (typically around 100 kHz) and therefore excellent *temporal* resolution. The *spatial* resolution of these probes, however, often is inadequate to resolve all the scales of the turbulence and thus the effects of spatial filtering on measured statistics have remained a topic of interest for years.

Ligrani and Bradshaw (1987a) and Ligrani and Bradshaw (1987b) found that the dimensions of hot-wire probes had significant effects on the measurement of streamwise Reynolds stress. They narrowed the size dependence to two factors: length-to-diameter ratio and length of wire and observed that the measured Reynolds stress was reduced by either increasing the wire length to more than 20 times the viscous length or decreasing the length-to-diameter ratio less than 150-200. Therefore, they concluded that in order to negate the effects of attenuation due to inadequate spatial resolution (i.e., "spatial

filtering") two conditions must be met. First, viscous-scale wire length, $l^+ = \frac{lu_\tau}{\nu}$, must be smaller than 20, where l is the wire length. Second, the length-to-diameter ratio of wire, l/d, where d is the wire diameter, must be larger than 200 to avoid the attenuation of frequency response due to heat conduction to the support prongs.

Many researchers examined the limitations proposed by Ligrani & Bradshaw. Alfredsson *et al.* (1988) performed experiments for measuring streamwise velocity fluctuations near the wall using three hot-wire probes, $l^+ = 2, 8, 10$. No dependence of the inner peak value on l^+ was observed, which confirmed the sufficiently small values of viscous-scale wire length consistent with Ligrani & Bradshaw results.

Until this time, most of the cited literature was reported at only a single Reynolds number, e.g., Ligrani & Bradshaw performed their studies at constant momentum thickness Reynolds number, $Re_\theta = \frac{\theta U_e}{\nu} = 2{,}620$, where θ is the momentum thickness and U_e is the free-stream velocity. Hence, it was felt that a study of the Reynolds number dependence of spatial filtering effects was required.

Klewicki & Falco (1990) performed an experiment in the range of Reynolds numbers, $1{,}010 < Re_\theta < 4{,}850$ and found the decreasing trend of hot-wire spatial resolution with increasing the non-dimensional wire length, l^+, measuring the near wall peak of longitudinal turbulent intensity. As a result, Ligrani & Bradshaw (1987b) condition for suitable range of l^+ ($l^+ < 20$) was not necessarily universal for all Reynolds numbers. Hutchins *et al.* (2009) continued the previous study and consistently found a dependency on the inner peak value and l^+. They proposed that the independent effects of Reynolds

number, Re_τ, and l^+, were responsible for high scatter of cited inner-peak values and proposed a correlation for relationship between them and measured inner peak value of

$$\left.\frac{\overline{u^2}}{u_\tau^2}\right]_{z^+=15} = 1.0747 \log_{10} Re_\tau - 0.0352 l^+ - 23.0833 \left(\frac{l^+}{Re_\tau}\right) + 4.8371. \quad (2.6)$$

They also proposed the error of using hot-wire with $l^+ = 20$, proposed by Ligrani & Bradshaw (1987b) with respect to Reynolds number is

$$|\%error|_{l^+=20} = 100 \times \frac{20(0.0352 + 23.0833/Re_\tau)}{(1.0747 \log_{10} Re_\tau + 4.8371)} \quad (2.7)$$

Based on this formula, the error of using hot-wire with $l^+ = 20$ has a inverse relation with Reynolds number, which means the error decreases with increasing the Reynolds number. By increasing the Reynolds number, numerator goes toward the constant value and denominator increases continuously.

They also investigated the proper length-to-diameter ratio and found results consistent with those of Ligrani & Bradshaw (1987b), which proposed that diameter-to-length ratio must be larger than 200 for diminishing the attenuation effects of hot-wires in finding the inner peak value.

Most recently, Smits *et al.* (2011) proposed a correction formula based on the attached eddy hypothesis of Townsend (1976) and showed that the attenuation is related to l/z instead of l^+ for $z^+ > 15$. Their correction formula, unlike that of Hutchins *et al.* (2009) is applicable across the entire height of the wall layer.

Smits *et al.* (2011) presented the correction as

$$\overline{u^2}_T^+ = [M(l^+)f(z^+) + 1]\,\overline{u^2}_m^+ \tag{2.8}$$

where

$$f(z^+) = \frac{15+\ln(2)}{z^+ + \ln[e^{(15-z^+)}+1]}, \tag{2.9}$$

$$M = \frac{\Delta\overline{u^2}^+}{\overline{u^2}_m^+}\Big|_{z^+=15} = \frac{6.13\,\tanh(\alpha l^+)\,\tanh(\beta l^+ - \mathrm{E})}{(\overline{u^2}_m^+)_{z^+=15}} \tag{2.10}$$

where $\alpha = 5.6 \times 10^{-2}$, $\beta = 8.6 \times 10^{-3}$, $\mathrm{E} = -1.26 \times 10^{-2}$.

$\overline{u^2}_T^+$ is the corrected streamwise turbulent intensity and $\overline{u^2}_m^+$ is the measured one.

2.2. The inner peak position and magnitude

According to the classical view, all inner region variables are independent of the outer region and are solely functions of z^+. In other words, they are independent of the large-scale geometry and are similar regardless of flow geometry. Furthermore, according to the definition of Re_τ, friction Reynolds number is a function of outer region length scale: turbulent boundary layer thickness, pipe radius, or channel half height. The combination of these two facts implies that inner region variables are independent of friction Reynolds number. In recent years, this concept was challenged, and the influence of Reynolds number, particularly on the statistical turbulence quantities, has been examined in detail.

As mentioned earlier, the streamwise turbulent velocity fluctuations profile has a peak near the wall, with its magnitude and position with respect to wall the focus of intense investigation due to its connection to the location of peak turbulence production. In spite

of the approximate consistence of its position at $z^+ \approx 15$, its magnitude has still been an active research topic. In this section, we will review the inner peak value, starting with two reviews covering up to 1996, and continue to the present time treating the three canonical flows separately.

To investigate the Reynolds number dependence of inner peak value of streamwise turbulent velocity fluctuations and its position with respect to the wall, Mochizuki and Nieuwstadt (1996) made a survey of 42 independent experimental and direct numerical simulation (DNS) data sets from all three types of canonical flows. The range of Reynolds numbers that were covered in their survey was $Re_\theta = 300 - 20{,}920$ for turbulent boundary layers, and $Re_\tau = 100 - 4{,}300$ for pipe or channel flows. In all the reviewed studies, $l^+ < 30$.

The results showed Reynolds number independence of the peak value and its position in all three kinds of flow. Interestingly, they found that the peak value and its position were equal in both internal and external flows, which was attributed to the equilibrium of the streamwise velocity fluctuations and the local wall shear stress. In the other words, the "inactive" motions imposed by the outer layer flow (Bradshaw, 1967) which are dependent on flow geometry (outer length scale) did not affect the peak value and its position.

In contrast, Klewicki & Falco (1990) found an empirical formula for the peak value dependence on Reynolds number of

$$\left.\frac{\overline{u^2}}{u_\tau^2}\right]_{z^+=15} = 8.5 \times 10^{-9}\, Re_\theta^2 + 4.8 \times 10^{-4}\, Re_\theta + 6.86\,, \qquad (2.11)$$

which was found by plotting data from eighteen independent experiments, with Reynolds number from $Re_\theta = 300$ to $Re_\theta = 20{,}000$.

Up until 1994, most well-known studies in the viscous wall region of turbulent boundary layers were at low to moderate Reynolds number, $Re_\theta < 5000$ (Gad-el-Hak and Bandyopadhyay, 1994). Since almost all practical applications featuring turbulent boundary layers are at high Reynolds numbers, the lack of results for this range of Reynolds numbers was conspicuous. It motivated the researchers to invent new laboratory facilities to reach higher Reynolds numbers, including the National Diagnostic Facility at the Illinois Institute of Technology (Hites, 1997), the Princeton Superpipe (Zagarola and Smits, 1998), the Minimum Turbulent Level wind tunnel at KTH (Österlund, 1999), the Stanford pressurized wind tunnel (DeGraaff and Eaton, 2000), the Surface Layer Turbulence and Environmental Science Test facility in Utah (Metzger, 2002), the High Reynolds Number Boundary Layer Wind Tunnel at Melbourne University (Nickels *et al.*, 2007) and the High Reynolds Number Test Facility at Princeton (Jiménez, Hultmark and Smits, 2010).

Note that low Reynolds number flows can still be useful for some purposes, such as studies of coherent near wall motions, which are also easier to perform at lower Reynolds numbers because of thicker viscous near wall regions (Smits *et al.*, 2011).

2.2.1. Boundary layer studies

Metzger and Klewicki (2001) performed experimental high Reynolds number research at Re_θ = 2000 and 5×10^6 in a laboratory turbulent boundary layer and the

atmospheric surface layer respectively. They found that the most energetic peak of the streamwise velocity fluctuation at $z^+ = 15$ rises logarithmically with Reynolds number following

$$u^+_{rms}]_{z^+=15} = 1.86 + 0.28\, log\, (Re_\theta) \tag{2.12}$$

where u_{rms} is the root-mean-square of the streamwise velocity fluctuations, or $\overline{u^2}^{1/2}$. For data acquisition, five hot-wires with $l^+ < 6$ mounted on a rack at different heights were employed.

The belief in classical scaling prompted researchers to seek some form of scaling which would collapse the inner region part of streamwise velocity fluctuations for different Reynolds numbers. In an attempt to reach this objective DeGraaff and Eaton (2000) proposed a new scaling method consisting of both internal and external velocity scales for normalization of velocity fluctuations, $\frac{\overline{u^2}}{U_e u_\tau}$. The basis of this idea was formed from their observations of the inner-scaled streamwise fluctuation profile, which changed proportionally to $Re_\theta^{0.1}$. The new scaling met their expectation and the streamwise velocity fluctuation profiles scaled by it, and plotted versus z^+, collapsed onto a universal curve regardless of the value of Reynolds number, for the range of the Reynolds numbers from $Re_\theta = 1{,}430$ to $Re_\theta = 31{,}000$. The data were acquired using laser-Doppler anemometer (LDA). In an attempt to validate the results, Metzger *et al.* (2001) used the same scaling method for an extended range of Reynolds numbers including the atmospheric surface layer data, $Re_\theta = 1{,}000 - 5 \times 10^6$. The proposed mixed scaling was found applicable in the near wall region for $z^+ < 30$.

Marusic and Kunkel (2003) proposed a similarity formulation based on a physical argument, the attached eddy model. They scaled the data with inner variables and found a dependency between the inner-peak value of the streamwise velocity fluctuation at $z^+ = 15$ and Reynolds number, Re_τ. Good agreement was seen between the proposed formulation and experimental data over a wide range of Reynolds numbers varying from laboratory to atmospheric flows; e.g., Metzger and Klewicki (2001). Their formulation was found the be valid to describe the streamwise turbulence intensity profile over the entire height of the boundary layer. Based on their formulation, they concluded that inner/outer interactions in boundary layers was probable and that the outer layer in boundary layer flows affects the inner layer down to the viscous sublayer.

Hutchins and Marusic (2007) found the Marusic and Kunkel (2003) formula to describe the behavior of the inner-peak value normalized by friction velocity precisely. They produced a curve fit to existing near wall peak data of

$$\left.\frac{\overline{u^2}}{u_\tau^2}\right]_{z^+=15} = 1.036 + 0.965 \ln(Re_\tau). \tag{2.13}$$

They also observed direct effects of superstructures occurring in outer region, i.e., "very long meandering positive and negative streamwise velocity fluctuation" on the near wall region. (See Section 2.3 for more details.)

Hutchins *et al.* (2009) believed that the effects of Reynolds number, Re_τ, and viscous-scaled wire length, l^+, on inner-peak value are not separable and must be considered simultaneously. Based on this hypothesis, they proposed that

$$\left.\frac{\overline{u^2}}{u_\tau^2}\right]_{z^+=15} = 1.0747 \log_{10} Re_\tau - 0.0352\, l^+ - 23.0833 \left(\frac{l^+}{Re_\tau}\right) + 4.8371 \qquad (2.14)$$

which covered the range of $3 < l^+ < 153$ and $316 < Re_\tau < 25{,}000$.

2.2.2. Pipe flow studies

Although many studies can be found regarding the effects of Reynolds number on inner peak value of streamwise turbulent velocity fluctuations in turbulent boundary layers after 1996, the numbers of studies in pipe flow in this subject is surprisingly small.

Den Toonder and Nieuwstadt (1997) performed an experiment in a water pipe using the LDA measurement technique. The range of Reynolds numbers was low to moderate, $Re_D = 5000 - 25000$, where Re_D is the Reynolds number based on bulk mean velocity and pipe diameter. No relation between Reynolds number and inner-scaled rms values of streamwise velocity fluctuations were observed and the profiles collapsed for all four Reynolds numbers up to $z^+ \approx 30$.

Wu and Moin (2008) presented a DNS study in a fully developed pipe flow for $Re_D = 5{,}300$ ($Re_\tau = 180$) and $Re_D = 44{,}000$ ($Re_\tau = 1{,}142$). A finite-difference method with $300 \times 1024 \times 2048$ grids along r, θ and z directions was used. They compared their results with previous studies and, in this case, Reynolds number dependence of the inner peak value of streamwise turbulence intensity was observed.

In an attempt to resolve the discrepancies regarding the inner peak value, and overcome the problem of limited spatial resolution in hot-wire measurements seen in

previous studies, Hultmark *et al.* (2010) conducted an experiment in the Princeton Superpipe. The range of Reynolds number was from $Re_D = 24 \times 10^3$ to $Re_D = 145 \times 10^3$, based on pipe diameter. The length of single normal hot-wires was in the range of l = 0.4 - 1.8 mm, however the non-dimensional hot-wire length scale, l^+, was kept constant, $l^+ = 20$ for each Reynolds number.

They found that the inner-scaled peak value of streamwise velocity fluctuations and its position were independent of Reynolds number and were constant at $\left.\frac{\overline{u^2}}{u_\tau^2}\right]_{z^+=15} = 7.77 \pm 0.37$.

The inconsistency between the results of inner peak value in turbulent boundary layer flows and pipe flows was attributed to the outer layer structure differences in internal and external flows, which could change its interaction with inner layer. (See Section 2.3 for more details.)

2.2.3. Channel flow studies

After 1996, we surprisingly could find just a single experimental study in channel flows. This is due to the rising prevalence of DNS studies over this period and their common application to channel flows due to geometric simplifications.

Monty (2005) performed an experimental study measuring the velocity using hot wire probes. The range of Reynolds numbers in his study was $Re_m = 40 \times 10^3 - 182 \times 10^3$ (based on bulk velocity and channel full height) and the viscous-scale wire length, l^+, was not constant. The results were presented for both inner- and outer-scaled variables and

showed dependency of the inner peak magnitude on Reynolds number regardless the scaling variables.

The DNS method tries to solve the flow governing equations from the largest to the smallest flow scales with no models employed. The results are accurate and reliable, but the only limitation is that the current computers are not sufficiently powerful to permit solutions at high Reynolds numbers and/or complicated geometries (McDonough, 2011). The journey of using DNS in channel flows started with $Re_\tau = 180$. To the author's knowledge, $Re_\tau = 2003$ is the largest Reynolds number channel flow ever simulated (Hoyas & Jiménez, 2006).

To ensure the accuracy of a DNS study, two requirements must be met:

1- Large DNS domain to capture the largest eddies, which would be proportional to the outer length scale

2- Fine grid spacing to resolve the smallest eddies (Abe *et al.*, 2001).

Kim *et al.* (1987) was one of the first DNS studies in fully developed channel flow. In this study, Re_h = 3300, based on mean centerline velocity and channel half height (Re_τ = 180) and $192 \times 129 \times 160$ grid points in x, y, z directions were employed. After this study, the use of DNS in channel flows became widespread. Kim (1990) increased the Reynolds number to Re_τ = 395. Antonio and Kim (1994) studied the combined results of these two studies and found Reynolds number dependency of the near wall turbulent quantities.

Moser *et al.* (1999) conducted the DNS study for Re_τ = 180, 395 and 590. The grids

employed were $128 \times 129 \times 128$, $256 \times 193 \times 192$ and $384 \times 257 \times 384$ (in x, y, and z directions) respectively. The result showed the influence of Reynolds number on the inner peak value of streamwise turbulent velocity fluctuations, which increased with increasing Reynolds number.

Abe *et al.* (2001) increased the Reynolds number to $Re_\tau = 640$. They studied also $Re_\tau = 180$ and 395. The number of grid points was $256 \times 128 \times 256$, $256 \times 192 \times 256$ and $512 \times 256 \times 256$ (in x, y, and z directions) for $Re_\tau = 180, 395, 640$ respectively. The result was consistent with previous studies and confirmed the Reynolds number dependency of inner-peak value of streamwise velocity fluctuations.

In the Del Álamo *et al.* (2004) study, Reynolds number value reached $Re_\tau = 1900$, but at the expense of decreasing the DNS domain. The study, performed for $Re_\tau = 550, 964, 1901$ focused on the overlap layer, which respectively, had $192 \times 192 \times 257$, $384 \times 384 \times 385$, and $768 \times 768 \times 769$ grid points in the x, y, and z directions. In addition, Del Álamo and Jiménez (2003) studied channel flow using $Re_\tau = 180, 550$ in which the number of grid points was not mentioned. Hoyas & Jiménez (2006) investigated the results of two previous studies and increased the Reynolds number to $Re_\tau = 2003$ in their study using $6144 \times 633 \times 4608$ grid points. The focus of this study was on velocity fluctuations, and the inner-scaled peak value at $z^+ = 15$ was found to increase with increasing the Reynolds number.

The increasing trend of inner peak value of streamwise turbulent velocity fluctuations seen in the DNS results agrees with results of turbulent boundary layer studies, which are both in conflict with the pipe results. To seek the reason for this discrepancy, the next

section is devoted to the effects of outer region on the inner region, which is believed to be the source of the Reynolds number dependence of the inner peak.

2.3. The effects of outer region on the inner region

Townsend (1976) pioneered the hypothesis of the existence of large-scale motions within turbulent boundary layers. He attributed long tails in the temporal correlation of the streamwise velocity component found by Grant (1958) to these long-scale motions and noted that the near-wall region feels all attached eddies whose centers are above that height. Hence, velocity fluctuations are the sum of all the induced fluctuations contained within the upper layers.

Kline *et al.* (1967) revealed the existence of "surprisingly well-organized spatially and temporally" motions in the viscous sublayer, which lead to the formation of low-speed streaks very close to the wall up to buffer layer.

The long tails on the temporal correlation of the streamwise velocity component were not, however, limited to just buffer layers and expanded throughout the logarithmic layer and even into a portion of the wake region; they were attributed to the presence of Large-scaled motions, LSMs, with approximately 2-3δ length (Kovasznay *et al.*, 1970; Brown and Thomas, 1977 and Marlis *et al.*, 1982).

Meinhart and Adrian (1995) observed long growing zones of low streamwise momentum in the outer region, and particularly in the logarithmic region, using particle image velocimetry (PIV) methods. Zhou (1997) found that this uniform momentum could be the results of streamwise alignment of hairpin vortices, which were found to align

coherently in groups to form long packets and generate more hairpins as they propagate along wall.

Kim and Adrian (1999) found the same structure in the pipe flow and attributed these to the same hypothesis proposed by Zhou (1997). They also found the large structures to be 12−14 times of the pipe radius. Hutchins and Marusic (2007) found the same structure in the log-layer of the turbulent boundary layer and called it a "superstructure". They defined the motion as a "region of very long meandering positive and negative streamwise velocity fluctuations" and believed that these superstructures could be up to 20δ long, meandering along their length.

Monty *et al.* (2007) revealed that large-scale motions in pipe and channel flows were 25 times longer than pipe radius or channel half height. They observed two main differences between these very large-scale motions (VLSM) in channel flow and boundary layers. First, the VLSM persist for further distance from the wall in channels compared to turbulent boundary layers. Second, the width of the structure is at least 1.6 times smaller in boundary layers compared to channel or pipe flow.

Bailey *et al.* (2008) observed that the spanwise scale of VLSM in pipe flows is similar to that of channel flows but larger than in turbulent boundary layers. These motions were found to be independent of Reynolds number changes and surface roughness effects. They also showed that further away from the wall, outside the logarithmic region, the spanwise scale of the structures in pipe flows decreases faster in comparison with analogous scales in channel flows.

The structure of these VLSM/superstructures is described as very large elongated

regions of negative velocity fluctuations flanked by positive velocity fluctuations to each lateral side (Hoyas and Jiménez, 2006; Hutchins and Marusic, 2007; Marusic and Hutchins, 2008; Bailey *et al*, 2008; Marusic *et al.*, 2010). It has been consistently shown that the superstructures influence the near wall region flow and maintain a footprint on it.

Mathis *et al.* (2009a) found through Hilbert transformation of velocity data that the nature of this influence is to modulate the amplitude of small-scale fluctuations.

2.4. The comparison between three different kinds of canonical flow

Monty *et al.* (2009) compared measurements from the three different kinds of canonical flow at a matched Reynolds number of $Re_\tau \approx 3020$ and showed a very brief and clear view of these flows. The non-dimensional wire length, l^+, was also kept constant in the three experiments at $l^+ = 30$. Hot-wire sensor diameter was also adjusted to maintain near constant wire length-to-diameter ratios.

The results showed an excellent collapse in mean velocity profile of three kinds of flow up to $z < 0.15\delta$ and somewhat up to $z \approx 0.25\delta$. The variance of inner-scaled streamwise velocity fluctuations was also found to agree well up to $z < 0.25\delta$.

Tennekes and Lumley (1972) state that very close to the wall the effects of geometry between pipe and channel flows are negligible and the statistics show the same behavior. Monty *et al.* (2009) found good agreement between these two types of flow even in the core region despite the very different geometries. Pre-multiplied velocity spectra, $k_x \emptyset_{uu}$, where k_x is streamwise wavenumber and $\emptyset_{uu}$ is spectral density of streamwise velocity fluctuations, also confirmed a striking agreement between channel and pipe flow.

The inner-peak position of axial velocity fluctuations was consistently observed at $z^+ \approx 15$ and its magnitude was found to be equal for all three flows. Although the inner peak value in the boundary layer was slightly higher, it was found to agree with the other two flows within the expected error bounds and could therefore not necessarily be attributed to any differences in the peak value.

In spite of the fact that VLSM observed in internal flows and superstructures observed in external flows appear to have the same structure (Hutchins and Marusic, 2007 and Monty *et al.*, 2007), there are some differences between them that affects the flow even in the near-wall region. Monty *et al.* (2009) showed that in the logarithmic region, the largest scales of superstructures in boundary layers were smaller compared to the VLSM observed in channel/pipe flows. Beyond the logarithmic region, superstructures vanished rapidly in turbulent boundary layers; however, VLSM persisted for further distances from the wall. In addition, at further distances from the wall in internal flows, longer wavelengths carried the VLSM's energy.

Mathis *et al.* (2009b) used the same experimental approach to extend of their observations of amplitude modulation to pipe and channel flows. In spite of this difference in large-scale phenomena, they found good agreement in amplitude modulation in all three flows up to the edge of the logarithmic region ($z/\delta < 0.15$).

Chapter 3

EXPERIMENTAL FACILITIES, INSTRUMENTATION AND MEASUREMENT PROCEDURES

3.1. Turbulent Channel Flow Facility

3.1.1. General Layout

The wind tunnel used was designed and built as part of this research study. Design objectives were to: (1) produce a turbulent channel flow, which would experimentally reproduce idealized turbulent plane Poiseuille flow; and (2) maximize the Reynolds number for the existing laboratory space and flow source.

To reproduce turbulent plane Poiseuille flow, two constraints had to be met. First, to eliminate spanwise velocity gradients at the channel centerline, the test section of the wind tunnel had to have a large aspect ratio of width to height. Dean (1978) postulated that an aspect ratio of 7:1 is the minimum required to produce two-dimensional flow at the centerline. Second, to ensure that streamwise gradients of velocity and Reynolds stresses were eliminated such the turbulence was fully developed, the channel had to be sufficiently long. Monty (2005) measured mean velocity in a channel flow at multiple stations from $x/H = 72$ to $x/H = 205$, where H is the channel height and x is the streamwise distance along the channel. He found that the velocity spectra were dependent on streamwise location until at least $128H$. These two constraints therefore defined the geometry of the test section of the wind tunnel.

As the wind tunnel was to use an existing blower, the flow source, and hence maximum flow velocity, was fixed. Therefore, given also that no attempt was to be made to alter the viscosity of the air, maximizing the achievable Reynolds number, $Re_m = U_b H/\nu$, where U_b is the bulk (area averaged velocity) meant maximizing H in the existing laboratory space which was approximately 19 m long. Given that the existing blower and flow conditioning sections were already 2.5 m long, and that sufficient distance from the exit to the wall had to be provided at the channel exit to allow the flow to be free of any stagnation regions (approximately 1 m) this meant that the new sections required to produce the turbulent channel flow, including contraction, had to fit in a space approximately 15.5 m long. Assuming a contraction length of 2 m, and given the constraint that the channel had to be at least $128H$ long, it was therefore decided that a value of $H \approx 0.1$ m was the maximum channel height, which could provide fully developed channel flow within the existing laboratory space. To eliminate any effects of the wall on the centerline flow, an aspect ratio of 9:1 was selected, exceeding the minimum guideline of 7:1 provided by Dean (1978).

Based on these criteria, a new contraction and working section (consisting of development length, instrumentation section and exit section) was designed for the existing blower and flow conditioning sections. The final length of the facility was 17.9 m, with a 13.9 m long, 0.1016 m high and 0.9144 m wide working section. A diagram of the channel is provided in Figure 3.1, and a photograph of the facility is presented in Figure 3.2.

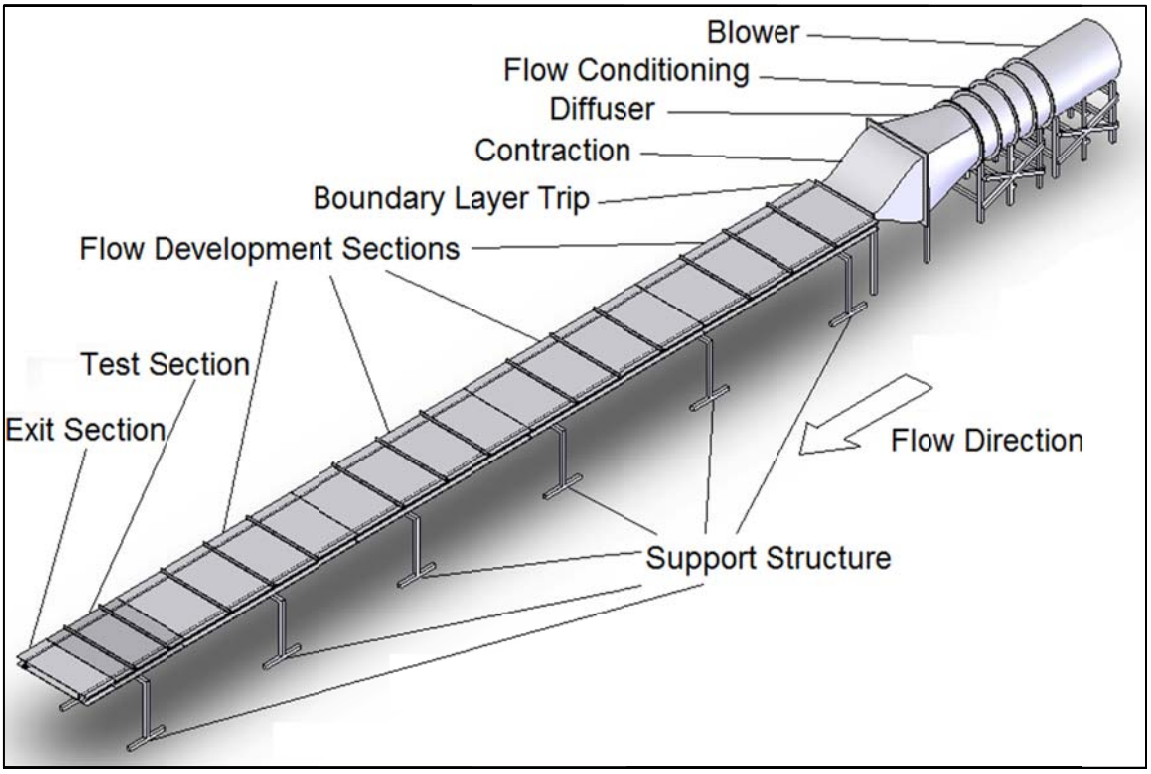

Figure 3.1: Schematic showing the separate sections of the turbulent channel flow facility

Figure 3.2: Photograph taken of the facility facing in the upstream direction. Note that the exit section has been removed.

The following sections are devoted to details of each part of the facility.

3.1.2. Blower and Flow Conditioning

Air was driven through the facility by a Peerless Electric Model 245 Centrifan in-line blower. The blower was 0.84 m in internal diameter and could provide 2.8 m^3/s when operating at 1445 RPM. The blower was powered by a Reliance 5.6 kW 3-phase motor controlled by a motor controller.

After leaving the fan, air entered a 1 m long, 0.84 m internal diameter settling chamber where the air passed through six fine-mesh screens to break up flow disturbances introduced by the blower produce an approximately steady, uniform flow at the exit of the settling chamber.

3.1.3. Diffuser

To pass the air from the existing circular cross-section blower and flow conditioning sections to the rectangular cross-section channel sections, and also to avoid having overly complex compound curves in the contraction, it was decided that a cross-section converter had to be manufactured.

The converter was manufactured by Bryant's Sheet Metal in Lexington Kentucky from welded 1.6 mm thick aluminum sheet and transformed from a 0.84 m diameter circular cross-section to a 0.91 m sided square cross section, thus creating a diffuser. To ensure that the flow did not separate inside the section, it was manufactured 0.91 m long,

resulting in a maximum sidewall angle of 13^{o} relative to the mean flow direction. Visualizations performed with strips of tissue paper attached to the sidewalls of the diffuser, once in place, showed no evidence of flow reversal or separation.

3.1.4. Contraction

After leaving the diffuser, the air enters the contraction. The design of contraction is one of the most important parts of a high-quality wind tunnel, as a well-designed contraction will produce a low-turbulence, uniform flow at the exit of the contraction, whereas a poorly designed contraction will introduce flow separation and unsteadiness. To simplify the contraction design, the width of the diffuser outlet was designed to be equal to the width of the working section. Hence, only a two-dimensional contraction was required to accelerate the flow into the working section of the channel.

The design used in this tunnel was based on recommendations provided by Monty (2005) who suggested using a cubic curve near the entrance followed by a parabolic curve towards the exit. Following these recommendations, the contraction was designed as shown in Figure 3.3 which the cubic and the parabolic curve met 0.76 m from the entrance of the contraction. The overall length of the contraction was 1.05 m and the contraction area ratio was 9:1, which is within the suggested ranges provided by Tavoularis (2005) and Barlow, Rae and Pope (1999).

The contraction was manufactured by Bryant's Sheet Metal in Lexington Kentucky from welded 1.6 mm thick aluminum sheet. At the exit, 44 mm aluminum angles were spot-welded to the outer walls of the contraction to provide flanges for connecting it to

following sections. However, this process introduced defects in the interior surface of the contraction, which could potentially introduce unwanted three-dimensionality and flow disturbances. Therefore, these defects were carefully removed by filing down raised protuberances as well as using automotive body filler to correct any indentations.

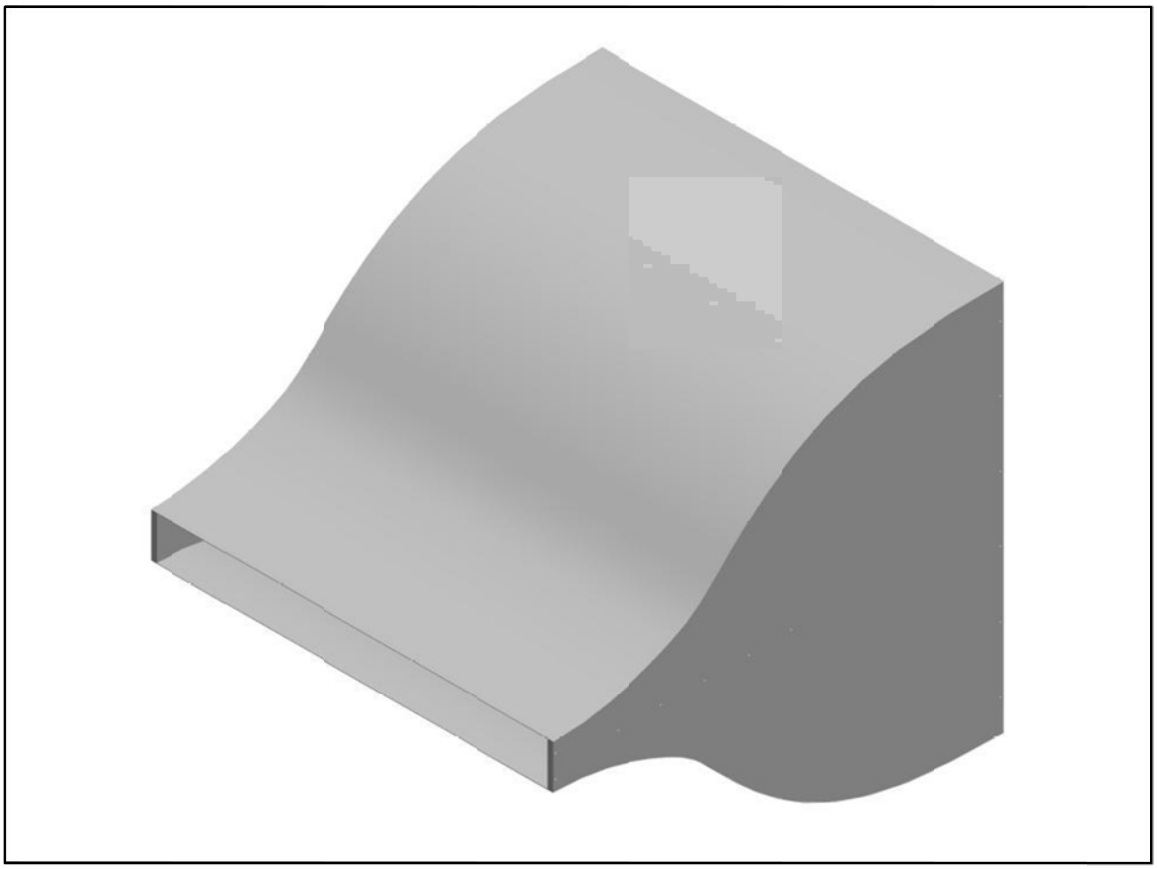

Figure 3.3: Isometric view of contraction of the channel. The diagram is not drawn to scale.

3.1.5. Working Section

The working section of the channel consists of multiple components: (1) a support structure; (2) a boundary layer trip section; (3) four flow development sections; (4) a test section, and (5) an exit section. The connection between each of the different sections

was sealed by silicone sealant to ensure constant mass flux throughout the entire length. Each section is described in further detail below.

3.1.5.1. Support Structure

Support and alignment for the working section, was provided by 7.62 m long, 0.15 m high aluminum I-beams. Four beams were used in pairs to provide support for the entire length of the working section. To prevent unwanted deflection of the working section elements on top of the beams, the beams were not aligned parallel with each other, but were instead positioned approximately 0.41 m apart at their upstream end and approximately 0.72 m apart at their downstream end.

These I-beams were in turn supported by six 1.2 m wide by 0.81 m tall supporting frames which were welded from 5 cm square steel tubing. Each frame was equipped with 4 leveling feet to allow adjustments to be made to the height of the working section over its length.

3.1.5.2. Boundary Layer Trip Section

To ensure an undisturbed transition from the contraction into the working section, a 0.3 m long section was manufactured, flanged and attached to the contraction exit. This short section allowed access to the internal connection between the two sections, which was filled with automotive body filler and sanded smooth to produce a disturbance-free connection.

The section was manufactured from 6.35 mm thick 6061 aluminum plates, which formed the upper and lower surfaces, and 0.3 m long 101.6 mm high aluminum C-channel were used as side-walls.

To ensure a regular laminar-turbulent transition point, a boundary layer trip was installed in this section. The trip, illustrated in Figure 3.4 consisted of a 50 mm wide section of 120 grit adhesive backed sandpaper and a 100 mm wide section of 60 grit adhesive backed sandpaper attached to the entire internal perimeter of the channel, 76 mm downstream from the contraction exit.

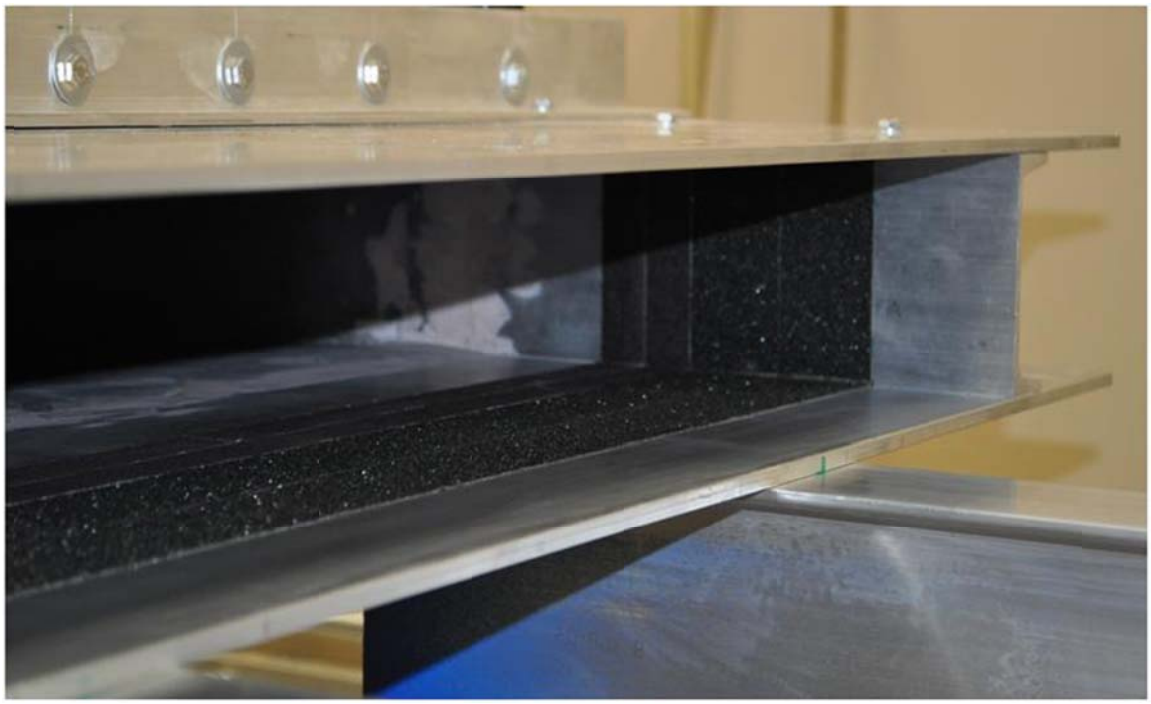

Figure 3.4: Photograph of boundary layer trip section, showing boundary layer trip and its placement.

This trip design is intended to introduce perturbations over a wavelength range of

0.11 to 150 mm and thereby improve the probability of initiating transition in the boundary layers formed along the walls.

3.1.5.3. Flow Development Sections

The flow development section of the channel consists of four separate 101.6 mm x 914.4 mm x 3.048 m long sections. The upper and lower surfaces of all four sections were made of 6.35 mm thick 3003 aluminum plate for the upper and lower surfaces with 101.6 mm high 6061 aluminum C-channel used to form the side walls.

Adjacent sections were connected 1.2 m long sections of aluminum C-channels with the same dimension as the sidewalls, inserted longitudinally between two sections. As well as maintaining a positive connection between each flow development section, these connections provided additional rigidity to the channel geometry.

To deter deflection of the upper surface of the channel, each section had three 50 mm x 50 mm 6061 aluminum angle mounted on the upper plate, which acted as stiffeners for the upper surface. Additional aluminum angle was positioned at the connection to ensure a smooth internal joint at the upper surface. Deflection of the lower surface was prevented by the aluminum I-beam support structure.

Each flow development section was equipped with 5 pressure taps located along the channel centerline, details of the taps are provided in Section 3.2.2.

A sketch of the cross-section of the working section is provided in Figure 3.5. Detailed engineering drawings are provided in Appendix A.

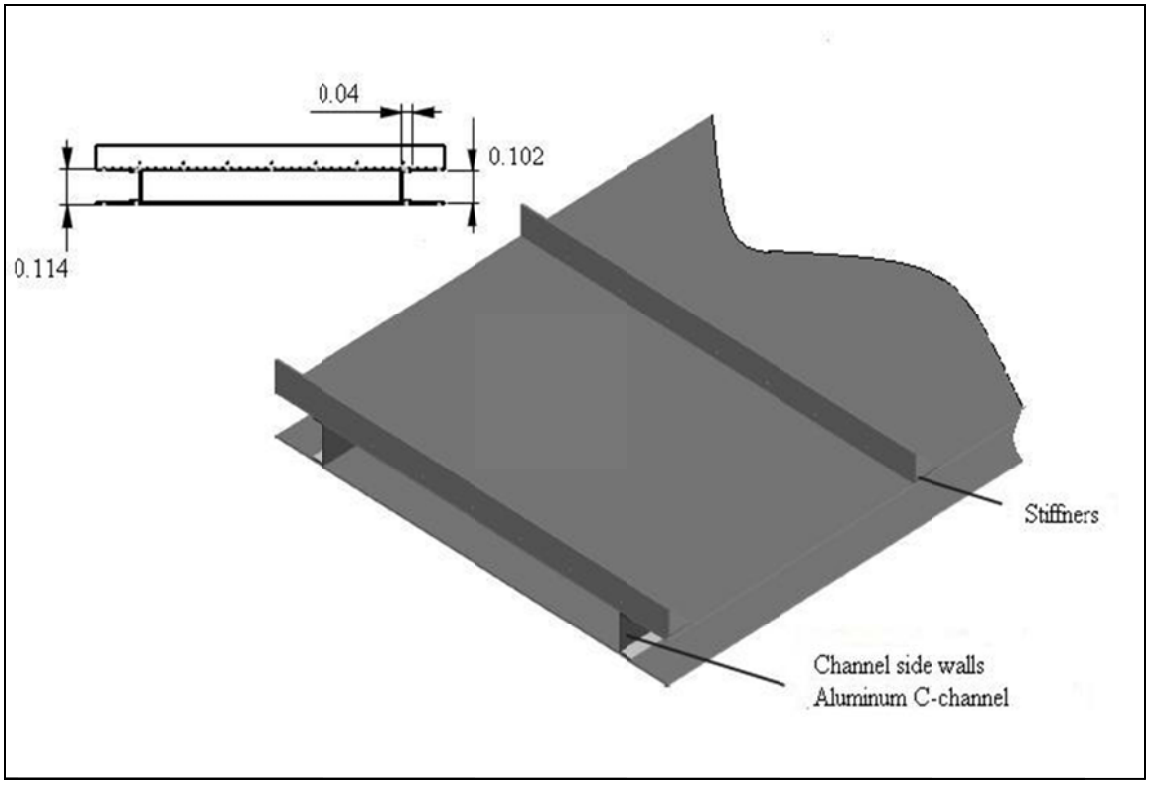

Figure 3.5: Isometric view of a Flow Development Section of the channel, illustrating the main features of its design. The diagram is not drawn to scale.

3.1.5.4. Test Section

The test section was designed to be a station where the primary measurements would be conducted. To allow measurements using optical techniques, such as particle image velocimetry and oil-film interferometry, the walls and upper surface of the test section were manufactured from optically clear, 12.7 mm thick, polycarbonate sheets. To ensure that the lower surface mated with the flow development section, it was manufactured from the same type of 6.35 mm thick 3003 aluminum plate. Two 50mm x 50mm 6061 aluminum angle stiffeners were mounted to the upper surface of the channel to prevent deflection of the upper surface.

To allow instrumentation access to the test section a 0.15 m diameter hole was located at the center of the lower surface, in which an insert containing test instrumentation could be placed. To allow measurement of the streamwise pressure gradient in the test section, and to verify flow two-dimensionality within the section, 21 pressure taps in three rows were located in the upper surface of the test section with 11 taps in the row along the channel centerline and 6 taps located in each row a spanwise distance of 203.2 mm to either side. Further details of the pressure taps are provided in Section 3.2.2.

Detailed engineering drawings of the test section are provided in Appendix A.

3.1.5.5. Exit Section

Preliminary testing revealed that exit conditions were introducing non-linearity and non-uniformity into the pressure gradient within the test section. To eliminate these effects, an additional 0.51 m long section was added after the test section. The upper and lower surfaces were manufactured from 6.35 mm thick 6061 aluminum plate, with 101.6 mm high 6061 aluminum C-channel used to form the side walls.

3.2. Instrumentation

Three types of experiments were conducted over the course of this study: (1) measurement of the velocity at the outlet of the contraction with a Pitot-static tube; (2) measurement of the streamwise pressure gradient; and (3) measurement of the wall-normal profiles of velocity using hot-wire probes. Each experiment required a

different experimental arrangement, as illustrated in Figures 3.6 to 3.8 which show connection diagrams between the instrumentation used for each of the experiments.

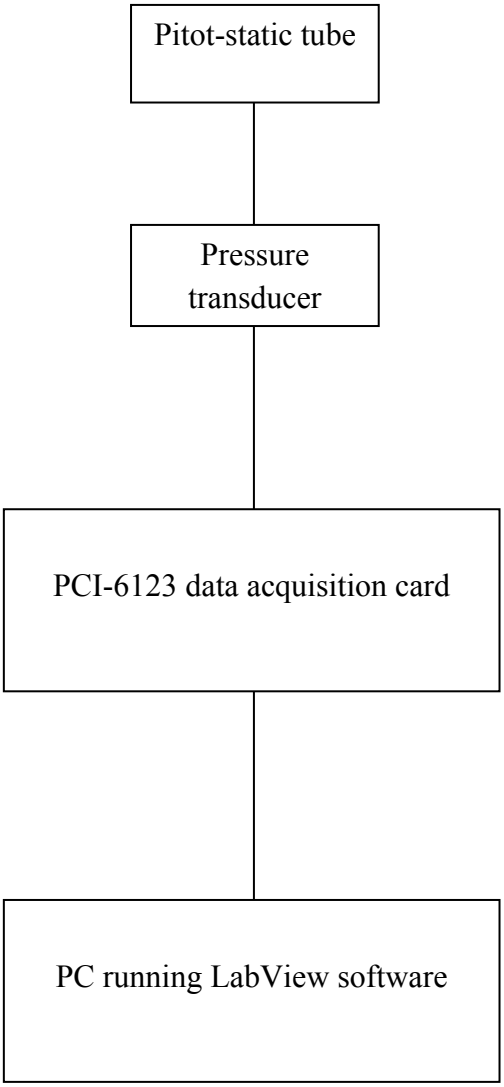

Figure 3.6: Diagram illustrating the connections of the instrumentation used for measurement of the velocity at the outlet of the contraction.

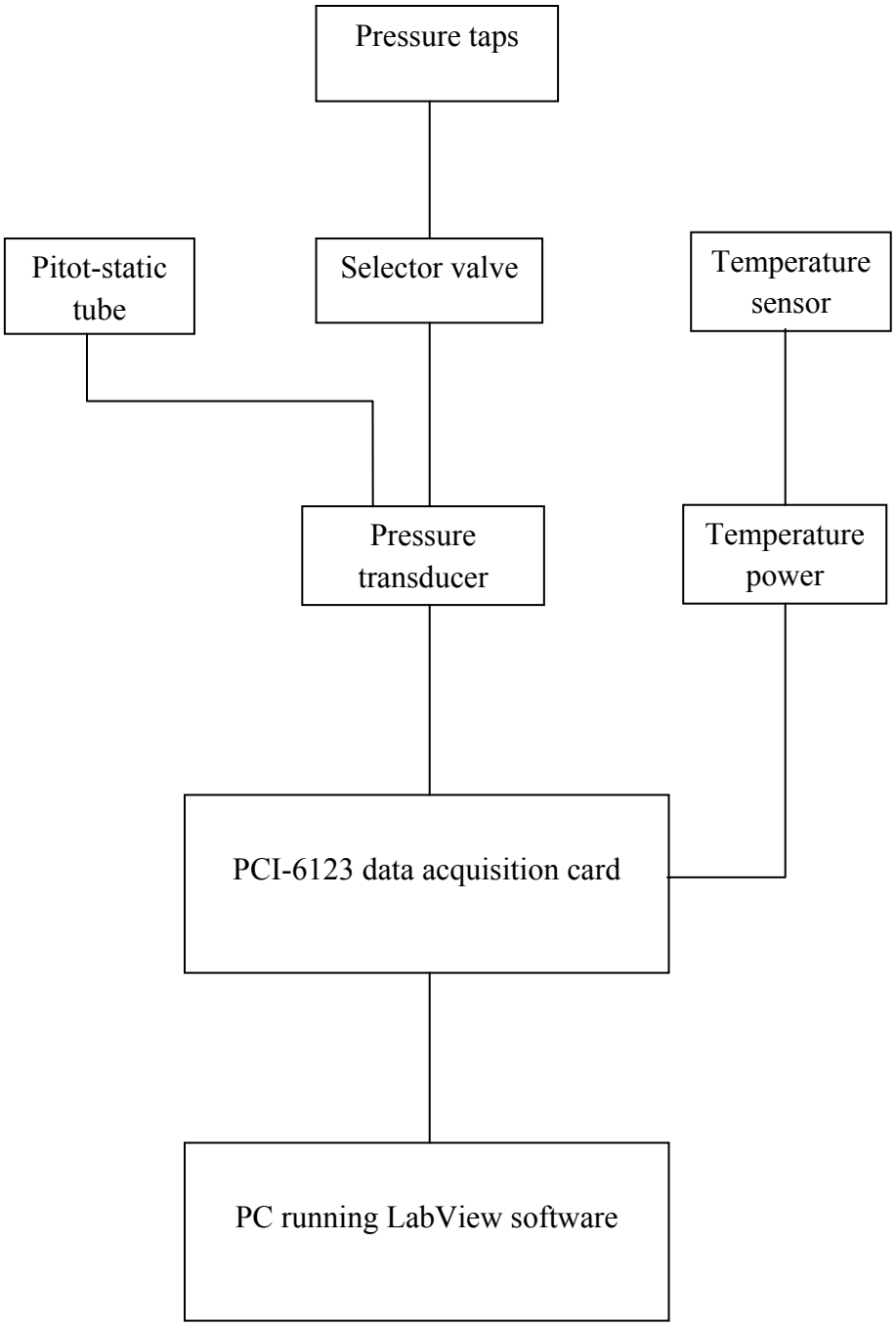

Figure 3.7: Diagram illustrating the connections of the instrumentation used for measurement of the streamwise pressure gradient.

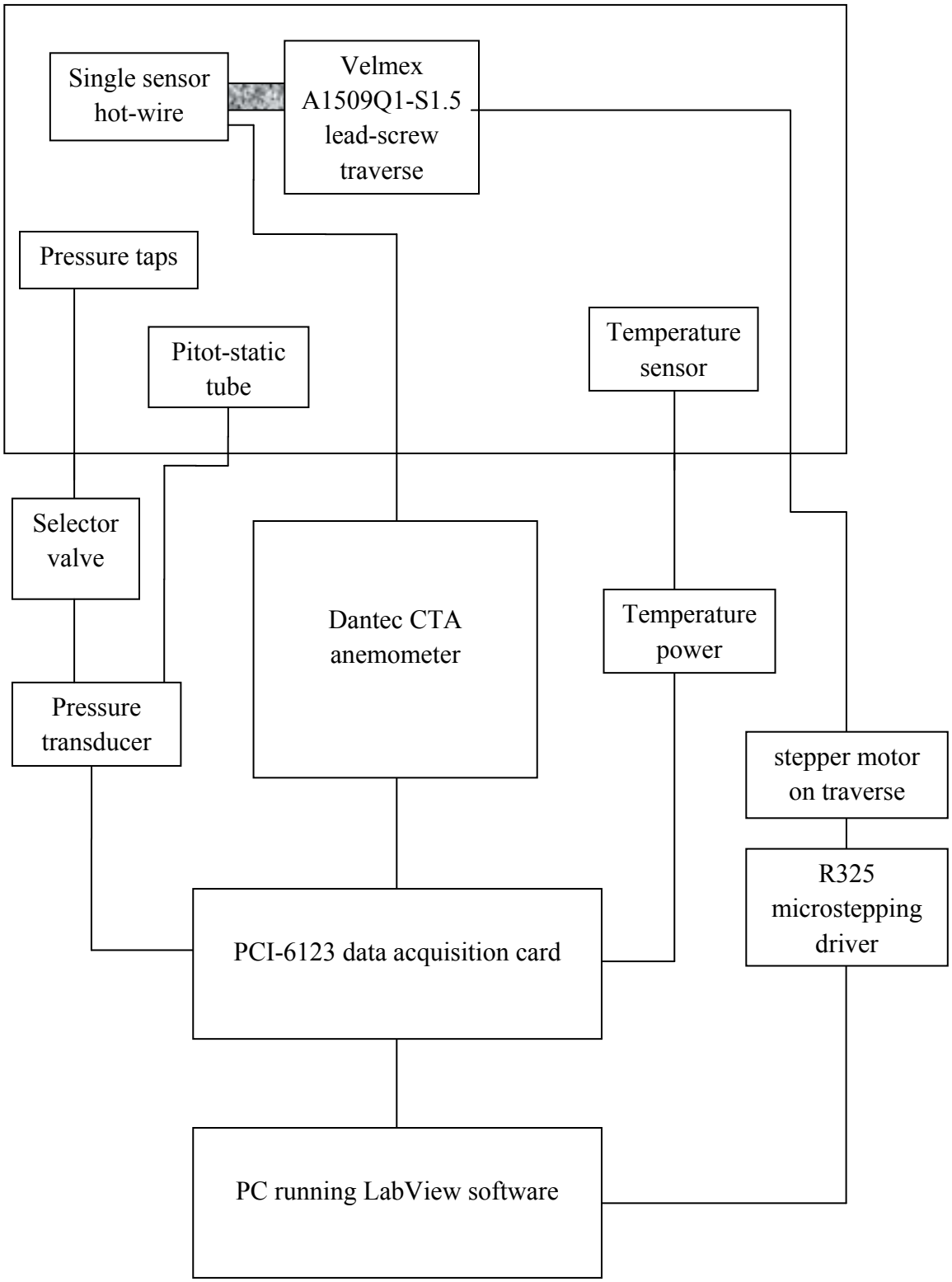

Figure 3.8: Diagram illustrating the connections of the instrumentation used for measurement of the wall-normal profiles of velocity.

3.2.1. Pitot-Static Tubes

Two different Pitot-static tubes were used over the course of this study, a Dwyer model 166-6 and a model 167-6. Both tubes were 3.2 mm in diameter and had a 0.15 mm insertion length. For the measurement of the velocity at the outlet of the contraction and during streamwise pressure gradient measurement, the model 166-6 was used, which had a 76.2 mm long streamwise-aligned element. For calibration of the hot-wires in the hot-wire probe measurements, the model 167-6 was used, which had a 50.8 mm long streamwise-aligned element.

3.2.2. Pressure Taps

For measurement of the streamwise pressure gradient, the entire length of the channel was equipped with wall-mounted pressure taps in the upper surface. In the flow development sections, 5 taps were located along the centerline of each of the 4 sections, spaced 0.61 m apart in the streamwise direction, for a total of 20 taps. Twenty-three pressure taps were inserted in the test section, 11 at the centerline spaced 101.6 mm apart and, to ensure two-dimensionality, two additional rows of six, spaced 406.4 mm apart, were located a spanwise distance of 203.2 mm to each side of the centerline row.

In the flow development sections, the pressure taps had a diameter of 1.3 mm for a depth of 3.2 mm. These holes were mated to threaded barbed fittings mounted on the exterior of the channel with matching internal diameter of 1.3 mm and 14.2 mm length and producing a total length to diameter ratio of 13. A similar arrangement was used for

the test section pressure taps, except the hole depth was 9.5 mm, due to the thicker material used in that section.

To minimize error caused by flow disturbances introduced by manufacturing defects, at the interface between the pressure tap hole and the internal surface of the channel, each tap was drilled inwards from the interior surface of the channel (minimizing burrs and lips) and were carefully sanded after machining. Note that the nature of the polycarbonate material meant that more manufacturing defects (in the form of chipping) were present in these taps which could not be completely eliminated by manual finishing of the surface.

Pressure taps were connected to a manually operated selector valve, manufactured by Aerolab L.L.C., by 1.5 mm internal diameter PVC tubing. The valve had 24 input ports and one output part, allowing selection between the pressure taps for connection to the pressure transducer. Pressure taps, which were not connected to the valve during a particular measurement run were sealed to prevent pressure gradient driven mass flux out of the tubing, which could disturb the flow through the channel. To allow the Pitot-static tube to be operated using the same transducer as the pressure taps, the total pressure line of the Pitot-static tube could also be connected to an input port on the valve.

3.2.3. Pressure Transducer

Pressure data were acquired using an NIST calibrated Omega PX653-03D5V differential pressure transducer with 0-746.5 Pa range. To simplify zeroing of the transducer, two-way valves were used to select between the input pressure lines or a separate line which connected the two input ports directly.

3.2.4. Temperature Probe

Temperature within the channel was monitored using an Omega THX-400-AP thermistor probe. The probe was powered by an Omega DP25-TH-A, which provided a digital display and linearized analog voltage output. This system had an accuracy of $\pm 0.2^{o}$C.

For the pressure gradient measurements, the sensing element of the probe was located at the channel mid-point, at the exit of the channel, 0.1 m from the channel centerline. For the hot-wire measurements, the probe was located 0.61 m from the inlet of the test section, at the channel mid-point, 0.05 m from the channel centerline.

3.2.5. Hot-Wire Probes

The single normal hot-wire probes used were constructed by soldering Wollaston wire onto Auspex boundary layer type hot-wire prongs. The Wollaston wire was then etched using 15% nitric acid to expose the 2.5 mm diameter 90% platinum-10% rhodium core. By using a micro-positioner to maneuver the wire inside a small bubble of acid formed as acid flowed through the tip of a syringe, the probes could be built to specific sensing lengths, l. Sensing lengths ranged from 0.5 mm to 1.63 mm, corresponding to l/d between 200 and 625, where d is the wire diameter. The l/d ratio has classically been used to quantify end conduction effects, and the Ligrani and Bradshaw (1987) criterion for $l/d > 200$ has been adhered to in this experiment. Hultmark *et al.* (2011) have suggested a new criterion for end conduction effects in hot wires that takes into account the effect of wire thermal conductivity, Reynolds number and operating overheat ratio in

addition to the length to diameter ratio. Their criterion, where it is required that $(l/d)(4Nu\gamma K_f/K_w)^{0.5} > 14$, is also satisfied in the current investigation. Therefore, the data are assumed to be free of end conduction effects. Here, γ is the resistance ratio, K_f the thermal conductivity of the fluid, K_w the thermal conductivity of the wire material and Nu the Nusselt number.

3.2.6. Hot-Wire Anemometer

The hot-wire anemometer used in this study was a Dantec Streamline research Constant Temperature Anemometer (CTA) system. The system was equipped with two channels and is capable of operating in both a 1:20 bridge mode in which internal resistors are used for bridge balancing, and a 1:1 bridge mode in which an external resistor provides balancing to the system. The anemometer also provided output signal conditioning in the form of user selectable output gains and offsets, as well as high and low-pass filtering. The system was controlled by custom-designed software through serial communications.

3.2.7. Probe Positioning

To position the hot-wire probe at precisely controlled positions a custom-built traversing system was used. This system was comprised of several components. Linear motion was provided by a Velmex A1509Q1-S1.5 lead-screw traverse with a 1 mm per rotation pitch. The lead screw was driven by a Lin Engineering 417/15/03 high accuracy stepper motor through a timing belt with a 2:1 increase in pulley diameter. The stepper

motor was controlled using a Lin Engineering R325 microstepping driver. This combination provided a potential positioning resolution of 5 nm per step. As positioning accuracy can be much greater than the resolution when using micro-stepper motor control, an Acu-Rite SENC50 E 5/M DD9 0.5 A156 quadrature linear encoder was mounted on the traverse to provide position feedback information. This encoder had 500 nm resolution and accuracy of ±3 μm. To allow the encoder quadrature signal to be read by the data acquisition system, the signal was first fed through a USDigital LS7184 quadrature clock converter microchip. The quadrature signal was then combined into a single clock pulse signal with a companion TTL direction signal.

The probe position could therefore be determined with high relative accuracy between measurement points. However, as detailed by Orlu *et al.* (2010), knowing the position of the probe relative to the wall is equally important when measuring turbulent wall-bounded flow. Since the hot-wire probe could not contact the wall, as it would be destroyed, an electrical contact limit switch was designed into the positioning apparatus. The switch was designed to output a 5 V signal, which would become grounded once a bar on the moving portion of the lead screw drive contacted a micrometer mounted on the fixed portion of the lead screw drive. Therefore, by carefully adjusting the micrometer while monitoring the probe position using a Titan Tool Supply Z-axis ZDM-1 measuring microscope, the limit switch could be set to trigger at a specific wall-normal position with an accuracy of ±5 μm.

3.2.8. Data Acquisition

Analog voltage signals were digitized using a National Instruments PCI-6123 data acquisition card mounted in a desktop PC. This acquisition card could sample up to 8 analog channels at 500kHz and 16-bit resolution, with each channel simultaneously sampled for zero time-shift between channels. In addition to the analog voltage inputs, the acquisition card had 8 digital input/output lines and two 24-bit counter-timers which were used for experiment control. Inputs and outputs to the acquisition card were passed through a National Instruments BNC-2110 connector block.

3.2.9. Experiment Control

The control center of the experiment was a computer in which the acquisition system was installed. Acquisition and experiment control were provided by custom-written Labview software. For contraction outlet and pressure gradient measurements, the software simply controlled digitization rates of the analog inputs and wrote the results to ASCII text. For the hot-wire measurements, the required software was more complex and completely automated the experiment. It would read in the desired probe position from an input file. Then, it would move the hot-wire probe to the desired position by outputting a square wave control input to the traverse stepper motor controller while monitoring the limit switch connected to a digital input line to ensure that the probe will not accidentally contact the wall. Simultaneously, the software had to count pulse and direction signals outputted from the LS7184 chip to recover the position feedback data from the linear encoder. Once the probe was in position, it would sample the analog inputs at the desired

rate and sample lengths. After acquisition was complete, the software would record the results to a binary data file and then proceed to move the probe to the next position.

3.3. Measurement Procedures and Conditions

3.3.1. Contraction Outlet Measurements

To validate the current contraction, the streamwise velocity was measured at the outlet of the contraction and boundary layer trip section before installation of the boundary layer trip and channel flow sections.

Wall-normal velocity profiles were measured using a model 166-6 Pitot tube at seven spanwise locations, y with a centerline velocity of U_{CL} = 27 m/s. Data were acquired using an Omega PX653-03D5V differential pressure transducer. To digitize analog voltage signals a National Instruments PCI-6123 data acquisition card was mounted in a desktop PC. (See more details about these instruments in Sections 3.2.3 and 3.2.8 above.) A manual lead screw traverse was implemented to change the vertical position of the Pitot tube with 0.127 mm positioning resolution.

In all pressure measurements, it is necessary to allow pressure in the pressure tubing reach steady state. The sufficient time before each measurement was found to be 15 seconds. In addition, to decrease the error due to data acquisition in transition time, sufficiently long averaging time should be employed, which was 45 seconds in present research.

3.3.2. Pressure Gradient Measurements

For measurement of the streamwise pressure gradient, twenty-four wall-mounted pressure taps in the upper surface of channel were used. Exit pressure was measured using a model 166-6 Pitot tube at the channel mid-point, at the exit of the channel. An Omega PX653-03D5V differential pressure transducer acquired data. To digitize analog voltage signals a National Instruments PCI-6123 data acquisition card was mounted in a desktop PC. (See more details about these instruments in Sections 3.2.3 and 3.2.8 above.)

The waiting time before each measurement was 15 seconds, and the data acquisition time was 45 seconds.

To investigate the two dimensionality of the channel, the pressure gradient was measured using nineteen pressure taps arranged in three spanwise rows located in the upper surface of the test section (see Sections 3.1.3.4 and 3.2.2 for more information about the pressure tap configuration) at three centerline velocities, 9.7 m/s, 19.6 m/s and 32.4z m/s.

3.3.3. Hot-wire Measurements of Streamwise Velocity Profiles

During the course of this research, streamwise velocity measurements were performed along profiles taken in the wall-normal direction. Profiles were measured using single normal hot-wire probes in the range of Reynolds numbers $\mathrm{Re}_\tau = 634 - 2115$ ($Re_m = 2U_b h/\nu = 25{,}970 - 95{,}920$, where U_b is the area-averaged, or 'bulk', velocity). Six cases were tested, which can be categorized into two divisions: in the first group, which consisted of four cases, the length of the sensing length of the hot-wire

probes, l, was kept constant and equal to 0.5 mm. In the second group, consisting of three cases, the viscous-scale wire length, l^+, was kept constant and equal to 20. The distance of the sensor from the wall, z_0, was measured using a depth-measuring microscope (see Section 3.2.7 for more details). The data were taken in 42 positions between z_0 and z = 60.78 mm + z_0 with high concentration on the near wall region. For all cases, the probe was located 0.61 m from the inlet of the test section and 126H downstream from the turbulence trip, at the channel centerline.

Single sensor normal hot-wire probes with 2.5 mm wire diameter and $0.5 - 1.63$ mm sensor length were employed; these were always aligned parallel to the wall and perpendicular to the flow stream (see Section 3.2.5 for more details). The resistance of the prongs/leads was 1.4 Ω. In all hot-wire selections, the Ligrani & Bradshaw (1987b) limitations were always considered, which means for all cases the viscous-scaled wire length, l^+, was equal to or, smaller than, 20; and the length-to-diameter ratio, l/d, was equal to or greater than 200. The Dantec anemometer was always set in the 1:1 bridge mode using an external resistor for bridge balancing (see Section 3.2.6 for more details about anemometer). All sensors were operated at an overheat ratio of 1.67, and output signal gain and offset values were set to maximize resolution of the analog-to-digital conversion. The probe frequency response of the sensors was determined to be at least 50 kHz, and the analogue signals were low-passed filtered at 30 kHz before sampling at 60 kHz.

Experimental conditions are presented in Table 3.1 for all the cases.

Table 3.1: Experiment conditions.

Case	Re_m	Motor Frequency (Hz)	Re_τ	U_b (m/s)	l^+	z_0 (μm)	Gain	Offset
1	25,970	10	619	3.88	5.64267	95	64	1.16
2	42,081	15.5	969	6.28	8.832	95	64	1.19
3	65,273	23	1,457	9.72	13.2787	95	32	1.21
4	95,921	33	2,113	14.35	19.2587	95	32	1.25
5	42,081	15.5	969	6.28	21.12	115	32	1.72
6	25,970	10	619	3.88	20.24	90	32	2.33

To ensure convergence of measured statistics, the data acquisition times were determined carefully and individually for each case based on the channel velocity, with each wall-normal position sampled. To stabilize the channel before taking data, a waiting time was considered for each hot-wire position from the wall. All the related times are presented in Table 3.2.

Hot-wire probes were allowed to anneal at operating temperatures for at least 12 hours after etching and before starting their use.

Table 3.2: Time schedule table for each case

Case	Re_m	Data taking duration (s)	Waiting time (s)
1	25,970	240	75
2	42,081	240	75
3	65,273	180	15
4	95,921	120	15
5	42,081	240	75
6	25,970	240	75

The hot-wire probes were calibrated at the beginning and end of each experiment case; the model 167-6 Pitot-static tube was used for this (see Section 3.2.1 for more detail about the Pitot-static tube). All calibrations were done on the centerline of the channel, where the velocity was maximum. The Pitot-static tube was fixed at the centerline, and the hot-wire probe was moved to this spot using the traverse mechanism (see Section 3.2.7 for more details).

In all the cases, the before and after calibration curves were checked against one another to ensure that there was no calibration drift during the measurement run. A sample set of calibration curves for case 3 is presented in Figure 3.9 showing excellent agreement between the two calibration curves.

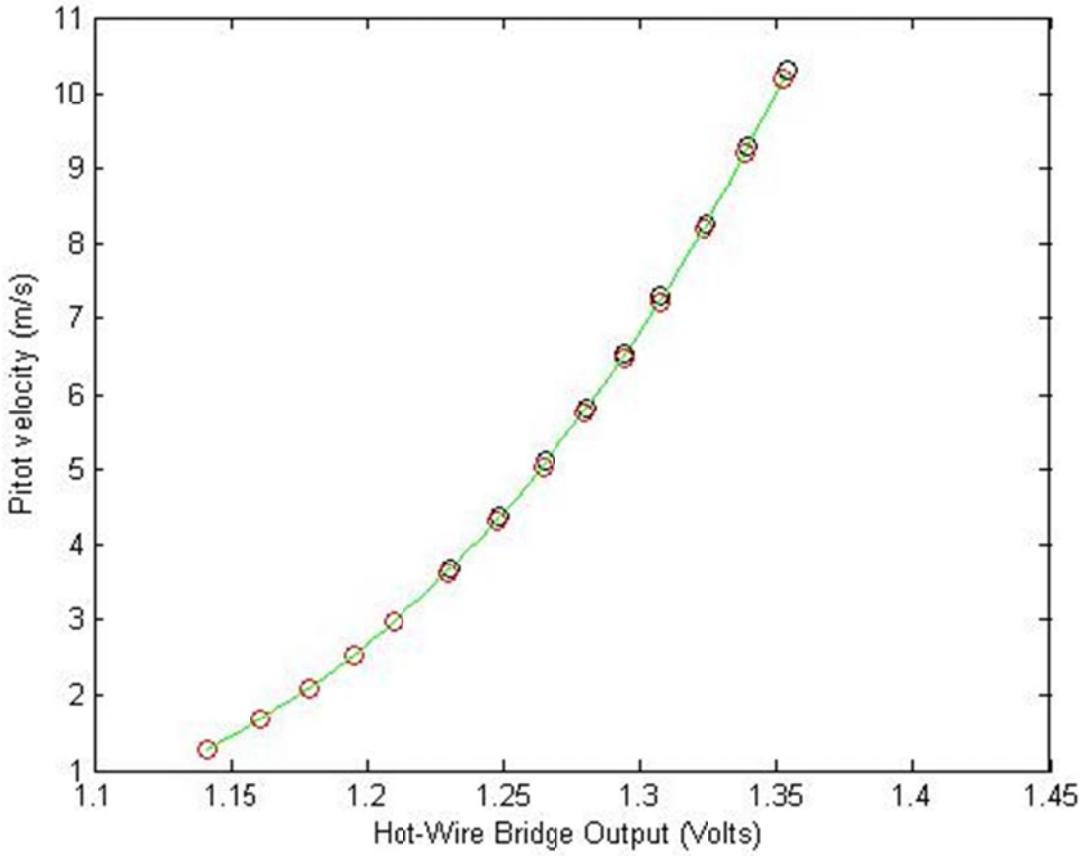

Figure 3.9: Sample calibration curve, related to case 3, Black circles, calibration data before profile measurement and Red circles, calibration data after measurement.

Chapter 4

CHANNEL FLOW VALIDATION AND CHARACTERIZATION

4.1 Turbulent Channel Flow Validation

To guarantee the accuracy and reliability of its results, any laboratory facility must be tested before starting any experiments, and the current channel flow facility is not an exception. Two crucial properties that a channel flow facility must have are: 1) two-dimensionality, and 2) fully-developed flow in the streamwise direction. In addition, the flow produced by the facility should also be characterized to understand the capabilities of the facility. In this chapter, we present results from tests performed to validate and characterize the flow through the channel.

4.1.1. Two-Dimensionality at Contraction Exit

A good contraction design must provide almost uniform flow at the exit. To validate the current contraction, the streamwise velocity was measured at the outlet of the contraction and boundary layer trip section before installation of the sandpaper trip or the downstream channel sections. Wall-normal velocity profiles were measured using a Pitot-static tube at seven y locations with a centerline velocity U_{CL} = 27 m/s. The results are presented in Figure 4.1 and show an almost uniform velocity over 92% of entire height of the contraction exit with virtually identical profiles at all seven locations.

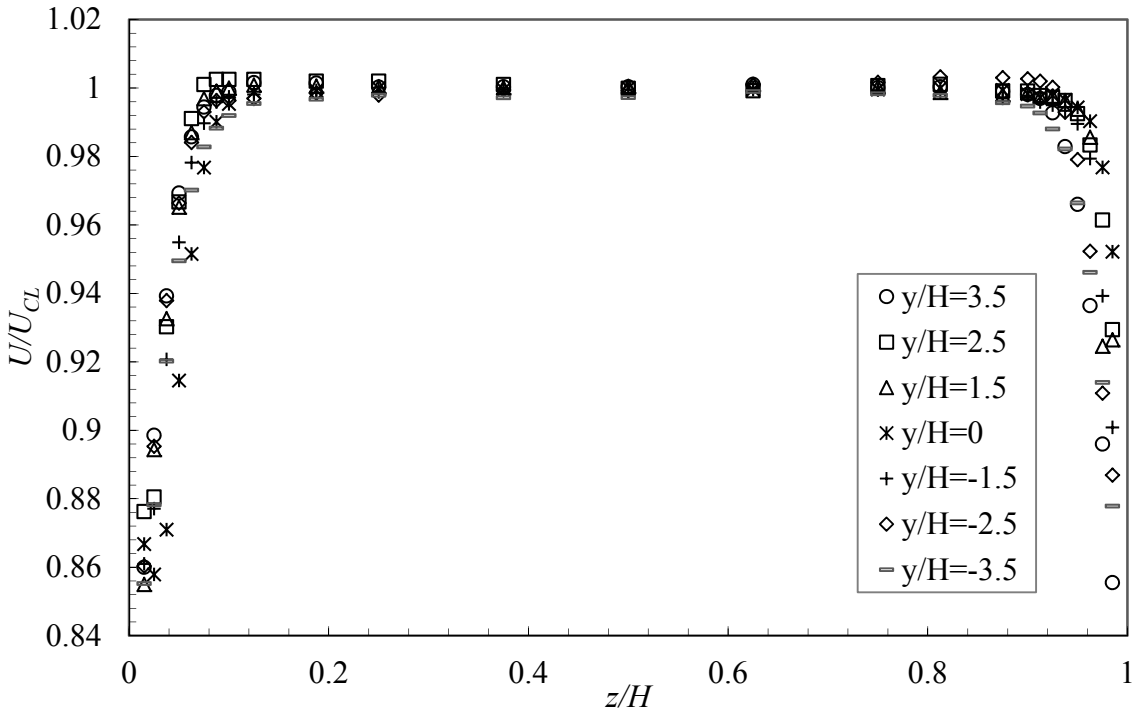

Figure 4.1: Exit velocity at outlet of contraction.

4.1.2. Two-Dimensionality in Test Section

To investigate two-dimensionality of the channel, the pressure gradient was measured using nineteen pressure taps arranged in three spanwise rows located in the upper surface of the test section (see Sections 3.1.3.4 and 3.2.2 for more information about the pressure tap configuration).

Results of the test for three centerline velocities, 9.7 m/s, 19.6 m/s and 32.4 m/s, are presented in Figure 4.2. Pressure measured from all the rows of pressure taps are in agreement indicating two-dimensionality of the flow in the range ±203.2 mm from the channel centerline. Small deviation from a linear trend in a few pressure taps can be attributed to surface roughness around them; effect of these is more obvious in highest

centerline velocity.

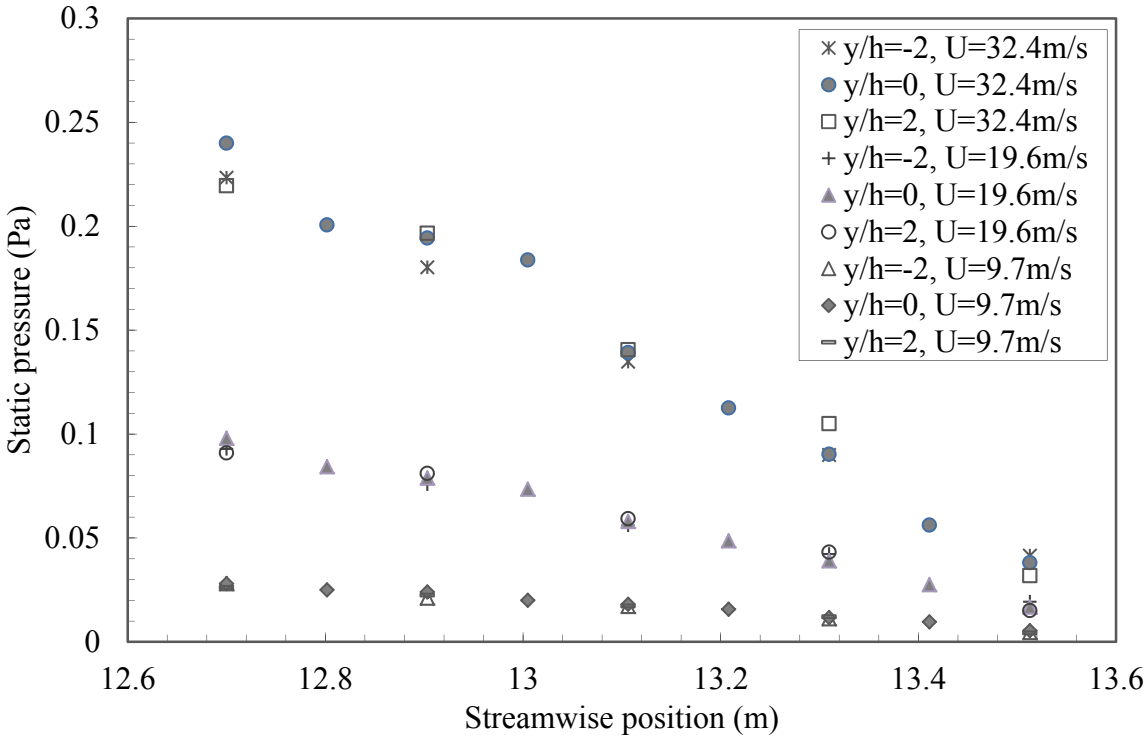

Figure 4.2: Surface pressure in the test section at three spanwise positions measured at three centerline velocities.

4.1.3. Blower Output Characterization

To characterize the relationship between motor controller frequency and velocity through the channel, the centerline velocity was measured using a Pitot-static tube while the motor controller was swept through its entire range of frequencies. The results, shown in Figure 4.3, indicate a linear dependence of the centerline velocity on the controller frequency with a maximum velocity of 33 m/s. The trend guarantees perfect uniform performance of motor controller.

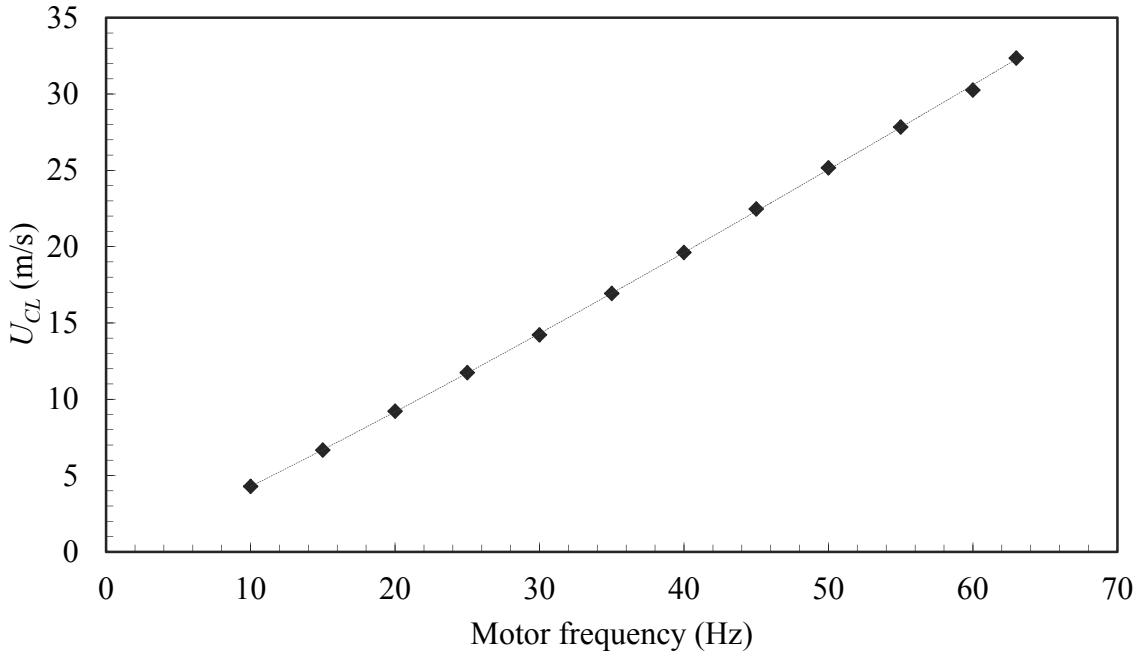

Figure 4.3: Centerline velocity as a function of motor controller frequency.

4.1.4. Surface Roughness Characterization

To ensure that the flow remained hydraulically smooth, and free of roughness effects, a piece of the aluminum material used for the test section floor was tested by stylus surface profilometry. The test was performed by scanning in two directions, along and across the grain of the aluminum for 60,000 locations in each direction. Along the grain of the aluminum, the standard deviation of the surface roughness height was found to be 267.6 nm, while the maximum and minimum roughness were 1245.5 and -725 nm respectively. For cross-grain direction, the results indicated a 334 nm standard deviation in roughness height, with a 425.3 nm maximum and -1816 nm minimum. The results confirm that the standard deviation of the surface roughness is less than 4% of the minimum viscous length expected in the channel (≈ 12μm), which confirms that surface

roughness effects can be expected to be negligible.

4.2. Characterization of Wall Shear Stress, τ_w

Wall shear stress, τ_w, is produced by the viscous forces exerted on the wall by the fluid flow. For Newtonian fluids, it is directly related to velocity derivative normal to the wall direction at $z = 0$, or

$$\tau_w = \mu \frac{\partial U}{\partial z} \Big|_{z=0}, \tag{4.1}$$

where μ is fluid dynamic viscosity. In laminar flows, it is possible to use Equation 4.1 to find τ_w due to gradual velocity change in the entire profile; however, this is not the case for turbulent flow due to the dramatic change in velocity in the near wall region. On the other hand, the scaling of turbulent wall bounded flows is driven by the wall shear stress (see Chapter 2), and therefore it must be determined in order to scale the measurement results and allow comparison between facilities.

Due to the crucial role of wall shear stress in wall-bounded turbulence, various methods to determine it have been proposed, including using measured velocity profiles, pressure differences, thermal techniques, electrochemical methods, optical techniques or liquid-crystal techniques (Tavoularis, 2005).

One of the most straightforward methods is measuring the wall shear stress based on pressure gradient, $\frac{dp}{dx}$. A simple momentum balance in channel flows relates these two quantities (Pope, 2000)

$$\tau_w = \varepsilon_T \frac{H}{2} \left(\frac{dp}{dx}\right) ; \quad (4.2)$$

where H is channel height, and ε_T is three-dimensionality factor which is equal to unity for flow between two infinite parallel plates. The area close to the center in channels with sufficiently high aspect ratio (7:1 and higher) can be assumed idealized turbulent plane Poiseuille flow having $\varepsilon_T = 1$ near the centerline (Monty, 2005). Zanoun *et al.* (2009) compared wall shear stress results determined from pressure gradient measurements to those determined using direct measurements by oil film interferometry and found agreement in results from these techniques.

Although only two pressure measurement points at a known streamwise separation would theoretically be enough to measure the pressure gradient in a channel flow, to reduce the impact of uncertainty in pressure and distance measurement on the measured pressure gradient, the gradient was determined from the pressure measured with twenty-four pressure taps over a 12.3 m length of the channel.

Note that Equation 4.2 is valid only when fully-developed conditions exist in channel or pipe flow which, according to Zanoun *et al.* (2009), occurs 30H downstream from the facility entrance. In this research, because of the large number of pressure taps, and for testing the flow situation in an earlier length of channel facility, the first pressure tap was selected at 30H and the last one at 126H from the turbulent trip. To diminish the effects of the channel exit on measurements, the last pressure tap was located at 14.25H from the end of the channel. The results of pressure measurements along the channel for the possible range of Reynolds numbers produced by the channel facility are presented in Figure 4.4.

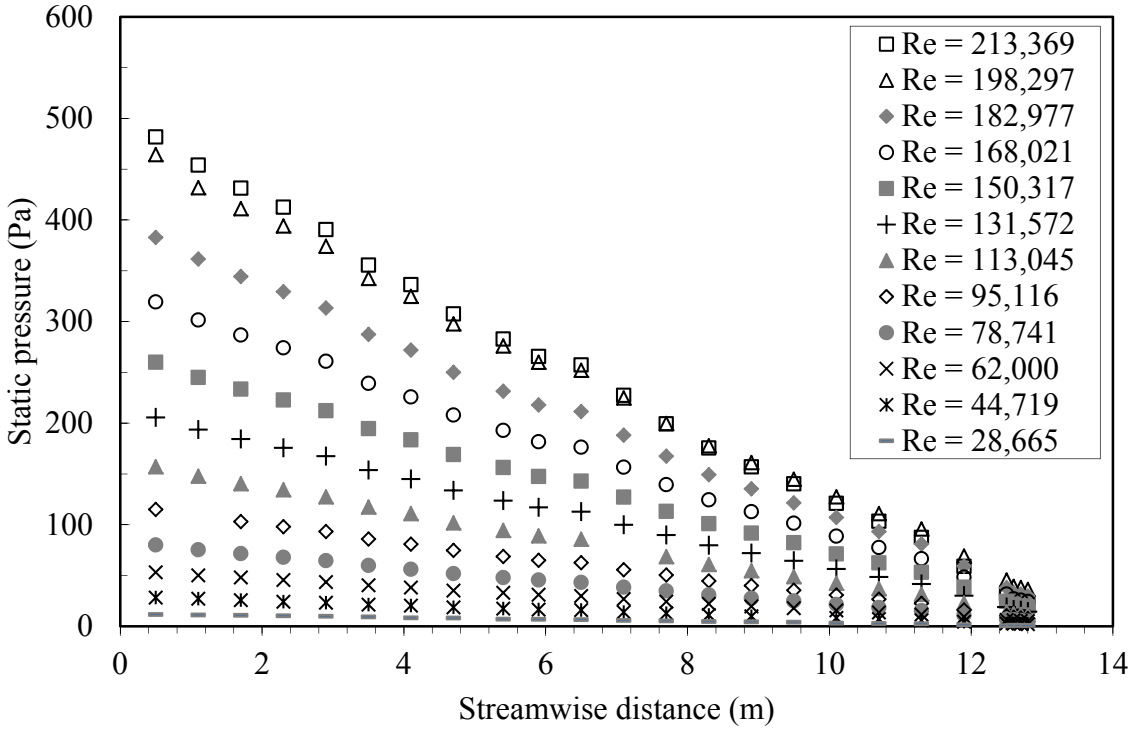

Figure 4.4: Streamwise pressure distributions for different Reynolds number based on centerline velocity and channel height.

The linearity of the results allows estimation of the pressure gradient through linear regression and determination of the corresponding wall shear stress from Equation 4.2. Small deviation from a linear trend in a few pressure taps can be attributed to surface roughness around them; effect of these is more obvious in higher velocities.

After finding wall shear stress, friction velocity and Karman number were calculated for the possible range of flow velocity in the channel and are presented in Figure 4.5a and 4.5b, respectively, as a function of U_{CL}. The results show a reasonable increasing trend with increasing channel velocity for both properties. The trends are almost linear, following $u_\tau = 0.052\ U_{CL}^{0.92}$ and $Re_\tau = 177.47\ U_{CL}^{0.91}$. (The formulas are presented in each Figure.) In addition, the dependence of the viscous length scale, δ_v on centerline

velocity is shown in Figure 4.5c. The expected inverse relation between these two parameters is clear in the plot, with a minimum expected viscous length of 10 μm. The trend can easily be explained through closer examination of Figure 4.5b. The friction Reynolds number, which describes the ratio of outer to inner length scales, logically increases with channel centerline velocity. Since in a channel flow the outer scale is h, which is a constant geometric property, increasing the friction Reynolds number implies a decrease of the inner length scale.

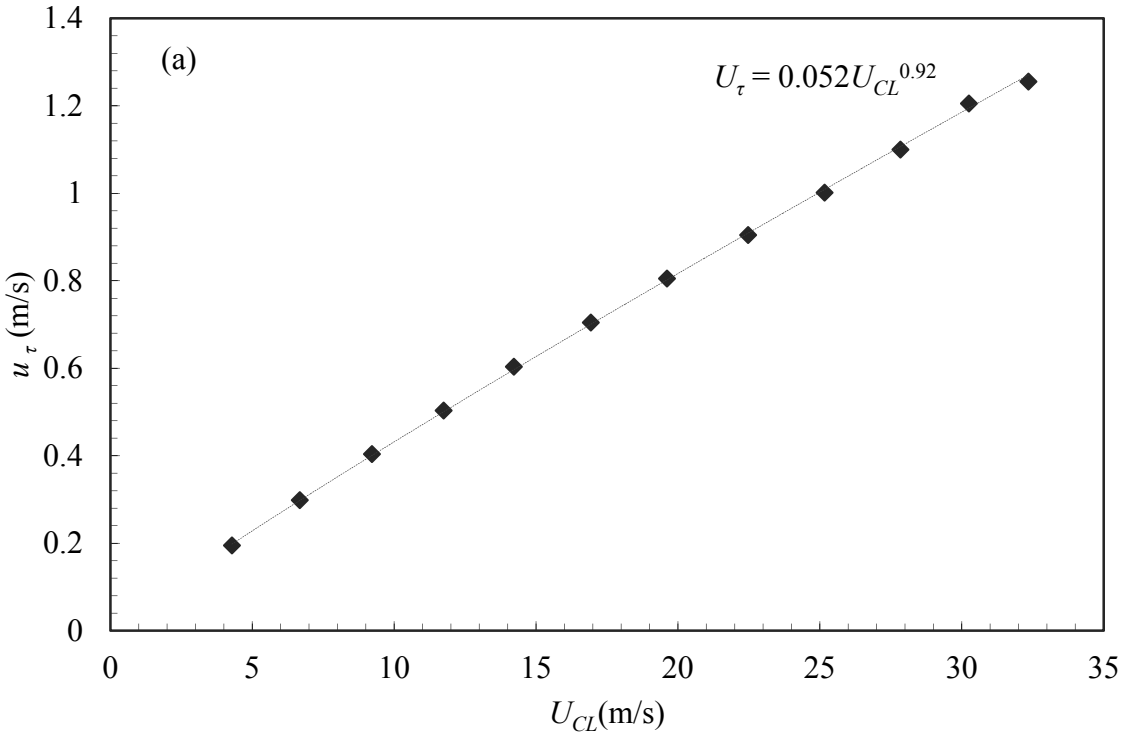

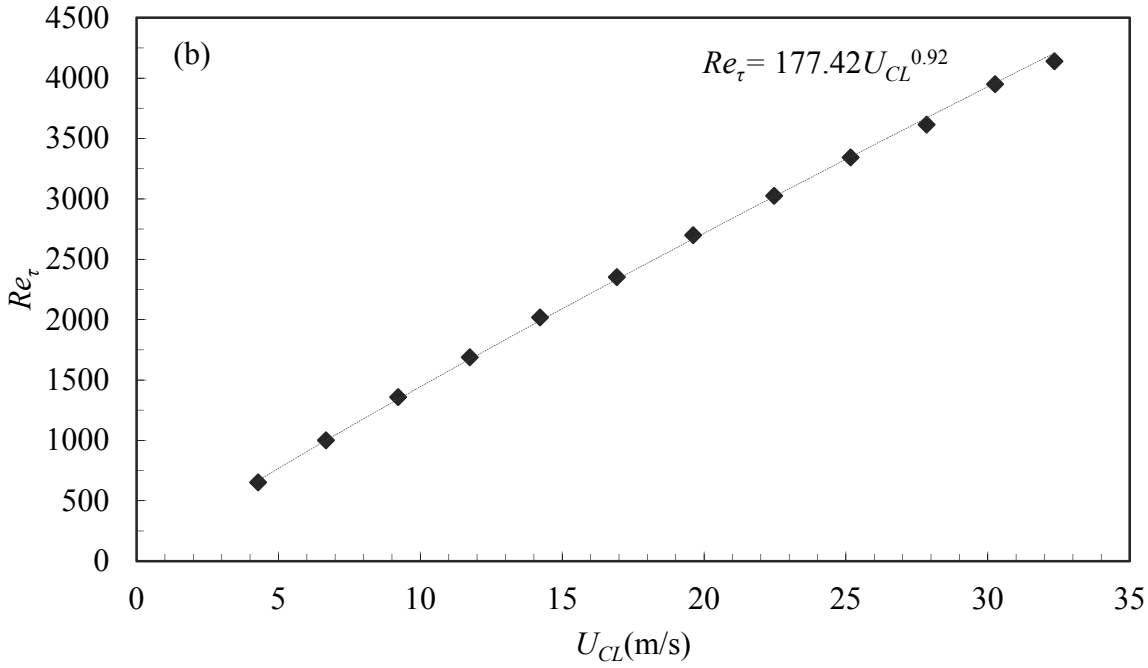

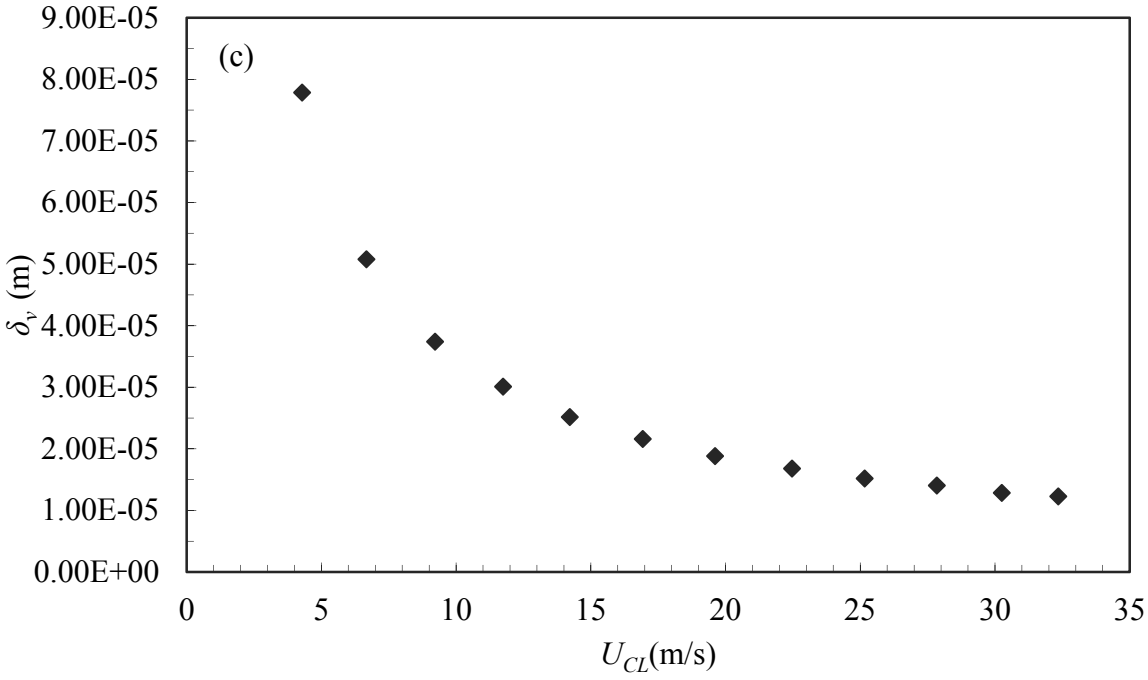

Figure 4.5: a) u_τ b) Re_τ and c) δ_v as a function of channel centerline velocity.

Local skin friction coefficient is a dimensionless number that is conventionally used to express wall shear stress in wall-bounded flows

$$C_f = \frac{\tau_w}{(\frac{1}{2}\rho U_b^2)}, \tag{4.3}$$

where U_b is bulk velocity.

Substituting τ_w in this formula using formula 4.1 shows that local friction coefficient can be calculated using

$$C_f = 2\,[\frac{u_\tau}{U_b}]^2. \tag{4.4}$$

Due to its importance in estimating skin friction drag force, the relation between friction coefficient and Reynolds number has been of interest for years. Dean (1978) proposed a power law, $C_f = 0.073\,Re_m^{-0.25}$(where Re_m is based on the channel full height and the bulk flow velocity), which was obtained by curve fit over a survey of 27 studies. Zanoun *et al.* (2003) proposed a revised power law of $C_f = 0.058\,Re_m^{-0.243}$. Monty (2005) found a logarithmic curve to be a better match for the data and proposed $\sqrt{\frac{1}{C_f}} = 4.175\,\log_{10}(Re_m\sqrt{C_f}) - 0.416$. Zanoun *et al.* (2009) proposed a further modified power law of $C_f = 0.0743\,Re_m^{-0.25}$ and a logarithmic formula of $\sqrt{\frac{1}{C_f}} = 1.911\,\ln(Re_m\sqrt{C_f}) - 1.282$. Figure 4.6 shows the skin friction coefficient determined from the present results versus Re_m, based on channel height and bulk velocity, along with previous studies for comparison. The results show good agreement with the logarithmic correlations of Zanoun (2009) and Monty (2005), thus confirming that the flow produced by the current

channel is comparable with the flow produced by other channel flow experiments. Deviation of C_f in Re_m = 40,515 can be attributed to experimental error at this point.

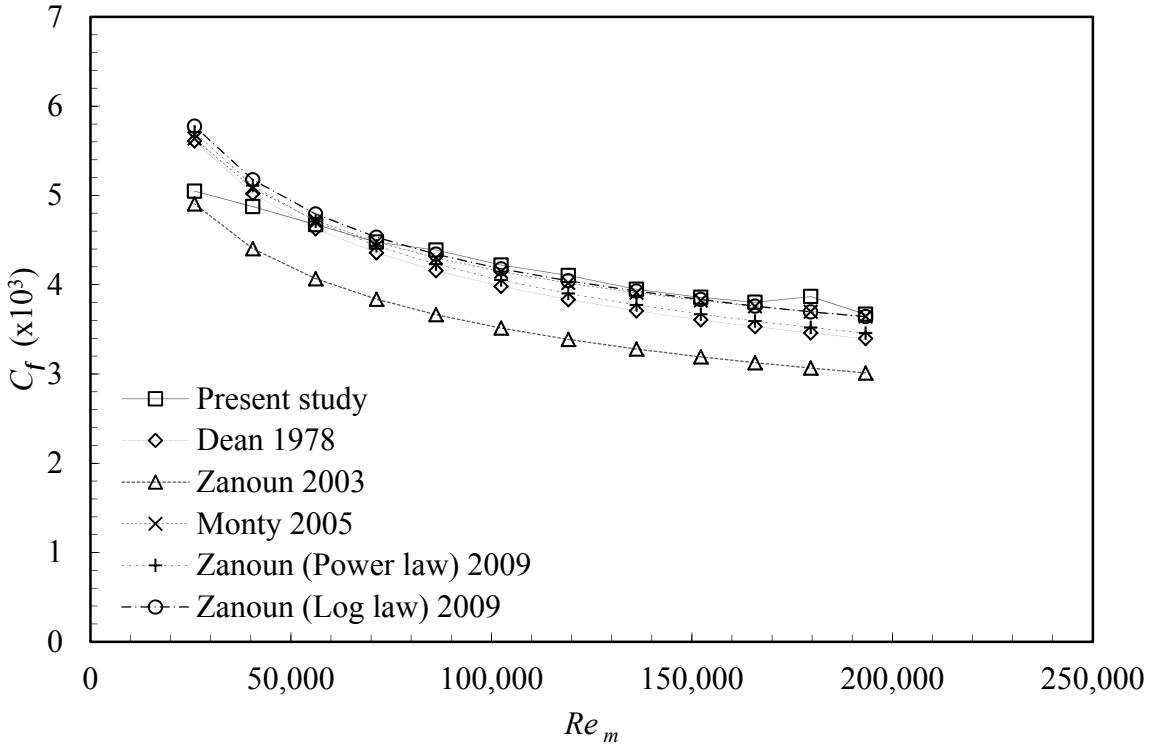

Figure 4.6: Skin friction coefficient versus Re_m, along with correlations proposed by previous studies for comparison.

Chapter 5

HOT-WIRE MEASUREMENT RESULTS AND DISCUSSION

In the following chapter, the measured mean flow velocity profiles scaled using inner and outer variables and corresponding streamwise velocity fluctuations profiles will be presented. The corrections presented by Smits *et al.* (2011) will also be assessed, and comparison between the corrections for measured inner-peak value of streamwise velocity fluctuation (Smits *et al.*, 2011; Hutchins *et al.,* 2009; and Chin *et al.,* 2010) will also be performed. The chapter will conclude by presenting the measured energy spectrum of the streamwise velocity fluctuations.

5.1. Mean Flow

Figure 5.1 presents the relationship of both U_{CL}/u_τ and U_b/u_τ to Reynolds number for cases $1-4$, hot-wires with constant l. A simple curve fit reveals the $U_{CL}/u_\tau \approx 4.9 \log_{10} Re_m$ relation between parameters, which illustrates that the ratio of outer and inner velocity scale is a function of Reynolds number.

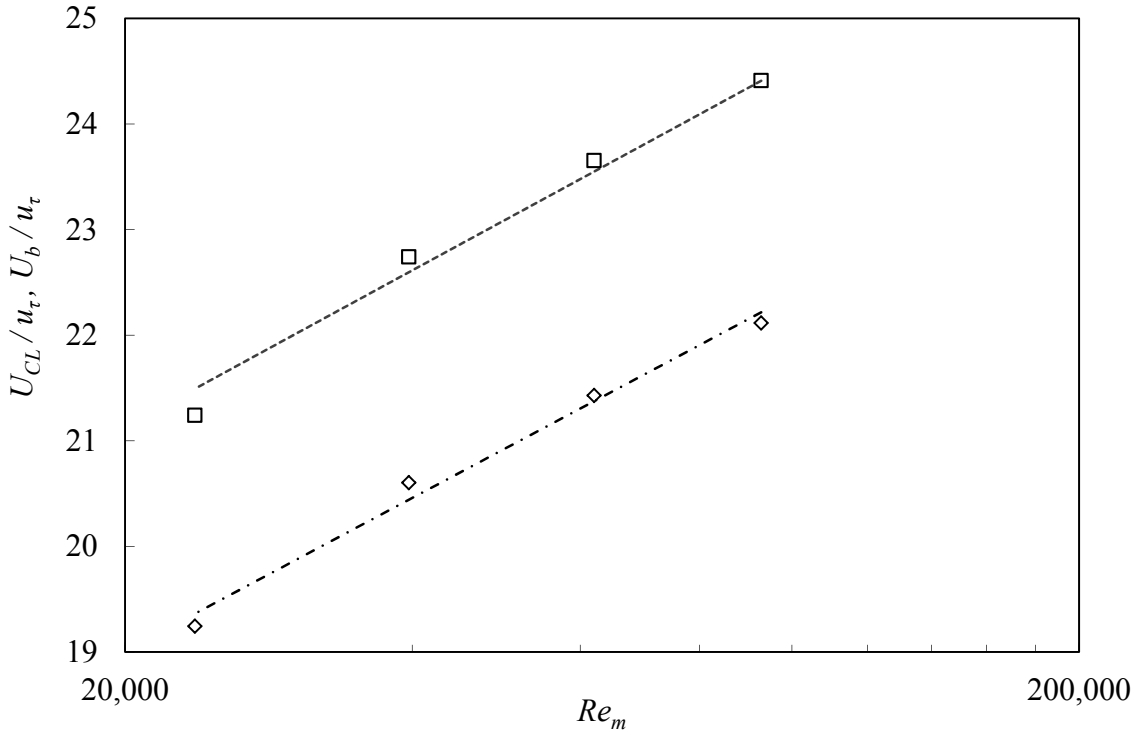

Figure 5.1: Reynolds number dependence of □, U_{CL}/u_τ and ◊, U_b/u_τ; ....., $U_{CL}/u_\tau \approx 4.9\ \log_{10} Re_m$; _ . _ , $U_{CL}/u_\tau \approx 4.8\ \log_{10} Re_m - 1.67$

In the following sections, the mean velocity profile scaled with inner and outer parameters is studied separately.

5.1.1. Inner Flow Scaling

The mean velocity profiles scaled with inner flow parameters are shown in Figure 5.2. The analytical formula for each part, and DNS from results Hoyas *et al.* (2006) at $Re_\tau = 2000$, are also added to this figure for comparison. Data show good collapse for all Reynolds numbers in the inner region, confirming Prandtl's law of the wall. This law states that the inner-scaled velocity profile is a function of z^+ only or

$$\frac{U}{u_\tau} = f(zu_\tau/\nu). \tag{5.1}$$

Very close to the wall ($z^+ < 2$), the deviation of U^+ values from $U^+ = z^+$ can be attributed to increasing heat conduction from the sensing wire to the wall. As described by Monty (2005), the velocity profile in outer region doesn't deviate greatly from the log law, compared to similar profiles in boundary layers and pipe flows.

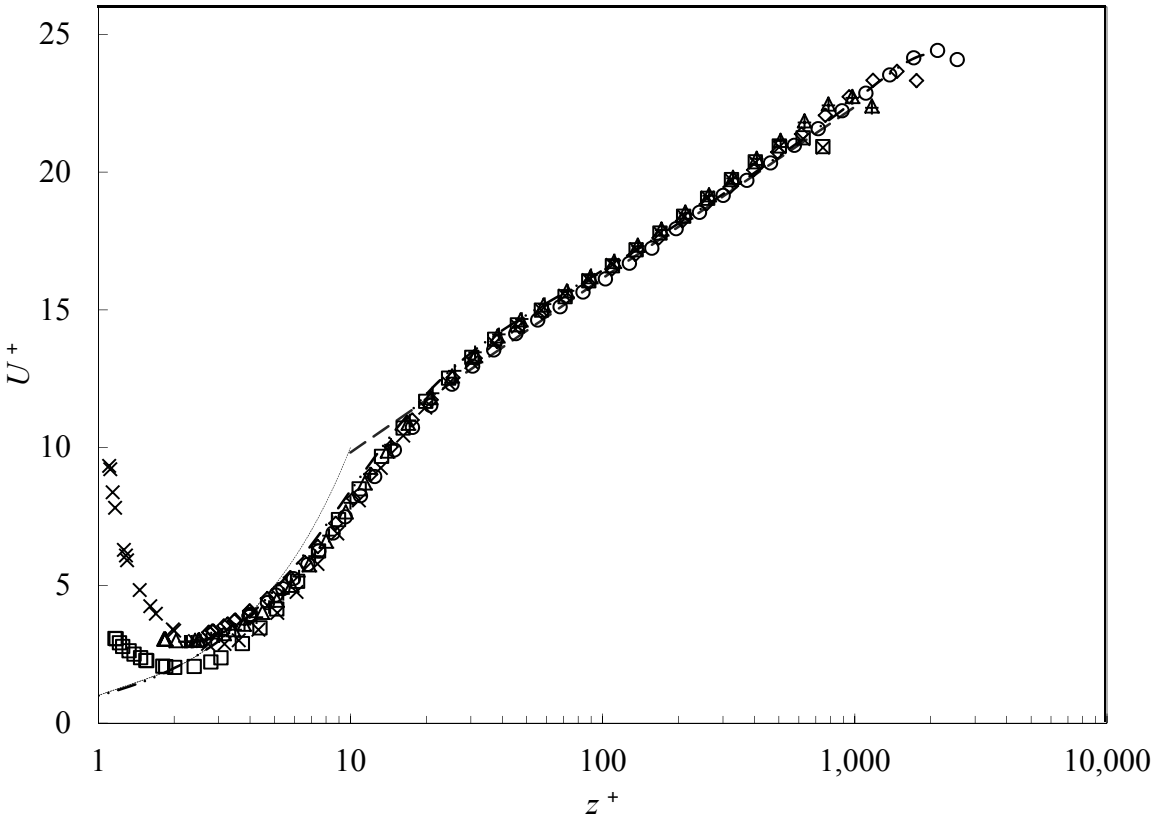

Figure 5.2: The mean velocity profiles scaled with inner flow parameters, □, Re_τ = 632, l = 0.5mm; Δ, Re_τ = 1000, l = 0.5mm; ◊, Re_τ = 1500, l = 0.5mm; ○, Re_τ = 2150, l = 0.5mm; ×, Re_τ = 632, l = 1.63mm; +, Re_τ = 1000, l = 1mm, ----, $U^+ = z^+$; _ _ _, Log law; _ ·· _, DNS results from Hoyas *et al.* (2006), Re_τ = 2000.

The relationship between U^+ and z^+ in the overlap region has been a controversial subject for years. The most popular form of governing Equations is the scaled velocity logarithmic formula

$$U^+ = \frac{1}{\kappa} \ln z^+ + A. \tag{5.2}$$

where κ and A are constant. Different values have been proposed for κ and A by many researchers. A few of them are presented in table 5.1.

Table 5.1: κ and A proposed by different researchers.

Researcher	κ	A
Coles (1962)	0.410	5.00
Zanoun *et al.* (2003)	0.370	3.71
Zagarola and Smits (1998)	0.436	6.1
Perry *et al.* (2001)	0.390	4.42
Monty (2005)	0.384	4.33

According to Hoyas & Jiménez (2006), Nagib *et al.* (2007) and Zagarola & Smits (1998), the Reynolds numbers in the current study is not sufficient to form the logarithmic part of the mean velocity profile, which prevented us from finding κ and A values.

The log law, however, is not the only proposed governing formula for this region of the mean flow velocity profile. Barenblatt (1993) and Barenblatt *et al.* (1997) proposed

proposed that a power law provides a better description for the velocity profile.

5.1.2. Outer Flow Scaling

Mean velocity profiles scaled with outer flow parameters are shown in Figure 5.3. The collapse of data in overlap and outer region for all Reynolds numbers is clear. The log law in the overlap region with outer scaling is often called von Kármán velocity defect law

$$\frac{U_{CL}-U}{u_\tau} = \frac{1}{\kappa}\ln(\frac{z}{h}) + B. \tag{5.3}$$

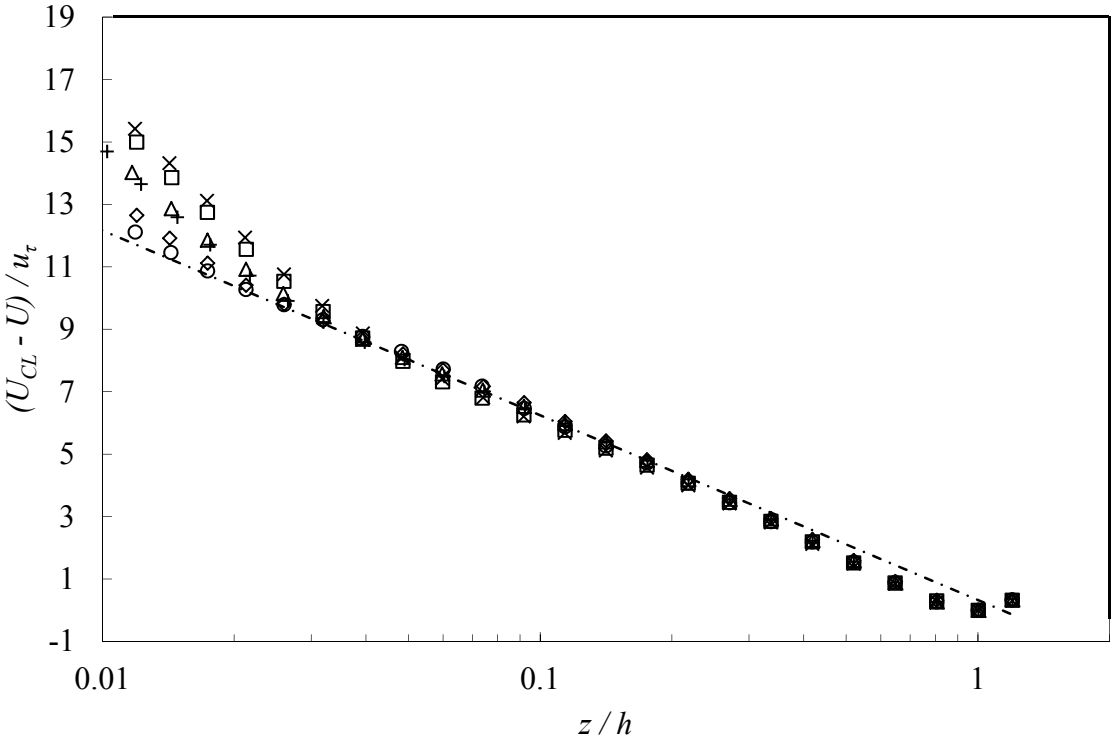

Figure 5.3: Mean velocity profiles scaled with outer flow parameters. □, Re_τ = 632, l = 0.5mm; Δ, Re_τ = 1000, l = 0.5mm; ◊, Re_τ = 1500, l = 0.5mm; ○, Re_τ = 2150, l = 0.5mm; ×, Re_τ = 632, l = 1.63mm; +, Re_τ = 1000, l = 1mm; _ . _, Monty (2005)

The velocity defect law with the constants, κ and B equal to 0.389 and 0.327 respectively, as proposed by Monty (2005) is also shown in the figure for comparison, and good agreement is found here.

5.2. Streamwise Velocity Fluctuations

5.2.1. Measured Data

In this section, the streamwise Reynolds stress, $\overline{u^2}$, will be presented. This component of turbulence intensity is the largest one among the three coordinate components due to the shear production energy being first fed to this component before being distributed to the remaining components (Kundu & Cohen, 2008). Therefore, the Reynolds number behavior of streamwise turbulent intensity has been an active research topic, fueled by a high degree of disagreement between different studies under what are expected to be identical conditions, particularly in its inner peak value. One of the most recognized contributions to this disagreement is limited spatial resolution in the measurement device, particularly at high Reynolds numbers.

In this study, to address the issue of spatial filtering, multiple approaches were used. First, the effect of viscous-scaled wire length, l^+, was investigated by comparing the Reynolds number dependence of profiles of the streamwise turbulence intensity with two sets of data: cases 1−4 with constant wire length, l, and cases 4−6 with constant viscous-scaled wire length, l^+. In addition, different corrections for spatial filtering were applied to the current data set and compared.

Figure 5.4 shows profiles of the streamwise Reynolds stress measured at four different Reynolds numbers and constant wire length (cases 1−4 in Table 3.1).

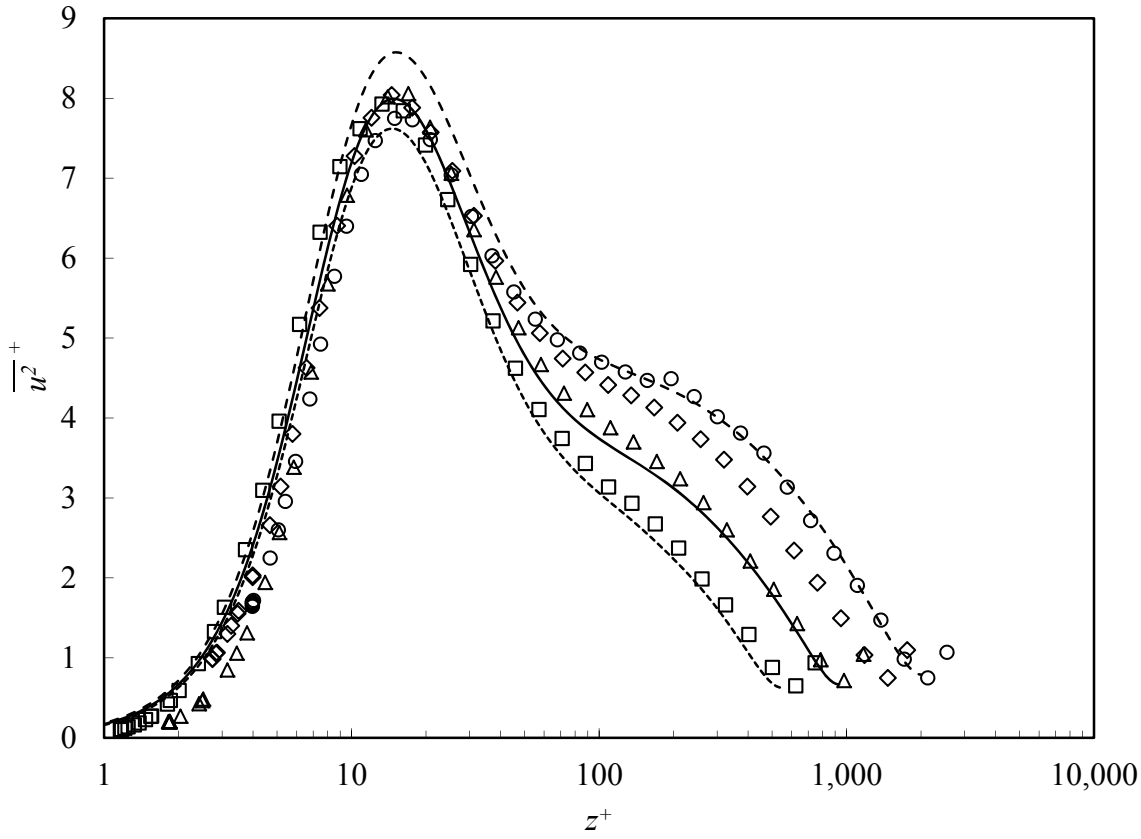

Figure 5.4: The streamwise velocity fluctuation measured with constant wire length and compared to the DNS results of Hoyas *et al.* (2006). □, $Re_\tau = 632$, $l = 0.5$mm; Δ, $Re_\tau = 1000$, $l = 0.5$mm; ◊, $Re_\tau = 1500$, $l = 0.5$mm; ○, $Re_\tau = 2150$, $l = 0.5$mm; ..... , DNS $Re_\tau = 550$; ___ , DNS $Re_\tau = 950$; ---- , DNS $Re_\tau = 2000$.

The inner peak appears clearly at $z^+ \approx 15$, with its magnitude appearing to be independent of the Reynolds number, at a constant value of 7.99 ± 0.07 for the first three Reynolds numbers. For the highest Reynolds number, however, the value of inner peak is 0.24 smaller and equal to 7.75. Figure 5.4 also compares the present results to the

DNS results of Hoyas *et al.* (2006). The results show excellent comparison everywhere throughout the channel, except in the inner peak and very close to the wall ($z^+ < 6$).

These results highlight the potential confusion which can be introduced by spatial filtering effects. From the very first studies on the spatial resolution of hot-wire probes, such as Ligrani and Bradshaw (1987b) and Alfredsson *et al.* (1988), attenuation was found to be a function of viscous-scaled wire length, l^+. In the other words, attenuation is not equal using hot-wires with different values of l^+, and consequently, the results of such a study are incomparable. In this set of data, in spite of the fact that the length of wire is constant, the value of l^+ increases Therefore, the spatial filtering effects increase with Reynolds number, serving to mask the Reynolds number dependence of the inner peak, where the scales of the turbulence are smallest.

To further illustrate this issue, in a second group of data l^+ was kept constant with increasing Reynolds number (cases 4−6 in Table 3.1). The corresponding profiles of the streamwise Reynolds stress, along with the DNS results of Hoyas *et al.* (2006), are presented in Figure 5.5.

Unlike the previous cases with constant l, the magnitude of the inner peak increases with Reynolds number, consistent with the behavior observed in the DNS results. The results for the highest Reynolds number, Re_τ = 2150, however, do not follow this trend, most likely due to experimental error.

Comparison between present experimental results and DNS results shown in Figure 5.5 presents excellent agreement across the entire wall layer, except for very close region

to the wall ($z^+ < 8$), for the first two Reynolds numbers. The larger Reynolds number results as previously observed, give a lower peak magnitude compared to equivalent DNS results.

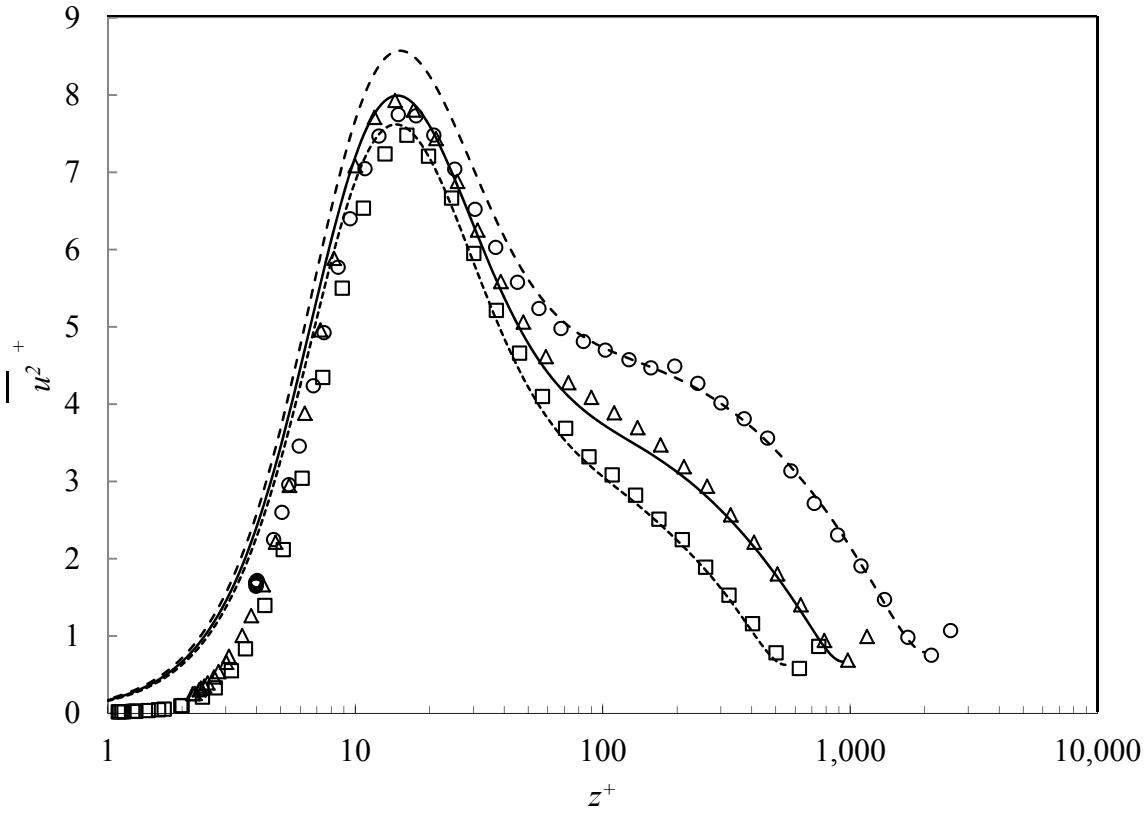

Figure 5.5: The streamwise turbulence velocity fluctuations with constant l^+, along with the DNS results of Hoyas *et al.* (2006). □, $Re_\tau = 632$, $l^+ = 20$; Δ, $Re_\tau = 1000$, $l^+ = 20$; ○, $Re_\tau = 2150$, $l^+ = 20$; ..... , DNS $Re_\tau = 550$; ___ , DNS $Re_\tau = 950$; ---- , DNS $Re_\tau = 2000$.

In addition to the peak of the turbulent intensity, the increasing trend is also obvious for the entire outer region for all Reynolds numbers with excellent agreement between experimental and DNS results.

Figure 5.6 shows the magnitude of the inner peak as a function of friction Reynolds

number for all cases measured and compares the results to the channel DNS values, the constant value proposed by Hultmark *et al.* (2010) for pipe flows, as well as the correlations presented by Hutchins & Marusic (2007) and Hutchins *et al.* (2009) for turbulent boundary layers (see Section 2.2.1). The obvious increasing trend of this value for the second data set confirms the nonexistence of any similarity with Reynolds number. More importantly, considering that the experiment instrumentation and procedures in the current channel flow experiment were carefully selected to match the pipe flow experiments of Hultmark *et al.* (2010), the results also indirectly validate the pipe flow results, thus confirming the observed Reynolds number independence of the pipe flow results.

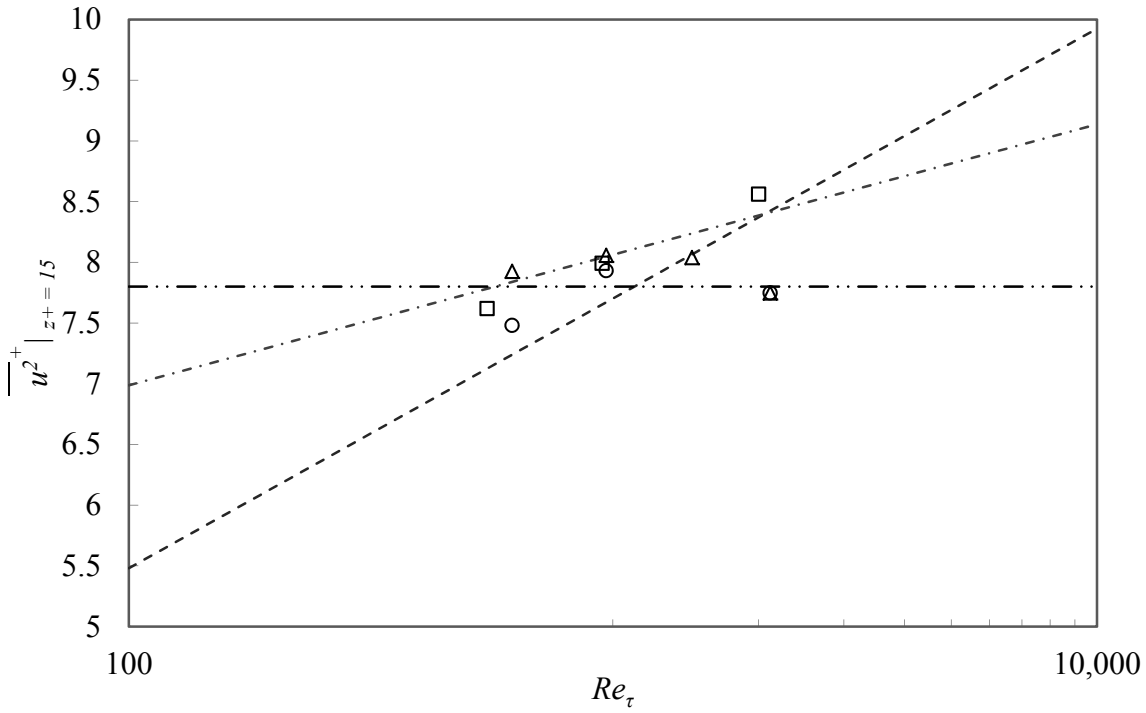

Figure 5.6: The comparison between inner-peak values for the present study versus friction Reynolds number. Δ, constant *l;* ○, constant l^+; □, DNS results; ---- , Hutchins & Marusic (2007); _ . _ , Hutchins *et al.* (2009); _ .. _ , Hultmark *et al.* (2010).

5.2.2. Corrected Data

In spite of hot-wire probe spatial resolution issues, the broad use of this measurement technique, especially in near wall turbulent measurements makes the possibility of correcting the data for spatial filtering effects an attractive proposition, with the most recent corrections proposed by Hutchins *et al.* (2009), Chin *et al.* (2010) and Smits *et al.* (2011). The Smits *et al.* (2011) correction, unlike the two earlier corrections can be applied to the entire wall layer whereas the Hutchins *et al.* (2009) and Chin *et al.* (2010) corrections are only applicable for inner-peak position at $z^+ = 15$. The validity of the correction was previously tested in turbulent boundary layer and pipe flow, showing very good performance. Here, we will investigate the applicability of the Smits *et al.* correction to turbulent channel flow.

Streamwise Reynolds stress profiles corrected using the Smits *et al.* correction are presented in Figures 5.7 and 5.8 for the matched l and matched l^+ sets of data respectively.

For the matched l data set, the agreement between the DNS and results from the current study in the outer layer remains unchanged with application of the correction. Unlike the uncorrected values however, the magnitude of the inner peak in the corrected profiles shows the expected increasing trend. When compared to the Hoyas *et al.* (2006) DNS results, the magnitudes of the inner peak is slightly higher in the experimental results, with maximum difference not more than 4.8 %, which is within the range which can be expected due to experimental error.

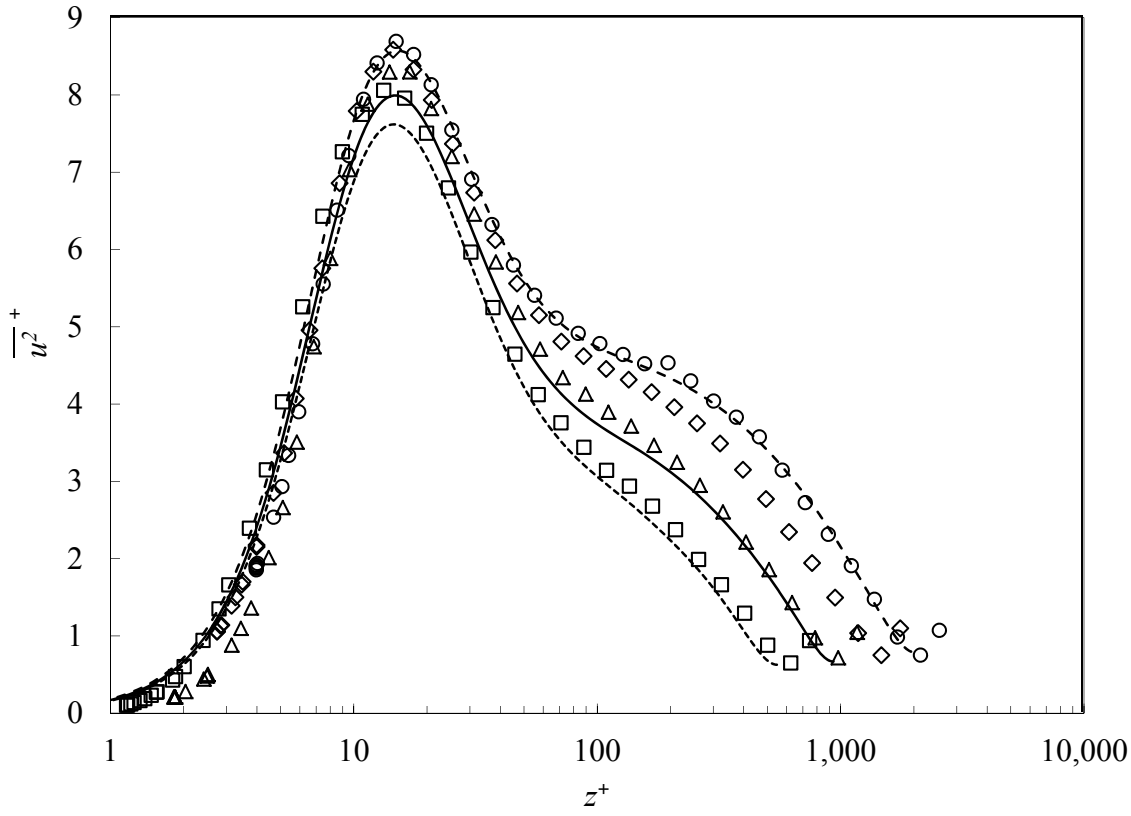

Figure 5.7: Corrected streamwise velocity profile for matched l data using Smits *et al.* (2011). □, $Re_\tau = 632$, $l = 0.5$mm; Δ, $Re_\tau = 1000$, $l = 0.5$mm; ◊, $Re_\tau = 1500$, $l = 0.5$mm; ○, $Re_\tau = 2150$, $l = 0.5$mm; ..... , DNS $Re_\tau = 550$; ___ , DNS $Re_\tau = 950$; ---- , DNS $Re_\tau = 2000$.

For the matched l^+ data, the increasing Reynolds number trend of inner peak magnitude is still present for the two lower Reynolds numbers but application of the correction does not improve the agreement of the largest Reynolds number data set with this trend.

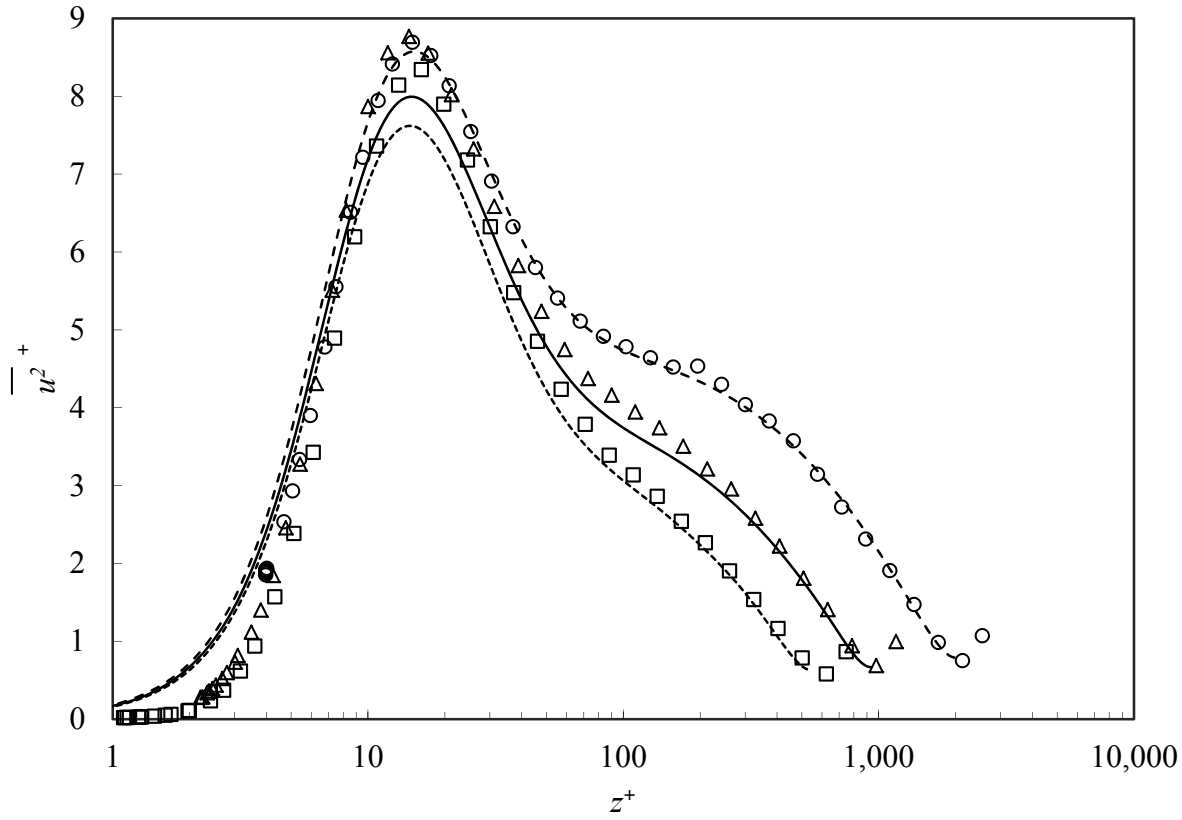

Figure 5.8: The corrected streamwise velocity profile for matched l^+ data using Smits *et al.* (2011). □, $Re_\tau = 632$, $l^+ = 20$; Δ, $Re_\tau = 1000$, $l^+ = 20$; ○, $Re_\tau = 2150$, $l^+ = 20$; ..... , DNS $Re_\tau = 550$; ___ , DNS $Re_\tau = 950$; ---- , DNS $Re_\tau = 2000$.

The peak value after executing the correction for each Reynolds number for the matched l and matched l^+ sets of data, along with the DNS results, are presented in Figure 5.9. Again, the formula by Hutchins and Marusic (2007) and Hutchins *et al.* (2009) for turbulent boundary layers, as well as the stated constant value provided by Hultmark *et al.* (2010) for pipe flows is also provided for comparison. The increasing trend of inner peak value after correction is clearly evident.

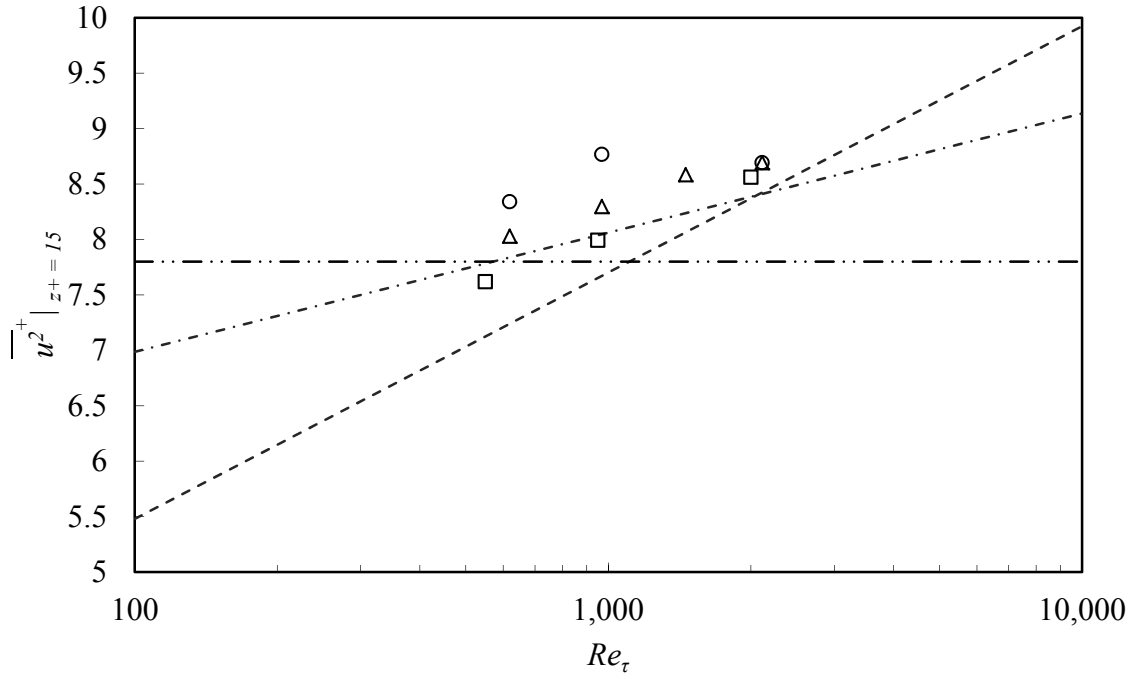

Figure 5.9: Comparison between inner-peak magnitude of current results after correction versus friction Reynolds number. Δ, matched l; ○, matched l^+; □, DNS results; ---- , Hutchins and Marusic (2007); _ · _ , Hutchins *et al.* (2009); _ ·· _ , Hultmark *et al.* (2010).

In next section, the streamwise turbulent intensity profiles for both sets of data in inner peak position were corrected using Hutchins *et al.* (2009) and Chin *et al.* (2010) correction formulas. The results along with the corrected peak values using Smits *et al.* (2011) formula, and also DNS results, are presented in Figure 5.10 and 5.11 for matched l and matched l^+ data sets, respectively.

In use of both Hutchins *et al.* (2009) and Chin *et al.* (2010) corrections, the value of difference between true streamwise turbulent intensity, $\overline{u^2}_T^+$, and the measured value,

$\overline{u^2}_m^+$, referred to as $\Delta\overline{u^2}^+$ is determined and added to the measured value through simply

$$\overline{u^2}_T^+ = \overline{u^2}_m^+ + \Delta\overline{u^2}^+. \tag{5.4}$$

Following Hutchins *et al.* (2009),

$$\Delta\overline{u^2}^+ = B_1\, l^+ - C_1\,(\frac{l^+}{Re_\tau}), \tag{5.5}$$

where $B_1 = 0.0352$ and $C_1 = 23.0833$. The Chin *et al.* (2010) correction is

$$\Delta\overline{u^2}^+ = A_2\, l^{+3} + B_2\, l^{+2} + C_2\, l^+ + D_2, \tag{5.6}$$

where $A_2 = -1.94 \times 10^{-5}$, and $B_2 = 1.83 \times 10^{-3}$, $C_2 = 1.76 \times 10^{-2}$ and $D_2 = -9.68 \times 10^{-2}$.

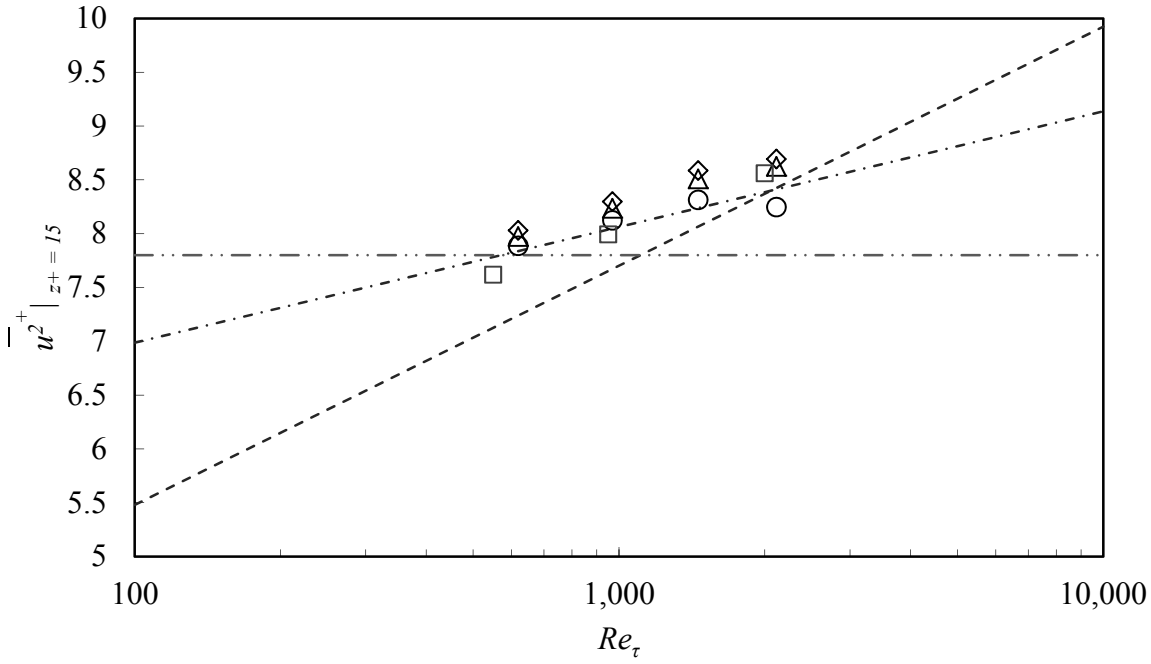

Figure 5.10: The inner peak values resulted from Hutchins *et al.* (2009) and Chin *et al.* (2010) correction formulas, for matched *l* data set. ◊, Smits *et al.*; ○, Hutchins *et al.*; Δ, Chin *et al.*; □, DNS results; ---- , Hutchins and Marusic (2007); _ . _ , Hutchins *et al.* (2009); _ .. _ , Hultmark *et al.* (2010).

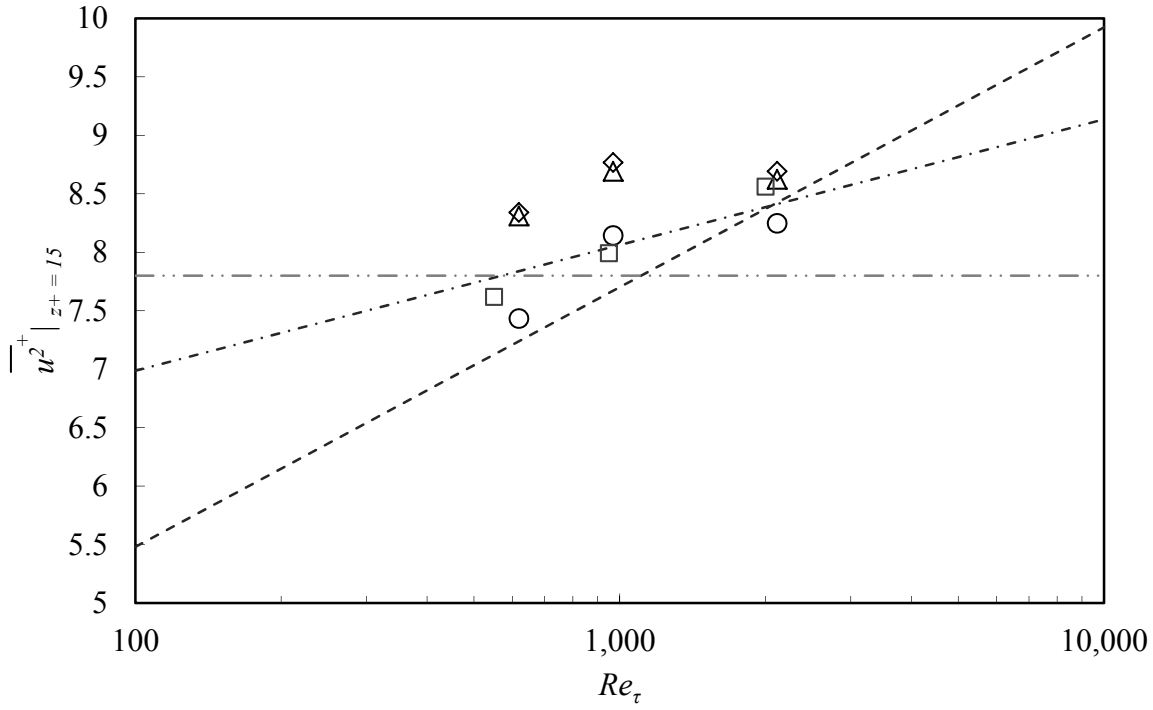

Figure 5.11: The inner peak values resulted from Hutchins *et al.* (2009) and Chin *et al.* (2010) correction formulas, for matched l^+ data set. ◊, Smits *et al.*; ○, Hutchins *et al.*; Δ, Chin *et al.*; □, DNS results; ---- , Hutchins and Marusic (2007); _ . _ , Hutchins *et al.* (2009); _ .. _ , Hultmark *et al.* (2010).

Profiles corrected using Smits *et al.* (2011) correction formula for different values of l and consequently different values of l^+ for constant Reynolds numbers are compared for Re_τ = 632, and 1000 in Figures 5.12 and 5.13.

Given that the correction, if successful, should cause both measured profiles shown on each figure to collapse, the good agreement between corrected profiles in the inner peak position and in the outer region, especially for the higher Reynolds number case, supports the validity of the correction. For the lower Reynolds number case, there is larger disagreement for $z^+ < 15$, however this is likely introduced by experimental errors due to the reliance on calibration data at very low velocities in this z^+ range. At low

velocities, accurate Pitot-static tube measurements become increasingly challenging to conduct due to the small pressure differences which must be measured.

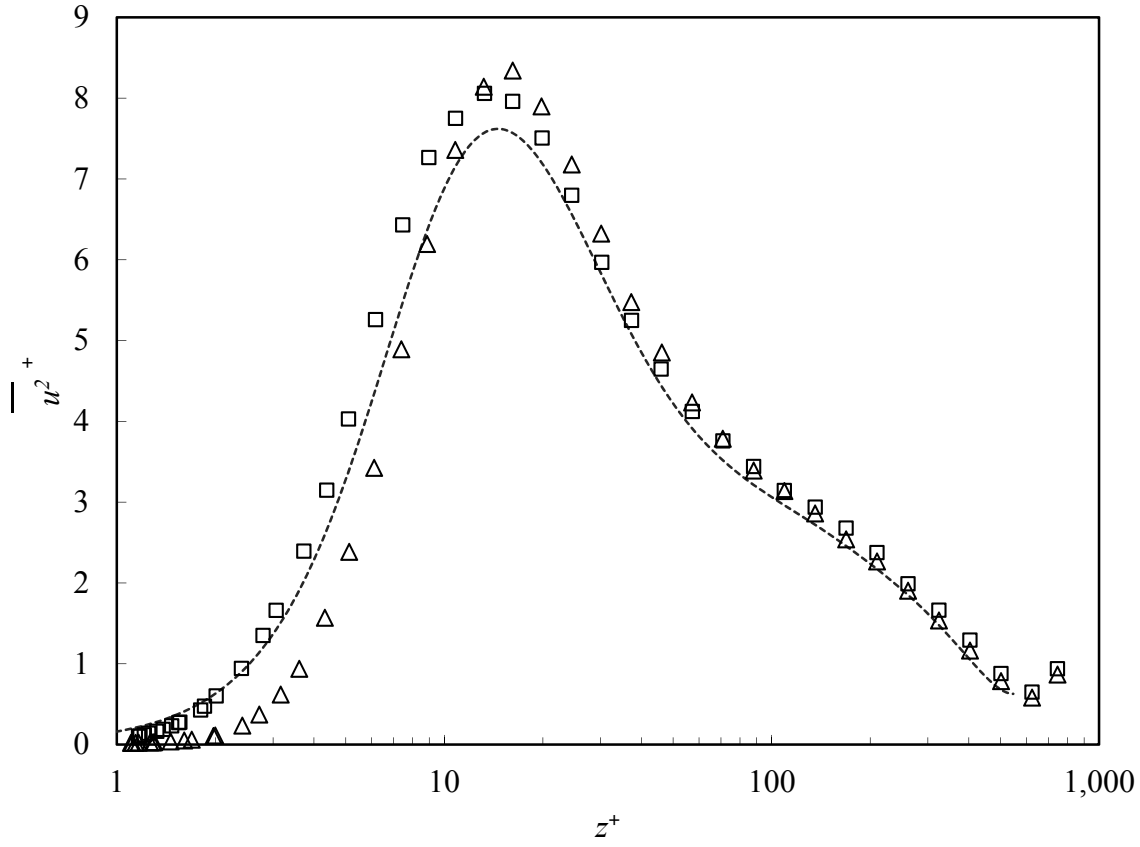

Figure 5.12: Corrected profiles for $Re_\tau = 632$ from matched l and matched l^+ data sets. □, $Re_\tau = 632$ after correction, $l = 0.5$mm; Δ, $Re_\tau = 632$ after correction, $l = 1.63$mm; ---- , DNS $Re_\tau = 550$.

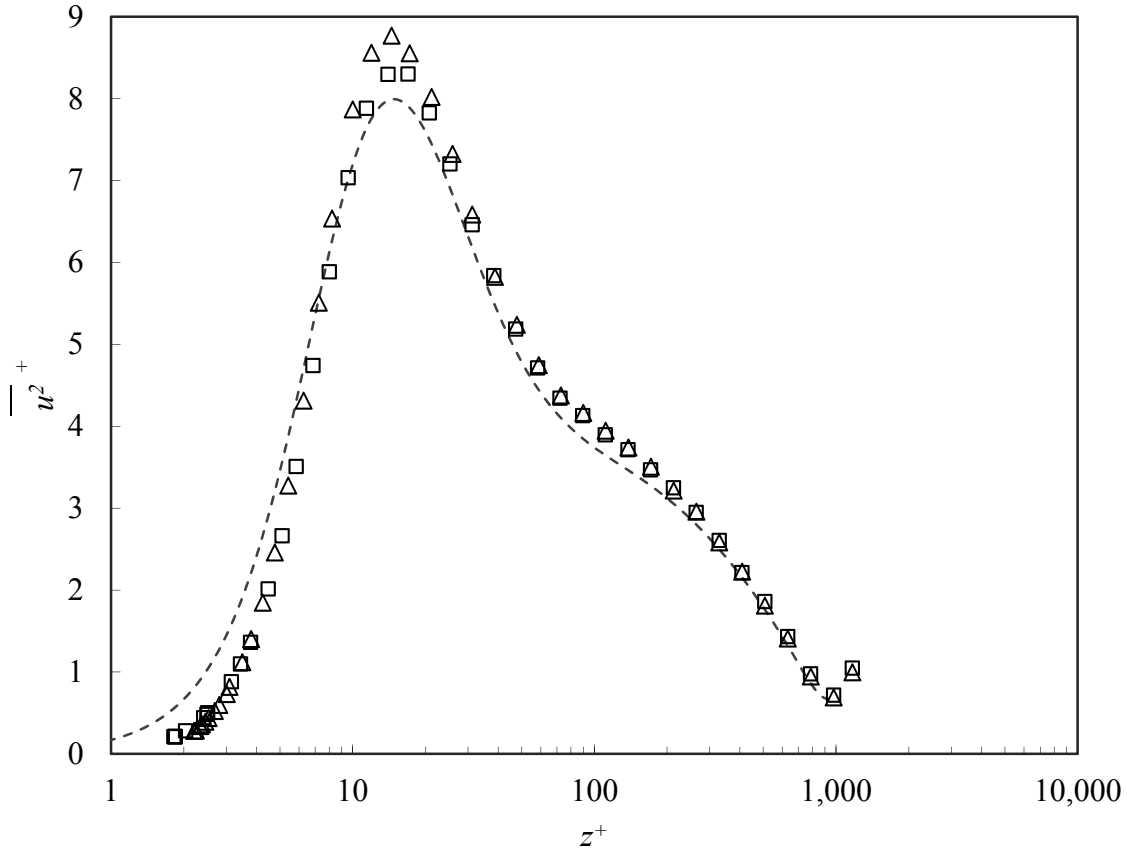

Figure 5.13: Corrected profiles for Re_τ = 1000 from matched l and matched l^+ data sets. □, Re_τ = 1000 after correction, l = 0.5mm; Δ, Re_τ = 1000 after correction, l = 1mm; ---- , DNS Re_τ = 950.

5.3. Energy Spectra

Energy spectra for the velocity signal at the peak position can potentially explain differences in the Reynolds number behavior of the inner-peak magnitude amongst canonical wall-bounded flows. To investigate the effects of hot-wire probe wire the energy spectra at constant Reynolds number, but different wire lengths, are presented for at z^+ = 15 at Re_τ = 632 and 1000 in Figures 5.14 and 5.15, respectively. To find the wavenumber, Taylor's frozen flow hypothesis was employed using the local mean

velocity. In these figures, energy spectra for both inner and outer scaling is presented. The results are consistent with expected behavior of attenuation over a wide range of wavenumbers. Note that at $Re_\tau = 1000$, the difference between the physical wire lengths was smaller, with more filtering affecting the shorter wire, causing the difference between the spectra to be reduced.

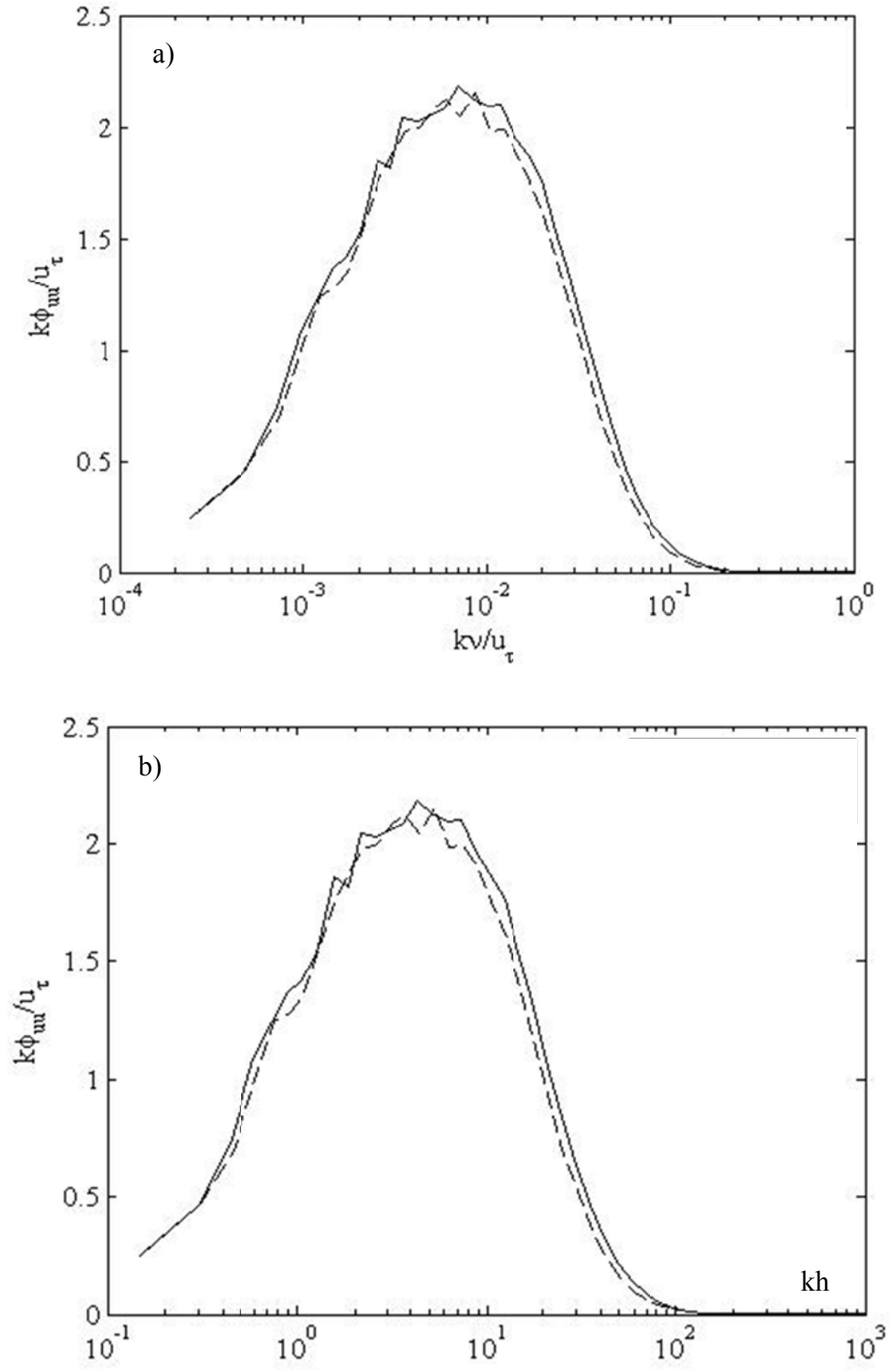

Figure 5.14: Energy spectra for $Re_\tau = 632$, ___ , $l = 0.5$mm; ---- , $l = 1.63$mm. a) inner scaling, b) outer scaling

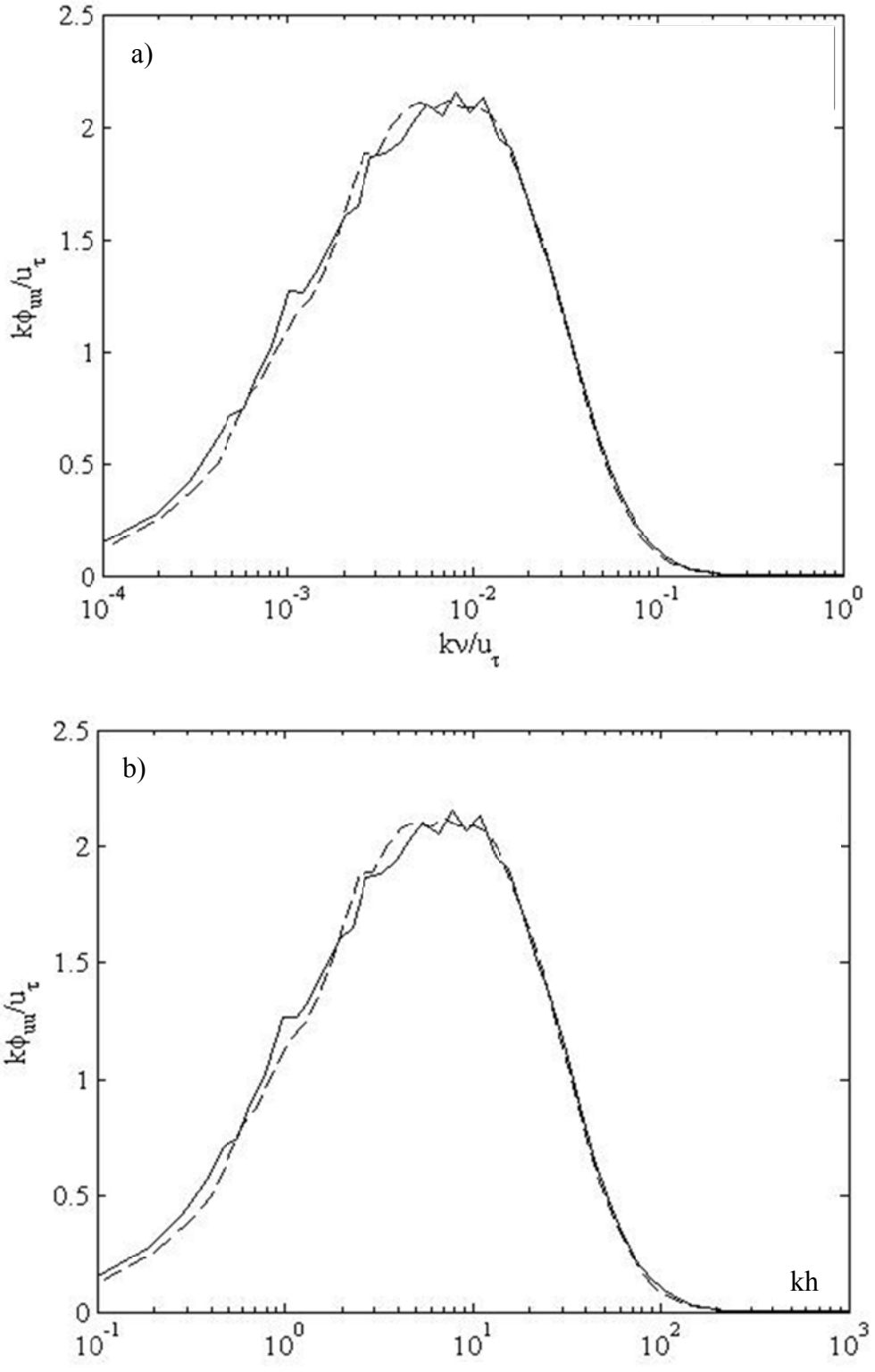

Figure 5.15: Energy spectra for Re_τ = 1000, ___ , l = 0.5mm; ---- , l = 1mm.. a) inner scaling b) outer scaling

Energy spectra for the matched l^+ data set at $z^+ = 15$ for both inner and outer scaling are presented in Figure 5.16.

The increasing trend of inner peak value of streamwise velocity fluctuations is evident from these plots. In energy spectra, the area under each curve corresponds to $\overline{u^2}^+$, which clearly increases with increasing the Reynolds number in Figure 5.16. Furthermore, this increase occurs at low wavenumbers indicating that it is caused by large-scale motions and is therefore likely caused by modulation of the near wall motions due to outer-scale influence on the inner region as suggested by Mathis (2009).

Therefore, the differences between the interaction of inner and outer regions in each kind of canonical flow can explain the different inner peak dependence on Reynolds number observed between these flows. The external structures in the outer layer of turbulent boundary layers have noticeable differences with VLSM in internal flow (see Section 2.3 for more details). In addition, the geometric constraints causing a reduction in scale of the VLSM in the outer layer for pipe flows compared to boundary layer and channel flows (Bailey *et al.*, 2008) provides reasonable grounds for the differences in inner peak behavior between pipe and channel flows.

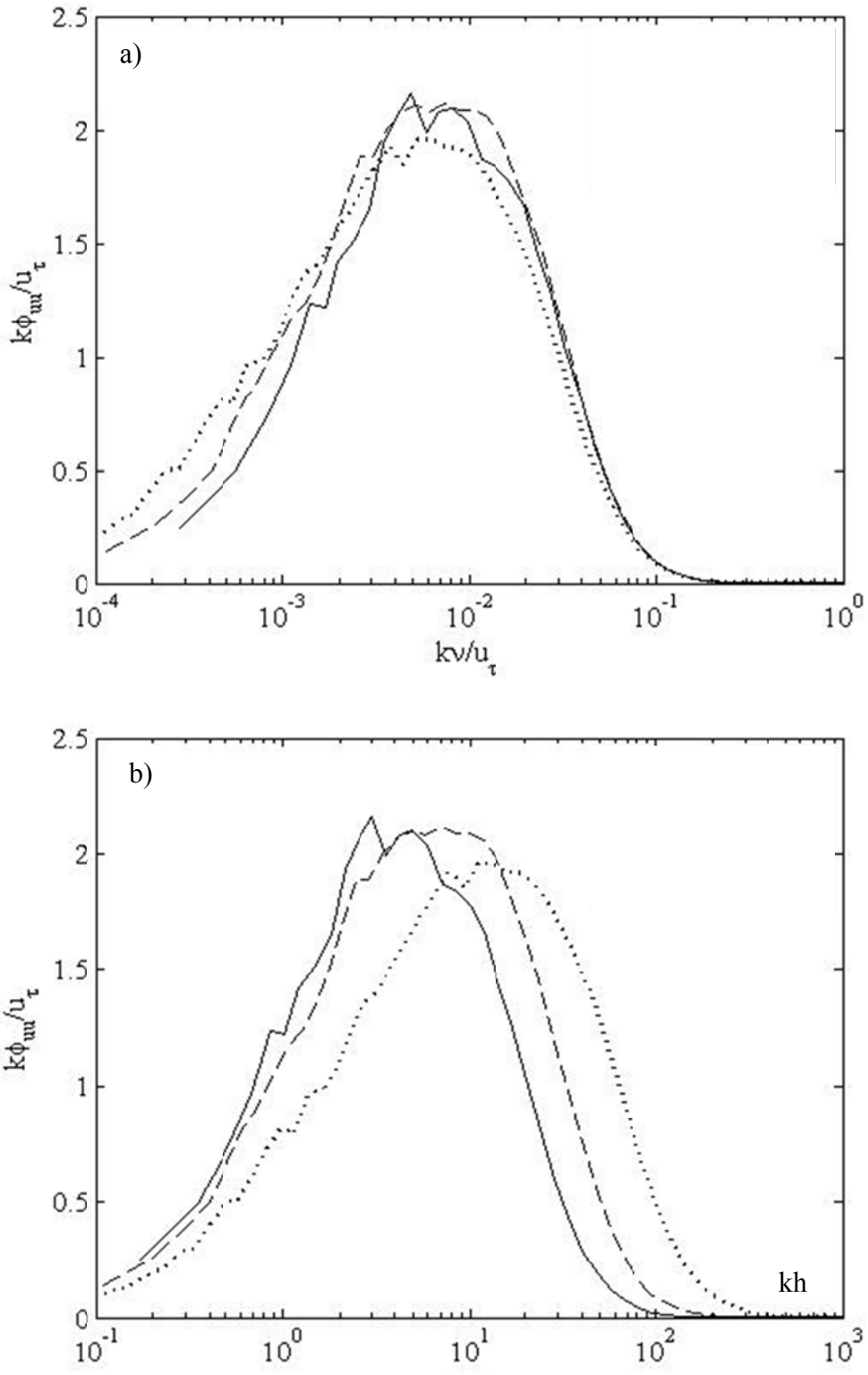

Figure 5.16: Energy spectra for matched l^+ data set for: ___ $Re_\tau = 632$; ---- , $Re_\tau = 1000$; ..... , $Re_\tau = 2150$.

Chapter 6

CONCLUSIONS

The slow rate of progress of computational methods used in the study of turbulent flows, due to the lack of sufficiently powerful computers to solve the complicated nonlinear differential equations governing turbulent flow at high Reynolds numbers, keeps experimental methods the most promising approach to resolve unsolved problems of turbulent flow.

Perhaps one of the most concrete outcomes of this study is the construction of a new channel flow facility capable of reaching higher Reynolds numbers in channels than has previously been available. In design, construction and erection of the facility, the lessons learned from previous studies found in the literature have been considered, resulting in an accurate experimental apparatus providing hope for improving our current knowledge of turbulence through the research presented here as well as those that to follow.

To address questions regarding the inner peak value of streamwise turbulence intensity, velocity was measured using hot-wire anemometry in the channel flow facility. Consistently with turbulent boundary layers, but inconsistently with pipe flows, the results show dependence of inner peak value on Reynolds number in channel flows – its magnitude increasing with increasing Reynolds number. Since the experimental instrumentation and procedures were selected to match the pipe flow experiments of Hultmark et al. (2010), this study can be considered as an indirect validation of their results, which *do* indicate independence of the pipe flow inner peak value on Reynolds number. Whereas it has come to be accepted that the behavior of turbulent fluctuations

near the wall could be different between internal and external flows, due to the existence of a pressure gradient in the former case, differences among internal flows was not expected.

Using energy spectra of streamwise velocity, the increasing trend of inner peak value of streamwise velocity fluctuations was found to occur at low wavenumbers. This indicates that large-scale motions, and therefore likely modulation of the near wall motions due to outer-scaled influence on the inner region as suggested by Mathis (2009), are the explanation for differences between internal flows as there are noticeable differences between outer layer motions in three kinds of flow (see, for example, Hutchins and Marusic, 2007; Marusic and Hutchins, 2008; Bailey *et al.*, 2008; Marusic *et al.*, 2010 amongst others).

In addition, results acquired using hot-wires with constant viscous scale wire length, l^+, and hot-wires with constant length, l, illustrated the crucial requirement of maintaining constant l^+ to minimize the effects of spatial filtering when studying Reynolds number dependence.

Moreover, recently proposed corrections to address the limited spatial resolution issue of hot-wire probes were employed to either the streamwise velocity fluctuation profiles or their inner peak values to investigate their suitability. The independence of measured profiles to hot wire probe sensing length following correction confirms the applicability of the Smits *et al.* (2011) correction. Furthermore, comparison between inner peak values following application of Smits *et al.* (2011), Chin *et al.* (2010) and Hutchins *et al.* (2009) corrections proves, as well, validity of the two latter corrections.

6.1. Future Work

Much yet remains unexplored in channel flow turbulence, leaving many possible studies which can follow the present one:

- Use the capabilities of the facility constructed for this study to push the Reynolds number range beyond that of previously reported measurements and simulations.

- Measurement of two other components of turbulent intensity and investigate the influences of Reynolds number on them.

- Examine the effects of surface roughness on the magnitude of inner peak and on the measurement process.

- Investigate of the inner-outer interaction using decomposition of velocity signature into small- and large-scale decomposition across the boundary layer using a cutoff spectra following Hutchins et al. (2009).

Appendix A

DETAILED ENGINEERING DRAWINGS

Part: Contraction-Side wall

Top view

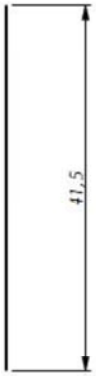

* Material: 1/4" Aluminum Plate
* 2 Required
* The tolerance of all dimension is 0.01
* Template will be provided for profile

Front view

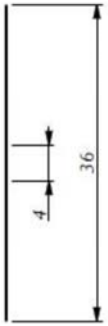

Right view

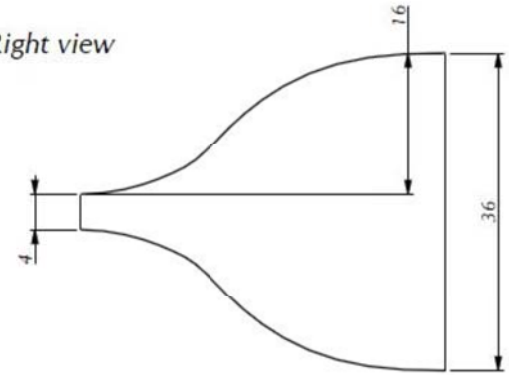

Part: Contraction_Top Bottom Sheet

Top view

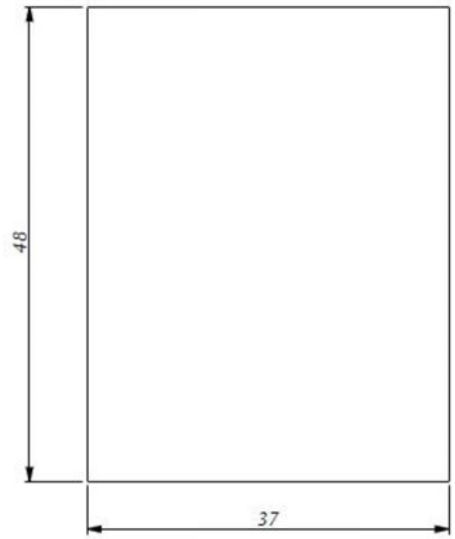

* Material: 16 gauge (0.0508") Aluminum sheet metal

* 2 Required

* The Top Bottom sheets are assembled by screwing to side walls.

* The Top Bottom Sheet should form to side wall.

* The tolerance of all dimension is 0.01

Front view

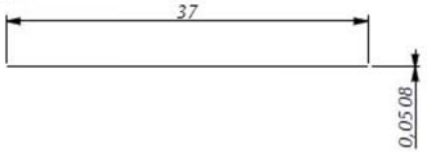

Right view

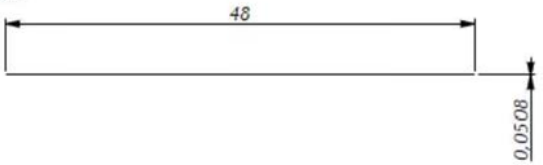

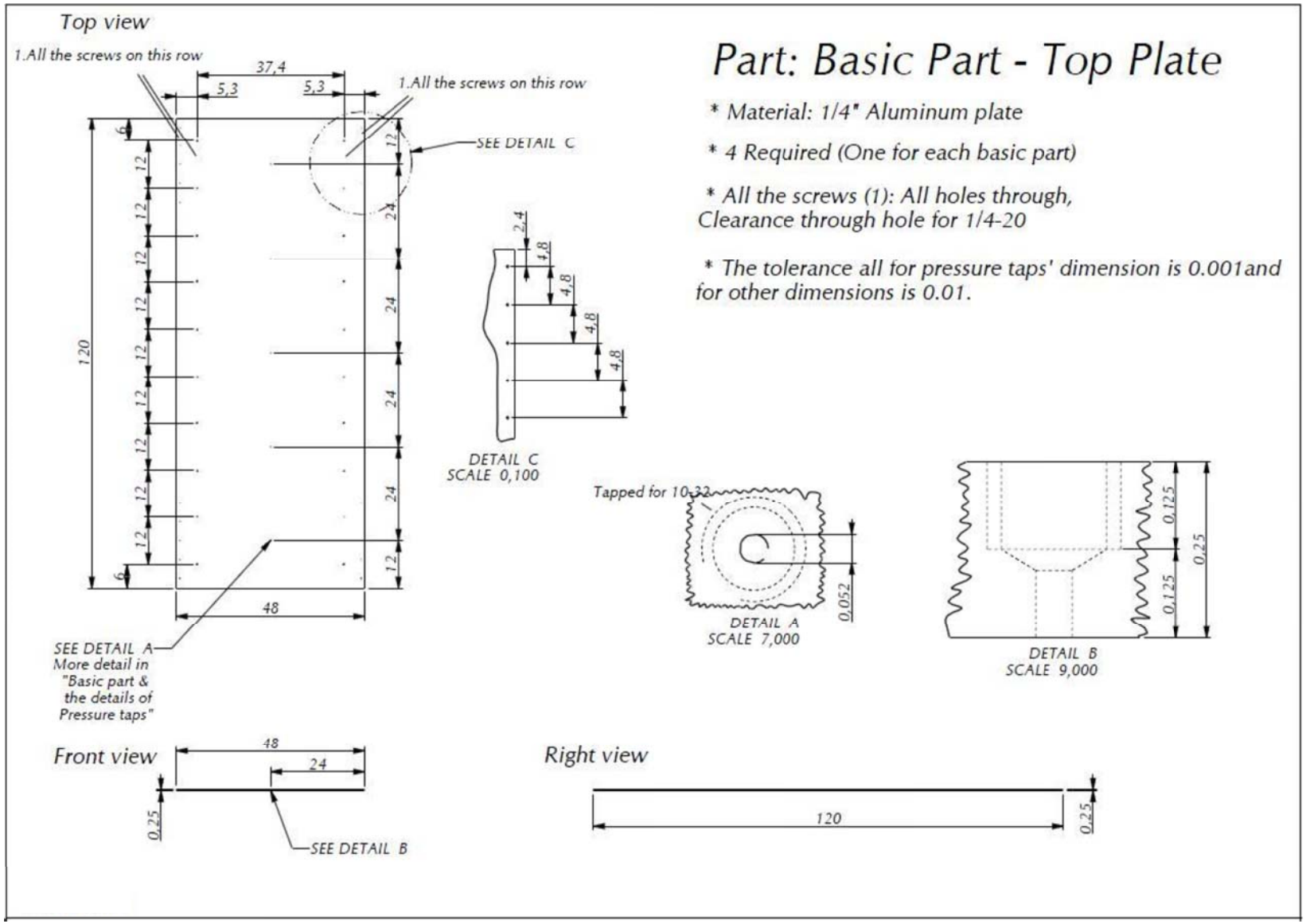
Top view
1.All the screws on this row
37,4
5,3
5,3
1.All the screws on this row
SEE DETAIL C
120
48
SEE DETAIL A
More detail in
"Basic part &
the details of
Pressure taps"
DETAIL C
SCALE 0,100
Tapped for 10-32
DETAIL A
SCALE 7,000
DETAIL B
SCALE 9,000
Front view
SEE DETAIL B
Right view
Part: Basic Part - Top Plate
* Material: 1/4" Aluminum plate
* 4 Required (One for each basic part)
* All the screws (1): All holes through,
Clearance through hole for 1/4-20
* The tolerance all for pressure taps' dimension is 0.001and
for other dimensions is 0.01.

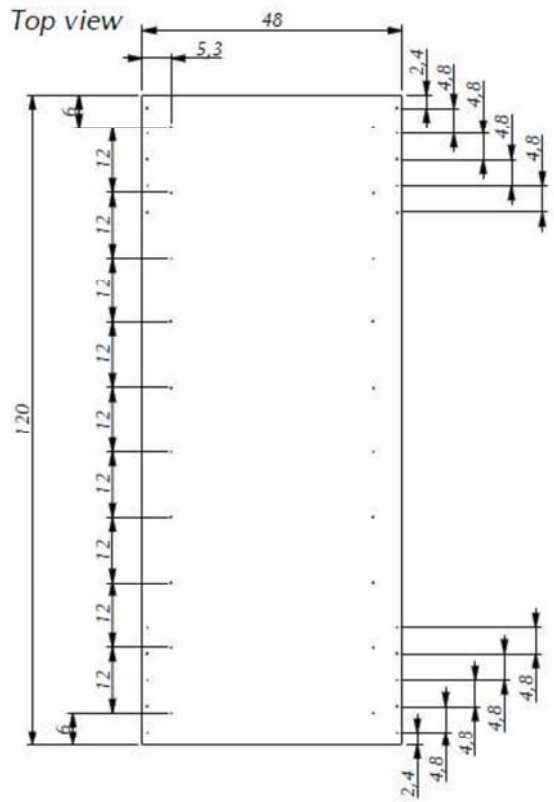

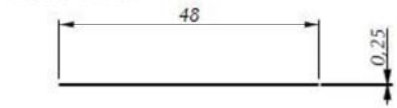

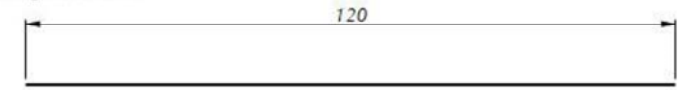

Part: Basic Part - Bottom Plate

* Material: 1/4" Aluminum Plate
* 4 Required (one for each basic part)
* All holes through, Clearance through hole for 1/4-20
* The holes in two rows are located the same.
* Bottom plate are the same as top plate except the absence of pressure taps.
* The tolerance for all dimension is 0.01

Part: Basic Part -Side wall

Top view

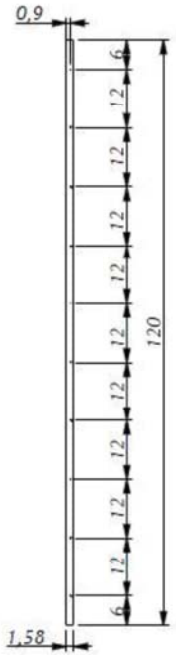

* Material: U Channel 6061-T6 Aluminum, Extruded
* 8 Required (2 for each basic part)
* All holes through, clearance for 1/4-20
* The holes on top and bottom wings of U channel locate the same.
* The tolerance for all dimensions is 0.01

Front view

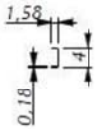

Right view

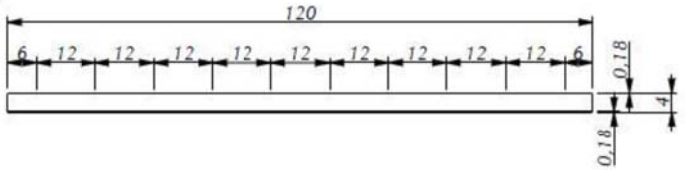

Assembly: Basic parts & pressure taps detail

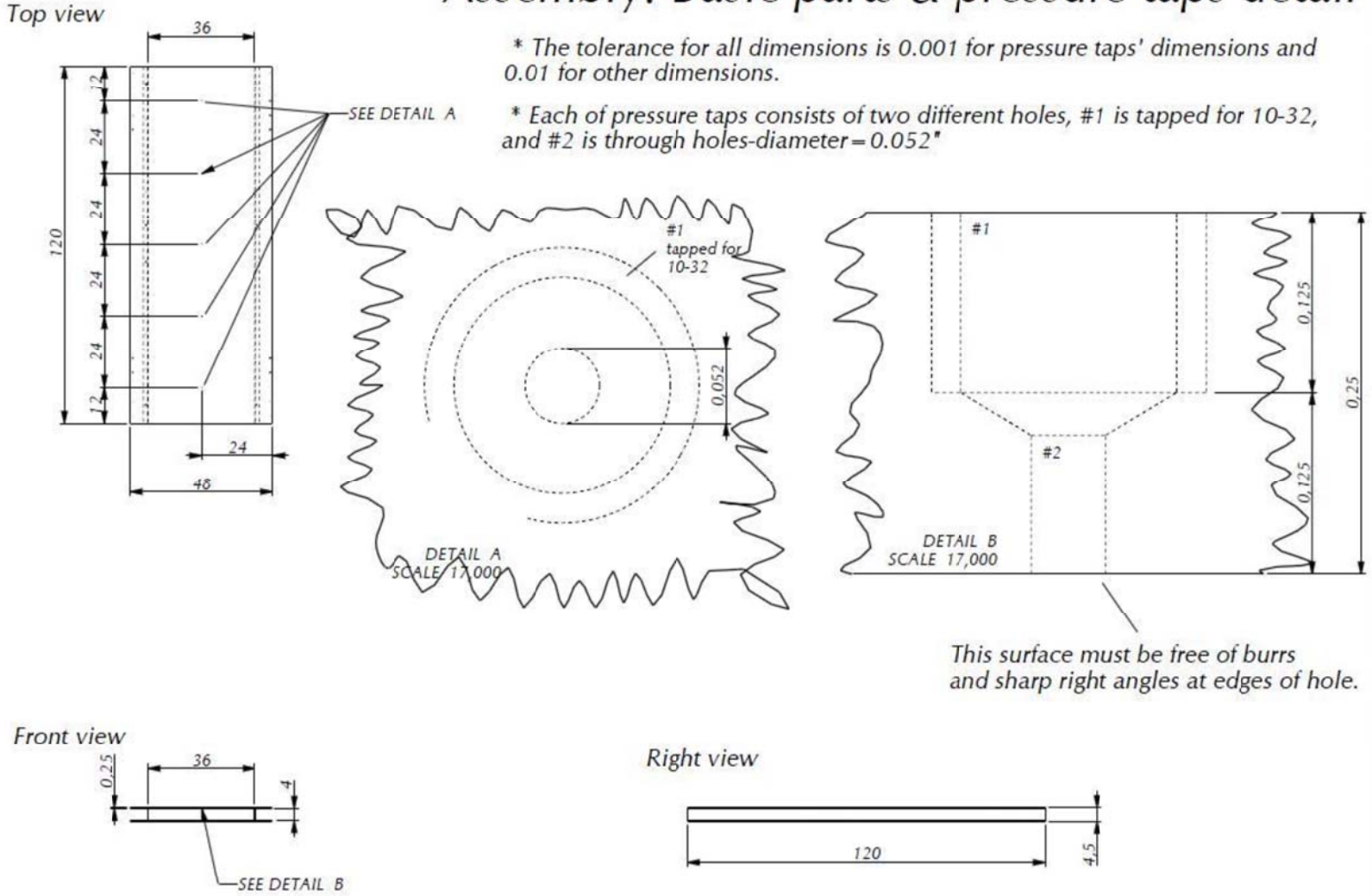

Part: Test Section - Top Plate

* Material: 1/2" Polycarbonate
* 1 Required
* All holes through,
Clearance through hole for 1/4-20
* The tolerance for pressure taps' dimensions is 0.001 and for other dimensions is 0.01.

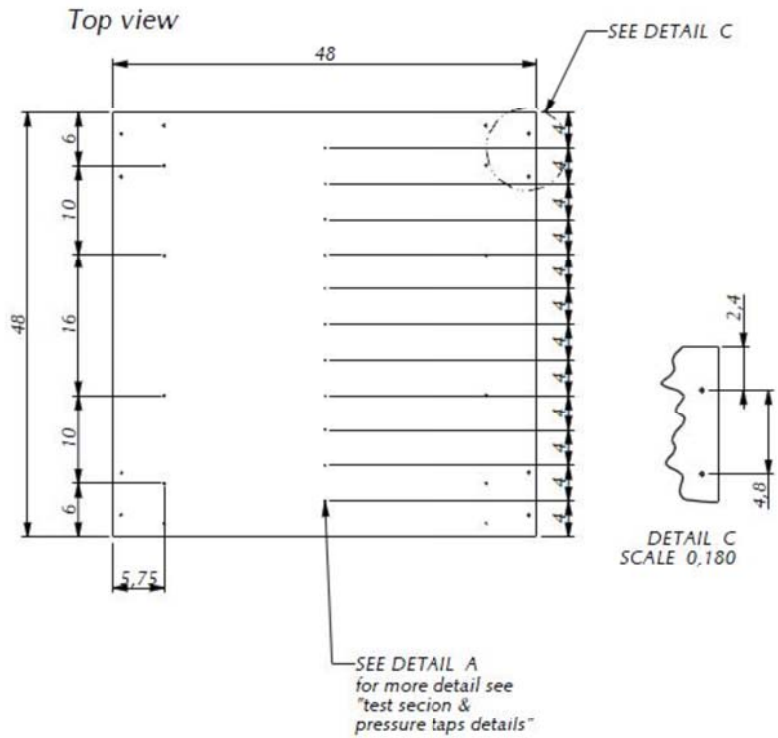

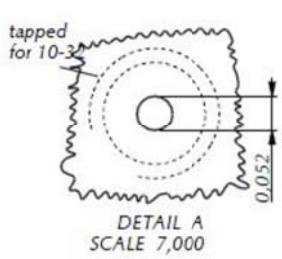

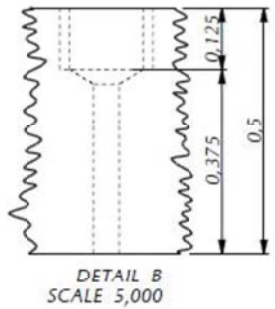

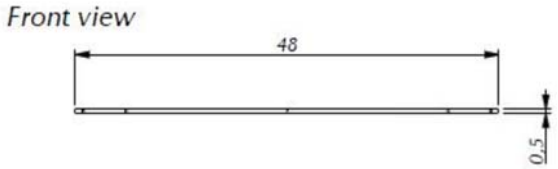

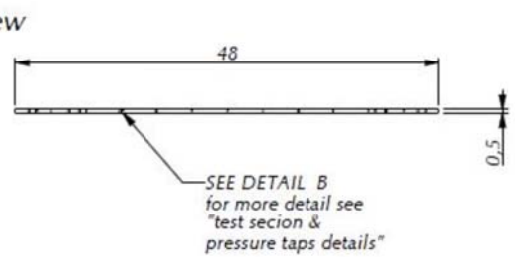

Part: Test Section - Bottom Plate

Top view

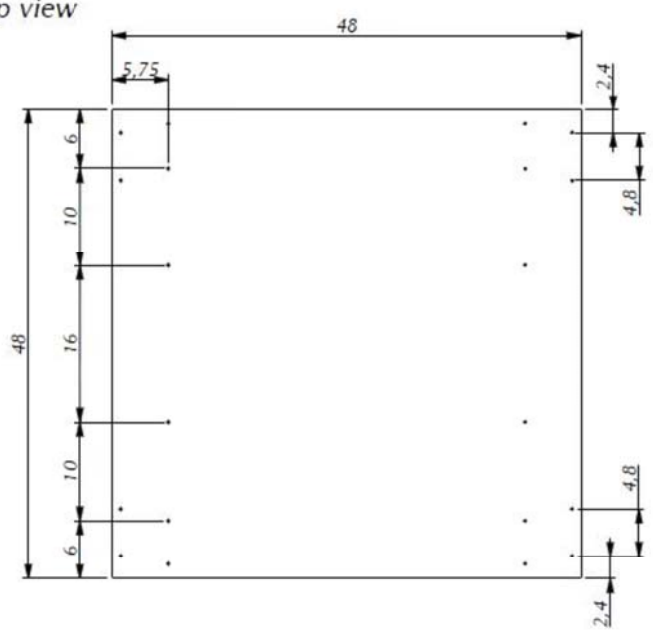

* Material: 1/2" Polycarbonate
* 1 Required
* All holes through,
Clearance through hole for 1/4-20
* Bottom plate are the same as top plate except the lack of pressure taps
* The tolerance for all dimensions is 0.01

Front view

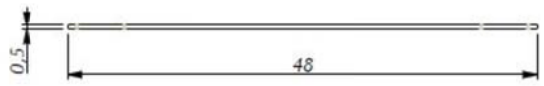

Right view

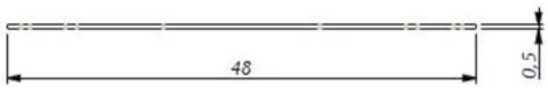

Part: Test Section -Side wall

* Material: 1/2" Polycarbonate
* 2 Required
* All holes, 0.5" deep, tapped for 1/4-20
* The holes on top row and bottom row are located the same.
* The tolerance for all dimensions is 0.01

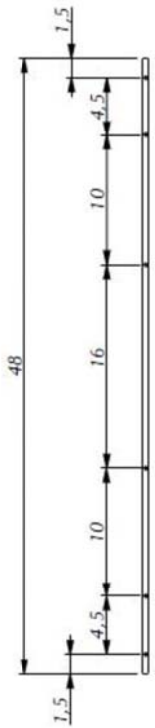

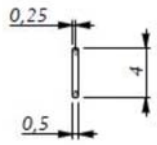

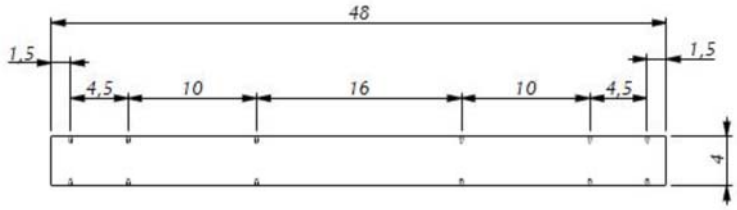

Assembly: Test Section & pressure taps details

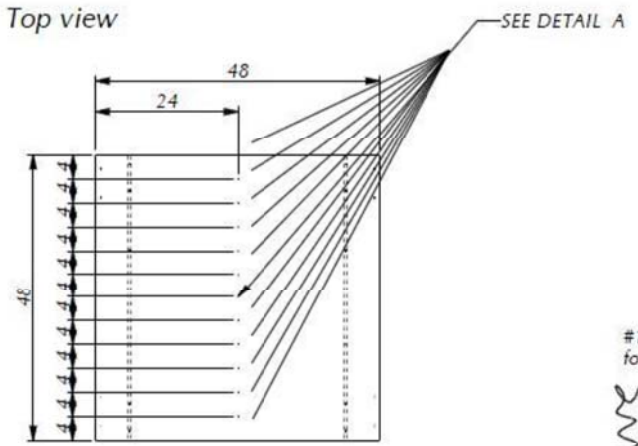

* The tolerance for all pressure taps' dimensions is 0.001 and for other dimensions is 0.01.

* Each of pressure taps consists of two different holes, #1 is tapped for 10-32, and #2 is through hole diameter – 0.052"

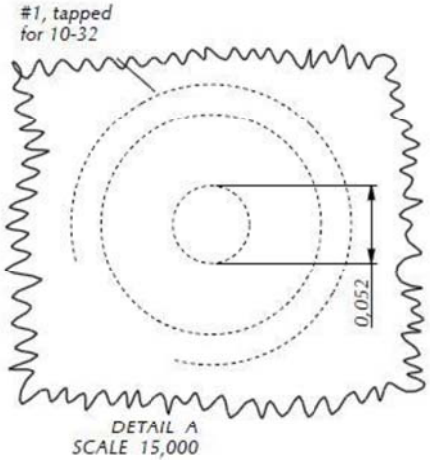

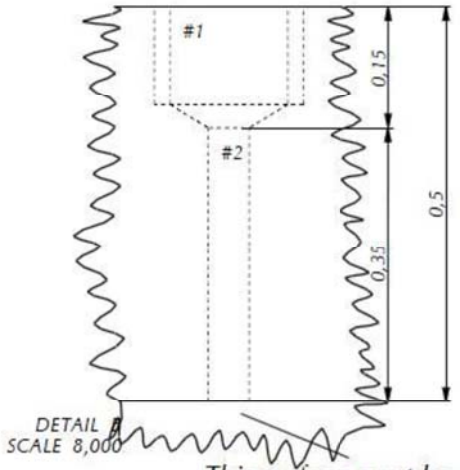

This surface must be free of burrs and sharp right angles at edges.

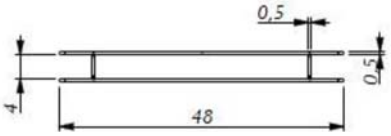

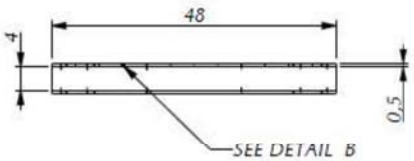

Part: Connector piece

* Material: U Channel 6061-T6 Aluminum, Extruded
* 10 Required (2 for each basic part)
* All holes through, clearance for 1/4-20
* The holes on top and bottom wings of U channel locate the same.
* The tolerance for all dimensions is 0.01

Top view

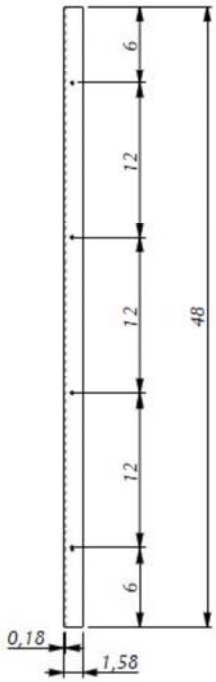

Front view

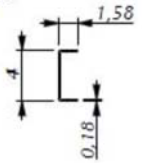

Right view

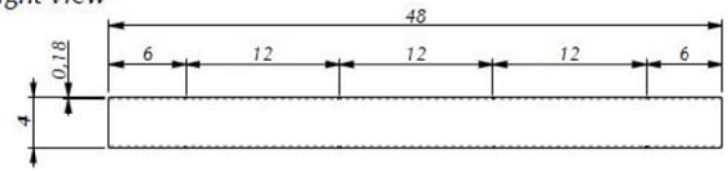

BIBLIOGRAPHY

Abe, H., Kawamura, H. & Matsuo, Y. 2001 Direct Numerical Simulation of a Fully Developed Turbulent Channel Flow With Respect to the Reynolds Number Dependence. *Transactions of the ASME* **123**, 382- 393

Alfredsson, P. H., Johansson, A. V., Haritonidis, J. H. & Eckelmann H. 1988 The fluctuating wall-shear stress and the velocity field in the viscous sublayer. *phys. Fluids* **31** (5), 1026-1033

Antonia, R. A. & Kim, J. 1994 Low-Reynolds-number effects on near-wall turbulence. J. Fluid Mech. 276, 61-80

Bailey, S.C.C., Hultmark, M. Smits, A. J. & Schultz,M. P. 2008 Azimuthal structure of turbulence in high Reynolds number pipe flow. *J. Fluid Mech.* 615 :pp 121-138

Barenblatt GI. 1993. Scaling laws for fully developed turbulent shear flows. Part 1. Basic hypotheses and analysis. *J. Fluid Mech*. **248**,513-520

Barenblatt GI, Chorin AJ, HaldOH,ProstokishinVM.1997. Structure of the zero-pressure-gradient turbulent boundary layer. *Proc. Natl. Acad. Sci. USA* **29**,7817-7819

Barlow, J. B., Rae, W. H. & Pope A. 1999 *Low-Speed Wind Tunnel Testing*. 3rd edn. John Wiley & Sons

Bradshaw, P. 1967 "Inactive" motion and pressure fluctuations in turbulent boundary layers. *J. Fluid Mech.* **30**, 241-258

Brown, G.L. & Thomas, A. S. W. 1977 Large structure in a turbulent boundary layer. *Phys. Fluids* **20**, S243

Bruns, J.M., Dengel, P. 1998 A miniature triple hot-wire probe for wall bounded flows. *Experiments in Fluids* **24** (5-6), 479-488

Chin, C. C., Hutchins, N., Ooi, A. S. H. & Marusic, I. 2009 Use of direct numerical simulation (DNS) data to investigate spatial resolution issues in measurements of wall-bounded turbulence. *Meas. Sci. Technol.* 20, 115401

Coles, D. E. 1962 The turbulent boundary-layer in compressible fluid. *Technical report R-403-PR*. The RAND Corporation, Santa Monica, CA.

Darcy, H. 1857 Recherches Experimentales Relatives au Mouvement de L'Eau dans les Tuyaux. *Mallet-Bachelier, Paris*. 268 p. & atlas

Dean, R. B. 1978 Reynolds number dependence of skin friction and other bulk flow variables in two-dimensional rectangular duct flow. *J. Fluids Eng*. **100**, 215–223

DeGraaff D. B. and Eaton J. K. 2000 Reynolds number scaling of the flat plate turbulent boundary layer. *J. Fluid Mech.* **422**, 319-346

Del Álamo, J. C. & Jiménez, J. 2003 Spectra of very large anisotropic scales in turbulent channels. *Phys. Fluids* **15**, L41

Del Álamo, J. C., Jiménez, J., Zandonade, P. & Moser, R. D. 2004 Scaling of the energy spectra of turbulent channels. *J. Fluid Mech.* **500**, 135-144

Den Toonder, J. M. J. & Nieuwstadt, F. T. M. 1997 Reynolds number effects in a turbulent pipe flow for low to moderate Re. *Phys. Fluids* **9** (11), 3398-3409

Du Buat, P. L. G. 1779 *Principes d'hydraulique*

Gad-el-Hak, M. & Bandyopadhyay, P. 1994 Reynolds number effects in wall bounded turbulent flows. *Appl. Mech. Rev.* **47**, 307

George, W. K. & Castillo, L. 1997 Zero-pressure-gradient turbulent boundary layer. *Appl.Mech. Rev.* **50**, 689-729

Grant, H. L. 1958 The large eddies of turbulent motion. *J. Fluid Mech.* **4**, 149

Hagen G. 1839 *Poggendorff's Annalen d. Physik u. Chemie* (2) **46**, 423

Hinze, J. O. 1975 *Turbulence,* 2end edn. McGraw Hill

Hites, MH. 1997 Scaling of high-Reynolds number turbulent boundary layers in the National Diagnostic Facility. *PhD thesis*, Ill. Inst. Technol

Hoyas, S. & Jiménez, J. 2006 Scaling of the velocity fluctuations in turbulent channels up to $Re_\tau = 2003$. *Phys. Fluids* **18**, 011702

Hultmark, M., Bailey S. C. C. & Smits, A. J. 2009 Scaling of near-wall turbulence in pipe flow. *J. Fluid Mech.* **649**, 103-113

Hultmark, M., Ashok, A. & Smits, A. J. 2011 A new criterion for end-conduction effects in hot-wire anemometry. *Measurement Science & Technology* **22** (5), 055401

Hutchins, N. & Marusic, I. 2007 Evidence of very long meandering features in the logarithmic region of turbulent boundary layers. *J. Fluid Mech*. **579**, 1-28

Hutchins, N., Nickels, T.B., Marusic, I. & Chong, M. S. 2009 Hot-wire spatial resolution issues in wall-bounded turbulence. *J. Fluid Mech.* **635**, 103-136

Jiménez, J. M., Hultmark, M. & Smits, A. J. 2010 The intermediate wake of a body of revolution at high Reynolds number. *J. Fluid Mech*. **659**, 516-539

Kim, J., Moin, P. & Moser, R. 1987 Turbulence statistics in fully developed turbulent channel flow at low Reynolds number. *J. Fluid Mech*. **177**, 133-166

Kim, J., Moin, P. & Moser, R. 1990 The Diskette of Collaborative Testing of Turbulence Models, *Bradshaw P. ed. Stanford University*

Kim, K. C. & Adrian, R. J. 1999 Very large-scale motion in the outer layer. *Phys. Fluids* **11** (2), 417-422

Klewicki, J. C., Falco, R. E. 1990 On accuracy measuring statistics associated with small-scale structure in turbulent boundary-layers using hot-wire probes. *J. Fluid Mech.* **219**, 119-142

Kline, S. J., Reynolds, W. C., Schraub, F. A. & Runstadler, 1967 The structure of turbulent boundary layers. *J. Fluid Mech.* **30**, 741

Kovasznay, L.S.G., Kibbens, V. & Blackwelder, R. F. 1970 Large-scale motion in the intermittent region of a turbulent boundary layer, *J. Fluid Mech*. **41**: 283

Kundu, P. K. & Cohen, I. M. 2008 *Fluid mechanics*. 4th edn.

Laghrouche, A., Adane, A., Boussey, J., Ameur, S., Meunier, D. & Tardu, S. 2005 A miniature silicon hot wire sensor for automatic wind speed measurements. *Renewable Energy* **30** (12), 1881-1896

Laufer, J. 1950 Investigation of turbulent flow in a two-dimensional channel. *Technical Report* **2123** N. A. C. A.

Ligrani P. M. & Bradshaw P. 1987a Subminiature hot-wire sensors: development and use. *J. Phys. E: Sci. Instrum.* **20** (3), 323-332

Ligrani P. M. & Bradshaw P. 1987b Spatial resolution and measurement of turbulence in the viscous sublayer using subminiature hot-wire probes. *Experiments in Fluids* **5** (6), 407-417

Marusic, I. & Kunkel, G. J. 2003 Streamwise turbulence intensity formulation for flat-plate boundary layers. *Phys. Fluids* **15** (8), 2461-2464

Marusic, I. & Hutchins, N. 2008 Study of the Log-Layer Structure in Wall Turbulence Over a Very Large Range of Reynolds Number. *Flow Turbul Combus.* **81**, 115-130

Marusic, I., Mathis, R. & Hutchins, N. 2010 Predictive Model for Wall-Bounded Turbulent Flow. *Science* **329**, 193-196

Mathis, R., Hutchins, N. & Marusic, I. 2009a Large-scale amplitude modulation of the small-scale structures in turbulent boundary layers. *J. Fluid Mech.* **628**, 311-337

Mathis, R., Monty, J. P., Hutchins, N. & Marusic, I. 2009b Comparison of large-scale amplitude modulation in turbulent boundary layers, pipe, and channel flows. *Phys. Fluids* **21**, 111703

McDonough 2011 Introductory lectures on turbulence Physics, Mathematics and Modeling. *Departments of Mechanical Engineering and Mathematics, University of Kentucky*

Meinhart, C. D. & Adrian, R. J. 1995 On the existence of uniform momentum zones in a turbulent boundary layer. *Phys. Fluids* **7**, 694

Metzger, M. M. & Klewicki, J. C. 2001 A comparative study of near-wall turbulence in high and low Reynolds number boundary layers. *Phys. Fluids* **13** (3), 692-701

Metzger, M. M., Klewicki, J. C., Bradshaw, K. L. & Sadr R. 2001 Scaling the near-wall axial turbulent stress in the zero pressure gradient boundary layer. *Phys. Fluids* **13** (6), 1819-1821

Metzger, M. M. 2002. Scalar dispersion in high Reynolds number turbulent boundary layers. *PhD thesis*, Univ. Utah

Mochizuki, S. & Nieuwstadt, F. T. M. 1996 Reynolds-number-dependence of the maximum in the streamwise velocity fluctuations in wall turbulence. *Experiments in Fluids* **21**, 218-226

Monkewitz, P. A., Chauhan, K. A. & Nagib, H. M. 2007 Self-contained high-Reynolds-number asymptotics for zero-pressure-gradient turbulent boundary layers. *phys. Fluids* **19**, 115101

Monty, J. P. 2005 Developments in smooth wall turbulent duct flows, *PhD thesis*, Univ. Melbourne

Monty, J. P., Stewart, J. A., Williams, R. C. & Chong, M. S. 2007 Large-scale features in turbulent pipe and channel flows. *J. Fluid Mech.* **589**, 147-156

Monty, J. P., Hutchins, N., NG H. C. H., Marusic, I. & Chong, M.S. 2009 A comparison of turbulent pipe, channel and boundary layer flows. *J. Fluid Mech*. **632**, 431-442

Moser, R. D., Kim, J. & Mansour, N. N. 1999 Direct numerical simulation of turbulent channel flow up to Reτ = 590. *Phys. Fluids* **11** (4), 943-945

Murlis, J., Tsai, H. M. & Bradshaw, P. 1982 The structure of turbulent boundary layers at low Reynolds numbers. *J. Fluid Mech*. **122**, 13

Nagib, H. M., Chauhan, K. A. & Monkewitz, P. A. 2007 Approach to an asymptotic state for zero pressure gradient turbulent boundary layers. *Philos. Trans. R. Soc. Lond. A* **365**, 755-770

Nickels, T. B., Marusic, I., Hafez, S. M., Hutchins, N. & Chong, M. S. 2007 Some predictions of the attached eddy model for a high Reynolds number boundary layer. *Philos. Trans. R. Soc. Lond. A* **365**, 807-822

Orlu, R., Fransson, J. H. M. & Alfredsson, P. H. 2010 On near wall measurements of wall bounded flows-The necessity of an accurate determination of the wall position. *Progress in Aerospace science* **46** (8), 353-387

Österlund JM. 1999 Experimental studies of zero-gradient turbulent boundary layer. *PhD thesis*, KHD, Stockholm

Panton, R. L. 2007 Composite asymptotic expansions and scaling wall turbulence. *Philos. Trans. R. Soc. Lond. A* **365**, 733–54

Perry, A. E., Hafez, S., & Chong, M. S. 2001 A possible reinterpretation of the Princeton Superpipe data. *J. Fluid Mech*. **439**, 395–401.

Pope, S. B. 2000 *Turbulent flows.* 1st edn.

Prandtl L 1904 Uber Flussigkeits bewegung bei sehr kleiner Reibung. *Verhaldlg III Int. Math. Kong. (Heidelberg: Teubner),* 484–491; Also available in translation as: *Motion of fluids with very little viscosity. NACA TM 452* (March 1928)

Prandtl, L. 1925 Bericht über die Entstehung der Turbulenz. *Z. Angew. Math. Mech.* **5**, 136-139

Reynolds, O. 1883 An experimental investigation of the circumstances which determine whether the motion of water shall be direct or sinuous, and of the law of resistance in parallel channels. *Royal Soc., Phil. Trans.,* 935-982

Schlichting, H. 1936 Experimental investigation of the problem of surface roughness. *Technical Report* **823** N. A. C. A.

Smits, A.J., Monty, J., Hultmark, M., Bailey S. C. C., Hutchins N. & Marusic, I. 2011 Spatial resolution correction for wall-bounded turbulence measurements. *J. Fluid Mech.* **676**, 41-53

Smits, A. J., McKeon, B. J. & Marusic I. 2011 High-Reynolds Number Wall Turbulence. *Annu. Rev. Fluid Mech.* **43**, 353-375

Sreenivasan, K. R. & Sahay, A. 1997 The persistence of viscous effects in the overlap region, and the mean velocity in turbulent pipe and channel flows. *R. L. Panton, Comp. Mech. Pub.* **1997**, 253-271

Tavoularis, S. 2005 *Measurement in Fliud mechanic.* 1st edn.

Tennekes, H. & Lumley, J. L. 1972 *A first course in turbulent*

Townsend, A. A. 1976 *The structure of turbulent shear flow*. 2nd edn., Cambridge University Press

Wei, T., Fife, P., Klewicki, J. C. & McMurtry, P. 2005 Properties of the mean momentum balance in turbulent boundary layer, pipe and channel flows. *J. Fluid Mech.* **522**, 303-327

Wu, x. & Moin, P. 2008 A direct numerical simulation study on the mean velocity characteristics in turbulent pipe flow. *J. Fluid Mech*. **608**, 81-112

Zagarola, M. V. & Smits, A. J. 1998 Mean-flow scaling of turbulent pipe flow. *J. Fluid Mech.* **373**, 33–79

Zanoun, E.-S., Durst, F. & Nagib, H. 2003 Evaluating the law of the wall in two-dimensional fully developed turbulent channel flows. *Phys. Fluids* **15** (10), 3079-3089

Zanoun, E.-S., Nagib, H. & Durst, F. 2009 Refined c_f relation for turbulent channels and consequences for high-*Re* experiments. *Fluid Dyn. Res.* **41** (2) 021405

Zhou, J., Meinhart, C. D., Balachandar, S. & Adrin, R. J. 1997 in Self-Sustaining Mechanisms in Wall Turbulence, edited by Panton R., *Computational Mechanics Publications, Southampton, UK* 109-134

VITA

Bahareh was born in Shiraz, Iran in 1979. She graduated with her B.S. from Shiraz University, School of Engineering, Mechanical engineering department in 2003. After her graduation, she worked as a Mechanical Engineer in cement industry for more than four years. Following this, she decided to continue her education through pursuing M.S. in Mechanical Engineering from the University of Kentucky. She also achieved CFD certificate during her M.S. from this university.

Publications:

- Bailey, S., Estejab, B., Robert, M., Tavoularis S. 2011 Long-wavelength Vortex Motion Induced by Free-stream Turbulence. *Seventh International Symposium on Turbulence and Shear flow Phenomena (TSFP-7), Ottawa, Canada* (Accepted)
- Estejab, B., 2007 Technical and economical comparison of Gas conditioning tower in cement industry. *Iranian Cement magazine*, Third issue in 2007 (Published)

Bahareh Estejab

07/26/2011